IOSR Journal of VLSI and Signal Processing (IOSR-JVSP)
e-ISSN: 2319 – 4200, p-ISSN No. : 2319 – 4197 Volume 1, Issue 6 (Mar. - Apr 2013), PP 01-06
www.iosrjournals.org

Design and Analysis of Johnson Counter Using Finfet Technology

Myneni Jahnavi[1], S.Asha Latha[2], T.Ravi[3], E.Logashanmugam[4]
[1](M.Tech-VLSI design ,Department of ECE, Sathyabama University, Chennai -119,India)
[2](Asst.Professor, Department of ECE, Sathyabama University, Chennai -119, India)
[3](Asst.Professor, Department of ECE, Sathyabama University, Chennai -119, India)
[4](Professor & Head, Department of ECE, Sathyabama University, Chennai -119, India)

Abstract : *Conventional CMOS technology's performance deteriorates due to increased short channel effects. Double-gate (DG) FinFETs has better short channel effects performance compared to the conventional CMOS and stimulates technology scaling. The main drawback of using CMOS transistors are high power consumption and high leakage current. Fin-type field-effect transistors (FinFETs) are promising substitutes for bulk CMOS in nano- scale circuits.FinFET, which is a double-gate field effect transistor (DGFET), is more versatile than traditional single-gate field effect transistors because it has two gates that can be controlled independently. Usually, the second gate of FinFET transistors is used to dynamically control the threshold voltage of the first gate in order to improve the performance and reduce leakage power. In this paper, we proposes a synchronous johnson counter by using FinFET Technology.FinFET logic implementation has significant advantages over static CMOS logic in terms of power consumption. The proposed counter was fabricated in 16nm FinFET technology in HSPICE.*

Keywords – *CMOS, Scaling, FinFET, Low Power Design, SET*

I. Introduction

Steady miniaturization of transistors with each new generation of bulk CMOS technology has yielded continual improvement in the performance of digital circuits.In the case of non portable devices, power consumption is also very important because of the increased in packaging density and cooling costs as well as potential reliability problems. Thus, power efficiency has increased importance, to meet the performance requirements of VLSI.The scaling of bulk CMOS, in fact faces significant challenges in the future due to fundamental material and process technology limits [1].Short channel effects such as sub-threshold and gate-dielectric leakages in conventional CMOS devices are primary limiters for scaling. Novel device architectures are therefore, necessary to continue reaping the benefits of scaling to very short gate lengths beyond 10nm. Double-gate CMOS (DGCMOS) devices offer an attractive alternative to other structures such as ultra-thin body (UTB) or conventional bulk CMOS in terms of performance and control of short-channel effects.

The emergence of FinFET provides a promising solution. FinFET, a double-gate device in which a second gate is added opposite to the traditional (first) gate, has long been recognized for its potential to better control short-channel effects.The additional back gate of FinFETs gives circuit designers many options. It can serve as a secondary gate that enhances the performance of the front (first) gate. For example, if the front gate voltage is VDD (transistor is ON) the back gate can be biased to VDD to provide bigger current drive, which reduces transistor delay. If the front gate voltage is 0 (transistor is OFF), the back gate can be biased to 0, which raises the threshold voltage of the front gate and reduces the leakage current. This can be achieved by simply tying the front gate and the back gate together[3]. Fin-FETs are predicted as one of the best possible candidates to replace the bulk MOSFETs beyond 32nm regime due to their improved subthreshold slope, reduced leakage current, better short-channel performance, and Compatible process flow with existing CMOS technologies.It has been shown that such a device has a very high potential for analog applications due to its high value of early voltage and, hence, a large intrinsic gain [4].

II. FinFET Structure

Double-gate devices have been used in a variety of innovative ways in digital and analog circuit designs. DG devices with independent gates (separate contacts to back and front gates) have been recently developed. In the context of digital logic design, the ability to independently control the two gates of a DG-FET has been utilized chiefly in two ways: by merging pairs of parallel transistors to reduce circuit area and capacitance, and the next way through the use of a back-gate voltage bias to modulate transistor threshold voltage. A parallel transistor pair consists of two transistors with their source and drain terminals tied together. In Double-gate (DG) FinFETs, the second gate is added opposite the traditional (first) gate, which have been recognized for their potential to better control short-channel effects (SCEs) and as well as to control leakage current.The structure of the FinFET is shown in the Fig.1.

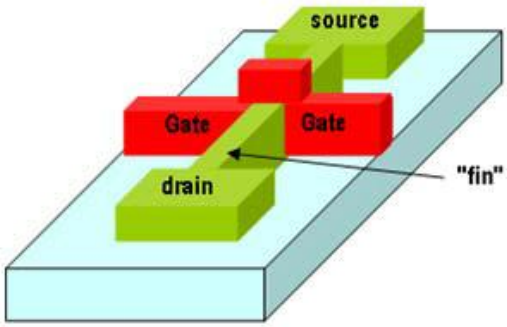

Fig 1.FINFET Structure

The two gates for FinFETs provide effective control of the short-channel effects without aggressively scaling down the gate-oxide thickness and increasing the channel doping density. The separate biasing in DG device easily provides multiple threshold voltages. It can also be exploited to reduce the number of transistors for implementing logic functions [5].

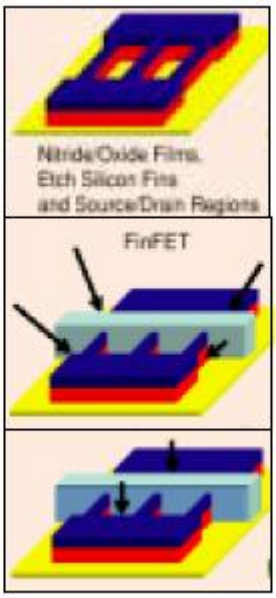

Fig 2. FinFET manufacturing process flow

1.1 Process Flow

The process flow is summarized in Figure 2. It involves the following basic steps: (i) Etching of Si fins out of the silicon layer of an SOI wafer, (ii) Gate formation around the fin, forming the front and back gates and (iii) spacer formation followed by S/D implantation. As we can see from Figure 1, the height of the silicon fin defines the transistor width. The thickness of the fin,on the other hand, defines the control of the back gate on the channel and hence the short channel behavior of the device.Silicon films on SOI wafers are used to define the fins and hence,the height of the fin is effectively constant for all transistors [2].

1.2 Device-Width Quantization

Each fin provides 2H of device width, where H is the height of the fin. The size of each fin also determines the increments in device widths available to the circuit designer. In planar devices, the device width quanta are dictated by the grid step size in the design database employed. This relatively unconstrained selection of device width allows designers to choose appropriate ratios of N-MOSFET and P-MOSFETdevices to achieve desired tradeoffs in performance, power, and robustness. Owing to the quantization constraint, it is much more difficult to achieve the required beta ratios in FinFETs [2].

III. SET D Flip flop

The proposed SET D flip-flop is illustrated in figure 3. When the clock is high, CLK signal is at logic level high and CLKB is at logic level low. In this state, the Master latch consisting of one pass transistor PT1 and inverter I1 is functional and the inverse of data at input D is stored to an intermediate node. When the clock is at logic level low, CLK signal is at logic level low and CLKB is at logic level high. In this state, the Slave latch consisting of pass transistor PT2 and a regenerative feedback loop consists of one pass transistor PT3 becomes functional and produces Q and QB after two inversions.The flip-flop as shown above in figure 3 is a negative edge triggered SETFF.

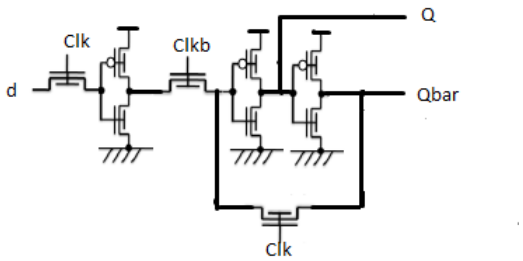

Fig 3.SG-FINFET SET D Flip flop implementation

The regenerative feedback loop that used in the design advantageously serves as even if the clock is stopped (permanently grounded) the proposed circuit is able to maintain the logic levels at Q and QB which proves the fact that the proposed SET is static in nature. The main advantage of the circuit is the reduced transistor count, which is only nine that is less than existing flip flop.So power is also reduced merely. Hence, it can be used to increase the chip density while maintaining a lower manufacturing cost at the same time. Moreover, the circuit can be made to function dynamically by merely removing the pass transistor from the regenerative feedback loop of the proposed design with only eight transistors. Since, we have used only N type FINFET transistors in the forward path, the design can be suitably used for high frequency applications and is easily portable to lower technologies.

IV. Design of Johnson Counter

Counters are usually suffer problem of power consumption because they are designed with conventional D,T or JK flip flops. They are not only increase power consumption but also design complexity is more. By choosing the flip flop with low power consumption makes the design power efficient. The johnson counter consists of four stages of cascaded D registers. The D register design has been implemented using CMOS inverter and two D latch with one clock and one input. Since it is synchronous counter clock input is applied to all flip flops simultaneously. A Johnson counter or switch tail ring counter, is a counter, where the inverted output from the last flip flop is fed back as an input to the first flip flop. Johnson counter, whose sequence length is equal to twice the length of the d flip flops in the counter. These counters find different applications like decoding, phase waveform generation etc. They can be implemented easily using D- or JK-type flip-flops. The 4 bit synchronous Johnson counter i.e shown in figure 2 is designed by using four SET D flip flops represented in figure 1 and figure 2.

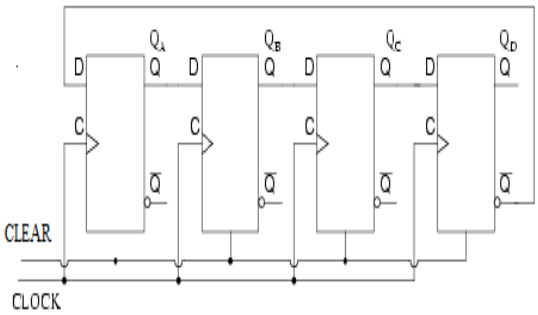

Fig 4.Johnson counter

In this counter, inversion of Q is fed back to input D causes the counter to "count" in a different way. Generally 4-bit Johnson counter passes four logic 0s and then four logic 1s thereby producing an 8-bit sequence pattern i.e., 1000, 1100, 1110, 1111, 0111, 0011, 0001, 0000 and this is shown in the following table1 below.

Table1. Truth Table for a 4-bit Johnson Counter

Clock Pulse No	FFA	FFB	FFC	FFD
0	0	0	0	0
1	1	0	0	0
2	1	1	0	0
3	1	1	1	0
4	1	1	1	1
5	0	1	1	1
6	0	0	1	1
7	0	0	0	1

To enable the counter according to desired Sequence shown in table 1, first it is necessary to clear all the flipflops.Initially QD is ‘0 and QDbar is ‘1’.The first clock shifts three 0s from (QA QB QC) to the right into (QB QC QD).After three clock pulses we have all 1s.So the output of last flip flop i.e QD is ‘1’ and QDbar is ‘0’.Thus we start shifting 1s to that right, replacing the zeros. Because of implementing the Johnson counter with proposed SET D Flip flop the power consumption is substantially reduced, the comparison results shown in section V.

V. Simulation Results

The design is implemented using HSPICE and the circuits are simulated using 16nm technology. The waveform of the SET DFF and Johnson counter using SET DFF are shown in fig 5 and fig 6.

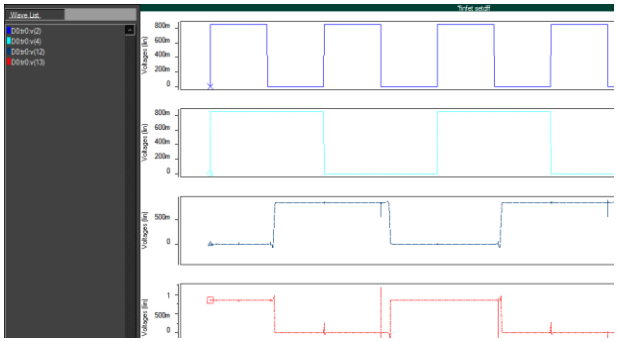

Fig 5. SG-Finfet SET D Flip flop

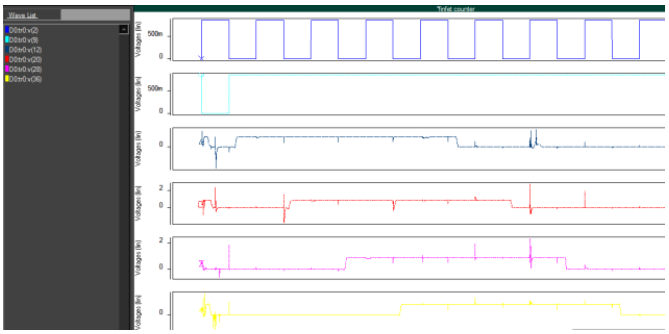

Fig 6.Johnson counter

Table 2.Comparison Table

Design	Parameters		No of Transistors	Avg Power (μW)
	Operating Frequency	Operating Voltage		
Flip flop	500MHz	0.85V	9	0.065
Counter	500MHz	0.85V	60	0.201

VI. Conclusion

This paper concludes that synchronous Johnson counter is implemented by FINFET 16nm technology using HSPICE . FinFET not only has superior performance over bulk silicon MOSFET, but also it is novel technology over bulk silicon MOSFET as the dominant transistor choice for sub micron technology. FinFET is equivalent to two MOSFETs operating in parallel. FinFET logic circuits achieve significant area and power reduction without transistor scaling.

References

[1] Anish Muttreja, Niket Agarwal and Niraj K. Jha,Dept. Of Electrical Engineering, Princeton University, Princeton, NJ 08544"CMOS Logic Design with Independent-gate FinFETs".

[2] Farhana Sheikh, Vidya Varadarajan, "The Impact of Device-Width Quantization on Digital Circuit Design Using FinFET Structures", *EE 241 SPRING 2004.*

[3] Michael C. Wang **,** "Independent Gate FinFET Circuit Design Methodology", *IAENG International Journal of Computer Science, 37:1, IJCS_37_1_06.*

[4] Varun P. Gopi and V. Sureshbabu,"Independently driven double gate FinFET scalable to 10nm" , *10th National Conference on Technological Trends (NCTT09) Nov2009.*

[5] Nirmal,Vijaya kumar, Samjabaraj, Nirmal et al, **,"** Nand gate using finfet for nanoscale technology", *International Journal of Engineering Science and Technology Vol. 2(5),* 2010, 1351-1358**".**

[6] Imran Ahmed Khan,Mizra Tariq Beg,"Comparitive analysis of low power master slave single edge triggered flip flops",*World applied sciences journal 16(special issue on recent trends on VLSI Design) 15-21,2012*

[7] V Narendar,Wanjul Dattatray,R Sanjeev Rai,R. A.Mishra," Design of High-performance Digital Logic Circuits based on FinFET Technology", *International Journal of Computer Applications (0975 – 8887) Volume 4*,1– No.20, March 2012.

[8] Michael C. Wang, Low Power, Area Efficient FinFET Circuit Design, *Proceedings of the World Congress of Engineering and Computer Science 2009 Vol I,WCECS 2009,* October 20-22, 2009, San Francisco, USA.

[9] Sherif A.Tawfik, VolkanKursun, "FinFET domino logic with independent gate keepers", Microelectronics Journal.

[10] Vladimir Stojanovic,Vojin G.Oklobdzija,"Comparitive analysis of master-slave latches and flip flops for high performance and low power systems*",IEEE Journal of Solid state circuits,vol 34,no.4,APRIL.*

[11] Simmy Hirkaney, Sandip Nemade, Vikash Gupta "Power Efficient Design of counter on 0.12 micron technology".

[12] Manoj sharma, Dr Arti Noor SoE, ,Shatish Chandra, Tiwari,Kunwar Singh,"An Area and Power Efficient design of Single Edge Triggered D-Flip Flop", *2009 International Conference on Advances in Recent Technologies in Communication and Computing.*

[13] Yu-Min Kuo,Shih-Hung Weng Shih-Chieh Chang , "A Novel Sequential Circuit Optimization with Clock Gating Logic".

[14] Abhilasha.K.G.Sharma,Tripti Sharma,Prof.B.P.Singh,"Optimum design of D Latch for low power applications*",IOSR Journal of Engineering,Apr 2012,vol 2(4)*

[15] Kunwar Singh,Satish Chandra, Tiwari Maneesha Gupta, **"**A High Performance FlipFlop for Low Power Low Voltage Systems" ,978-1-4673-0126-8/11/$26.00_c 2011, IEEE.

M.Jahnavi was born in Vijayawada on 3rd June 1989. She received his Bachelor Degree in Electronics and Instrumentation Engineering, from JNTU University, Kakinada, Andhra Pradesh.,India in the year 2010. Currently she is doing M.TECH., VLSI DESIGN in Sathyabama University,Chennai,Tamil Nadu,India.

S.Asha Latha was born in Chennai, Tamilnadu, India in 1983. She received her Bachelor Degree in Electrical and Communication Engineering from Bharathidasan University in the year 2004, Master Degree in VLSI DESIGN from Bharath Institute of Higher Education & Research Deemed University in the year 2006. Currently she is doing Ph.D in Sathyabama University. she is working as Assistant Professor in Department of ECE in Sathyabama University. Her interested areas of research are Wireless Sensor Networks, Cryptography, Nano Electronics, VLSI Design.

T.Ravi was born in Namakkal, Tamilnadu, India in 1978. He received his Bachelor Degree in Electrical and Electronics Engineering from Madurai Kamaraj University in the year 2001, Master Degree in Applied Electronics from Sathyabama Deemed University in the year 2004. Currently he is doing Ph.D in Sathyabama University. He is working as Assistant Professor in Department of ECE in Sathyabama University. His interested areas of research are Nano Electronics, VLSI Design, Low Power VLSI Design and Mixed Signal circuits. He has Research publications in National / International Journals /Conferences. He is a member of VLSI Society of India.

Dr.E.Logashanmugam was born in Madurai, Tamilnadu, India in 1969. He received his Bachelor Degree in Electronics and Communication Engineering from Madurai Kamaraj University in the year 1991, Master Degree in Electronics Engineering from Anna University, Chennai in the year 2001 and Ph.D., from Sathyabama University, Chennai, in the year 2009. His interested areas of research are VLSI Design, Nano Electronics, Image Processing and Cryptography. He has 60 Research publications in National / International Journals / Conferences to his credit. He has 22 years of experience in teaching and presently working as Head of Department , ECE, Sathyabama University, Chennai, Tamilnadu, India. He is a member of ISTE and IEEE.

IOSR Journal of VLSI and Signal Processing (IOSR-JVSP)
ISSN: 2319 – 4200, ISBN No. : 2319 – 4197 Volume 1, Issue 6 (Jan. - Feb 2013), PP 07-09
www.iosrjournals.org

2.5v 900 MHz 0.13µm CMOS cascode low noise amplifier for wireless application

Rupesh P.Raghatate[1],
[1](*M-tech SEM-I (B.D.college of engineering*,wardha)

Abstract : *This paper presents low noise amplifier (LNA) for wireless application as RF front end which has been implemented in 0.13µ RF CMOS technology. The LNA was designed using inductive source degeneration cascode topology which produces better gain and good stability. From the simulation results, the LNA exhibits a gain of 26.46 dB, noise figure (NF) of 1.16 dB at 115µW , output return loss (S22) of −6.55dB, input return loss (S11) of −14.46dB, reverse isolation (S12) of −39.76 dB, and a power consumption is 7 mA from a 2.5V power supply.*

Keywords - *Low noise amplifier; RF front-end, cascode, CMOS, inductive source degeneration.*

I. INTRODUCTION

Nowadays ,there have been many extensive studies and efforts to improve the noise figure in RF transceiver also CMOS integrated circuit for wireless application is receiving much attention, due to their potential for low cost . A key building block for the RF front-end is the low noise amplifier (LNA) which precedes a high noise stage plays a critical role in determining the over-all noise figure (NIF) of the transceiver. From a cost standpoint, the LNA is implemented in 0.13µm RF CMOS technology. Recent works in designing LNA have there have been a difficulty in attaining both low noise figure and low power consumption simultaneously. This paper describes the implementation of LNA using 0.13µm CMOS technology which meets low noise figure, higher gain and low power consumption simultaneously at 900 MHz frequency. Following text is divided into three sections; section II describes LNA design section III gives simulation results, section IV presents the conclusion.

II. LNA DESIGN

1) Circuit Topology

A fig (1) shows a cascode topology, A single-stage cascode amplifier topology with inductive degeneration at the source is used. A cascode topology is chosen to minimize the power dissipation and to improve 1-dB compression point. Here a cascode transistor M2 provides high impedance which improves isolation between input and output that increases stability of amplifier. The work is focused on developing the LNA circuit for 900 MHz application. The use of inductive degeneration provides input matching and noise matching with better gain and stability along with low power consumption simultaneously.

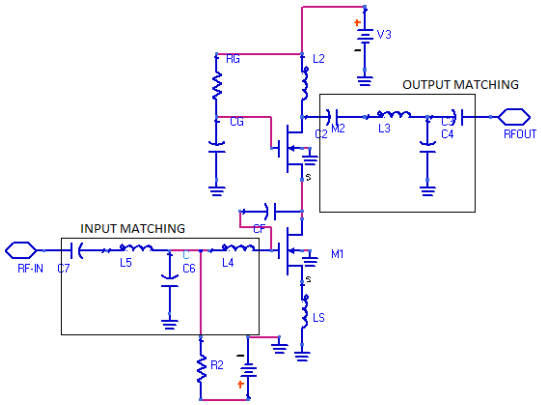

Fig.1: Schematic of LNA

2) Low noise amplifier:

Low noise amplifier is an important block in wireless receiver .it determines the receiver performance .the figure (1) shows schematic of LNA .circuit shown in dashed box both at input and output side are matching components of LNA while rest of the circuit is actual LNA.

The LNA is full of trade off between optimum gains, optimum input matching, low power consumption, lowest noise figure and linearity. The gain of LNA should be high enough to reduce noise contribution of subsequent stages; also noise must be as low as possible to minimize the impact on receiver noise performance. The input impedance of LNA is matched to 50Ω(characteristic impedance of antenna).The transistor M1 and M2 are depletion mode devices .resistor R2 and V2 are used to set voltage condition at M1 gate .RG is used to provide voltage at M2 while CG is used to eliminate any noise from the bias network .LS is used for stability. The input is coupled to gate of M1 with coupling capacitor Cs .the input is matched to 50 Ω using matching network and inductor LS .In this LNA design transistor M1 have gate width of 10 µm and 20 fingers ,transistor M2 has gate width of 5 µm and 1 finger. The transistor M1 is biased at 0.5 v and M2 is biased at 2.5v respectively, CF forms feedback network for M1 .The feedback degrades noise while improves linearity and offers easy input matching for LNA. A simple gain equation of LNA is given by following equation,

AV=RF OUT /RF IN

Feedback network affects gain of LNAQ but provides better stability.

III. SIMULATION RESULTS

All simulation for this LNA has been performed using Agilent's ADS-2009 using TSMC 0.13µm CMOS .a fully integrated 900 MHz LNA in 0.13µm RF CMOS has been designed, LNA employ lumped inductor and capacitor for matching input and output .fig (2) shows gain (S21) and (S12) of LNA .the S21 is -26 dB at 900 MHz, the S12 is -40 dB at 900 MHz.fig(3)shows input and output reflection co-efficient (S11) and (S22) of LNA .the S11 is lower than -10dB while S22 is -6dB at 900 MHz .fig (4)shows stability of LNA which is greater than 1 for all frequencies.fig(5)shows noise figure of LNA .the noise figure is 1.04 dB at 900 MHz . The LNA is biased with VDD 2.5v and consumes 7mA current.

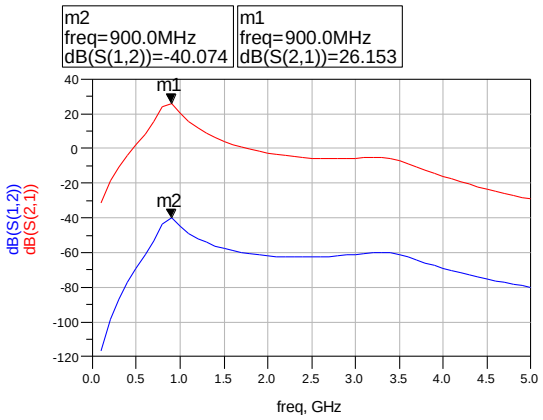

Fig2: *gain and isolation of LNA*

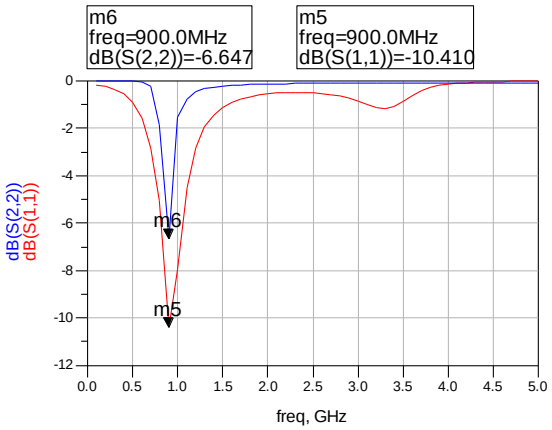

Fig3: *input and output reflection co-efficient*

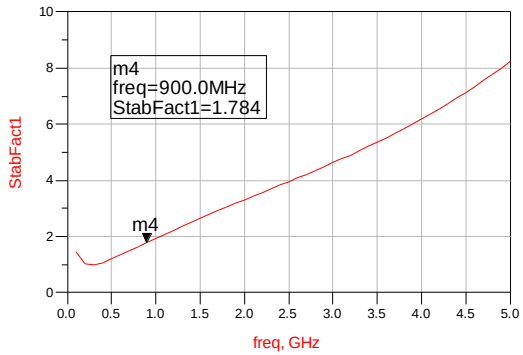

Fig 3: stability factor

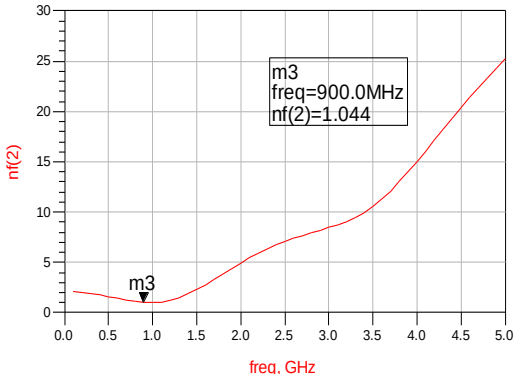

fig 4: noise figure

Table 1: summary of LNA parameters

LNA	Measured parameter
Supply voltage	2.5v
Technology used	TSMC 0.13 µm CMOS
RF frequency	900 MHz
Voltage gain (S21)	26 dB
Noise FIGURE	1.04dB
S11	-14 dB
S22	-6 dB
Power dissipation	115µW
Current consumption	7 mA
Reverse isolation	-40 dB

IV. CONCLUSION

The TSMC 0.13 µm CMOS high frequency model is used to design 900 MHz receiver front end. This paper presents 900 MHz LNA with noise figure 1.04 dB with power consumption of 115 µW from 2.5v power supply .the LNA exhibits gain of 26 dB. From both performance standpoint and cost standpoint, these results show that CMOS is very competitive with available technologies.

REFERENCES

JOURNAL PAPERS:

[1] Brian A. Floyd, Jesal Mehta, Carlos Gamero, and Kenneth K. O, A 900-MHz, 0.8-pm CMOS Low Noise Amplifier with 1.2-dB Noise Figure, *Silicon Microwave Integrated Circuits and Systems Research Group (SiMICS) Dept. of' Electrical and Computer Engineering, University of Florida, Gainesville.*

[2] Andrew N. Karanicolas, A 2.7-V 900-MHz CMOS LNA and Mixer, *Member, IEEE*

[3] Arjuna Marzuki, GaAs pHEMT cascode LNA for wireless application, *International journal of computer and electrical engineering ,vol.1,No.2,June 2009,1793-8163.*

[4] Jon Guerber,Design of an 2.4GHz CMOS LNA, *ECE 621,winter 2010.*

IOSR Journal of VLSI and Signal Processing (IOSR-JVSP)
e-ISSN: 2319 – 4200, p-ISSN No. : 2319 – 4197 Volume 1, Issue 6 (Mar. – Apr. 2013), PP 10-18
www.iosrjournals.org

Power Efficient Sum of Absolute Difference Algorithms for video Compression

D.V. Manjunatha[1], G. Sainarayanan[2]
[1](Department of ECE, Don Bosco Institute of Technology/ Visveswaraya Technological University, India)
[2](Department of EEE, New Horizon College of Engineering/ Visveswaraya Technological University, India)

Abstract : *Video Compression (VC) is one of the resource hungry key element in video communication and is commonly achieved using Motion Estimation (ME). In this paper we proposed power efficient one bit full adder and one of the simple and easy metric called Sum of Absolute Difference (SAD) for estimating the motion vectors in motion estimation. SAD is primarily used to detect motion in the video sub system. Here we proposed power efficient 4X4 and 8X8 SAD architectures. The proposed 4X4 SAD proves that 29%, 63.23% and 61.31% improvement in leakage power, dynamic power and total power respectively as compared with existing 4X4 SAD. Similarly the proposed 8X8 SAD which proves that 57%, 46.16% and 46.78% improvement in Leakage Power (LP), Dynamic Power (DP) and Total Power (TP) respectively as compared with that of existing 8X8 SAD at the gate level. The designs are implemented in ASIC methodology using cadence tools.*
Keywords - *SAD, ME, VC, CSA, DSP, LP, DP, TP, FPGA etc.*

I. INTRODUCTION

Many recent multimedia applications of digital video systems such as video conferencing, video-on-demand, video-phone, distance learning and digital TV, object tracking and many more have become popular products because of their convenience. Such applications require video compression with ever higher compression ratios, better visual quality and high bandwidth. The high efficiency video compression commonly uses the efficient hardware architectures. In general the development of hardware architectures are designed to form the integrated circuits which allows parallel processing of data from various sub blocks of the architectures, however hardware architectures suffers from limitations such as algorithm flexibility due to timing dependencies, which arises from the dataflow of various blocks of the architecture. Thus the development of good architecture of video codec in integrated circuits is very important. The customization of video codec is the video compression in the modern state of the art real time Digital Signal Processing (DSP) systems.

Video compression is one of the techniques in video processing system to reduce resource usage. The two primary challenges addressed during video compression are:

- Limited Network bandwidth.
- Limited Storage capacity.

Hence the two important metrics of a video encoder are low computational complexity & low power hardware implementation. Present day world, compression ratio plays the major role in the field of video processing. The motion in the video scene will reduce the efficiency of the compression ratio. Hence the motion estimation field has seen the highest research topic and interested issue in the past a few decades. In short the motion estimation means the estimation of the displacement (or velocity) of image structures from one frame to another in a time sequence of 2-D images of the video in order to achieve video compression in video coding.

The efficiency of the compression ratio can be increased by exploiting the similarities between the video frames. The simple metric system is the SAD algorithm, where the absolute differences between the corresponding elements are added up.

There are varieties of video coding standards in the video processing systems; the modern video coding standard is H.264/AVC. This coding standard uses the Variable Block Size Motion Estimation (VBSME), in this standard; the computation requirements are much higher than the previous coding standards such as H.263/ MPEG-IV. In H.264/AVC, each picture frame is divided into many macro blocks.

Each macro block is further divided into seven different sub-block sizes they are 4×4, 4×8, 8×4, 8×8, 8×16, 16×8 and 16×16 as shown in figure below

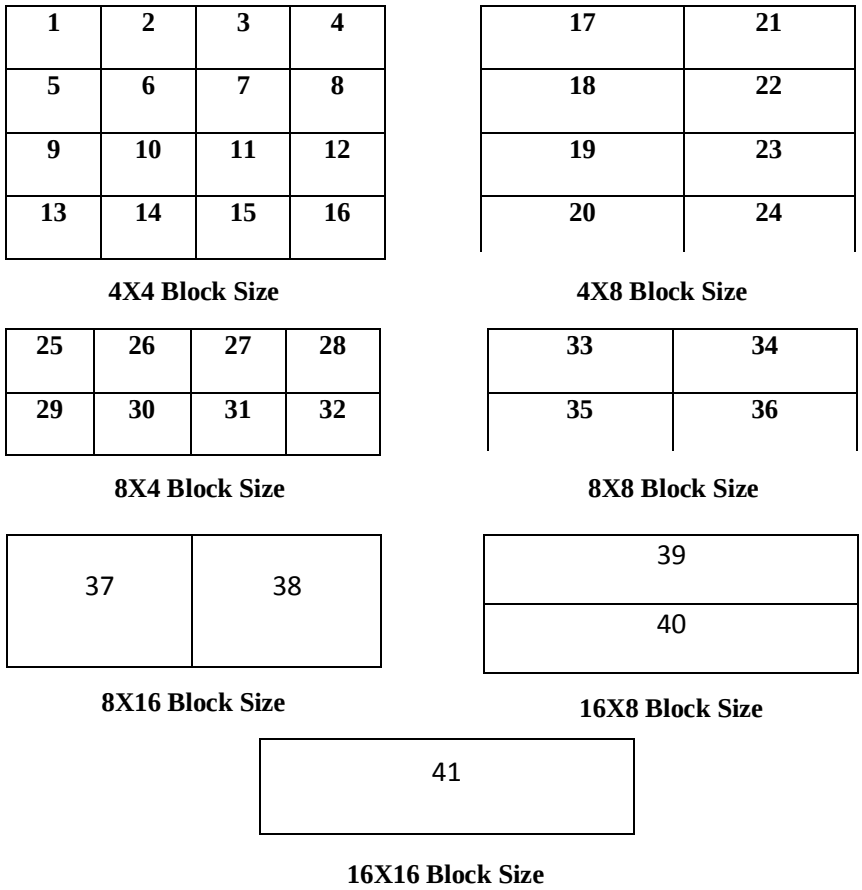

Figure 1: Different block sizes of motion estimation in h.264.

In this work we first identify the low power architecture at the level of 1bit addition (full adder) here five full adder architectures are synthesized based on, which architecture is giving the low power solution, such a full adder is used in the ripple carry parallel adder and the carry save adders, then these adders are used in basic sub block sizes of VBSME such as 4X4 and 8X8 are used in SAD architectures. Using these two SAD architectures remaining SAD architectures can be obtained for achieving variable block size motion estimation in video coding (compression). There are many tradeoffs encountered during the design of such modules (will be discussed in results section).

II. RELATED WORK

Several methods of finding the motion vectors have been presented in the literature, where there is a tradeoff between the power dissipation, area and the latency in the optimality of hardware implementation. The work presented by [1-6] shows that motion estimation aims at reducing the temporal redundancy between successive frames in a video sequence. Innovation has put much emphasis on improving the video-coding giving rise to new standard H.264/AVC [7, 8].

The coding efficiency in this new standard is increased to about 40–60% as compared with the Motion Picture Experts Group (MPEG)-2 and H.263 standards. Chen et al. [9] have presented H.264/AVC encoder which employs 1024 SAD processing Elements (PE) which uses 305k gates. Vanne et al. [10] have proposed SAD architecture and compared much architecture in terms of area and delay.

Yufei et al. [11] proposed the SAD architecture with 1st and 2nd stage pipeline; Stephan Wong, et al. [13] describes the parallel hardware implementation of the SAD operation in field-programmable gate arrays (FPGAs). A novel SAD16 unit which performs a 16 x1 SAD operation is proposed by C Hisham, et al [14], the work done in [9-13] presented the SAD architectures in terms of gate count and delay optimization.

The work by S. Kappagantula, et al. [15] presents that the two types of redundancies can be reduced using the predictive coding but more compensation can be reached by using it together with motion estimation. The work by S. Vassiliadis, et al. [16] proposes that the sum of absolute differences algorithm is used in determining the motion vectors in video coding. This paper is organized as follows: Section 3 describes the various existing gate level realizations and the proposed low power 1-bit binary full adder. Section 4 describes

the higher order adder architectures in the adder exploration. Section 4 gives the details about the existing and proposed SAD architectures at 4X4 (16 samples) and 8X8 (64 input samples) level. Section 5 describes the results and discussion, finally we conclude in section 6.

III. 1BIT ADDER ARCHITECTECTURES

The 1bit adder is the most basic elements of many critical data paths of the digital arithmetic circuits and digital signal processors. A 1 bit full adder is basically a combinational logic circuit, which performs binary addition operation on 3 single bit binary numbers and produces two outputs called sum and the carry. There are many efficient full adder architectures in the literature namely i) 2 EXNOR gate and 1 MUX architecture ii) 1 EXNOR and 2 MUX based Full adder iii) EXOR, AND & OR gate Architecture iv) EXOR and Nand Gates Architecture and v) The proposed low power NAND, AND & OR Gate architecture.

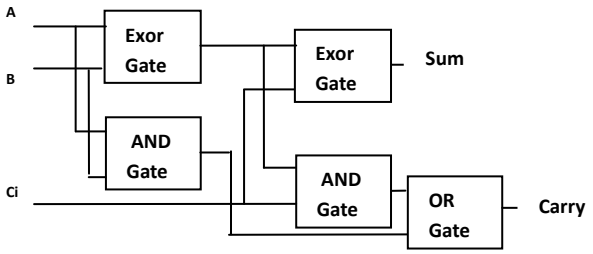

Figure 2: EXNOR & MUX architecture of Full Adder

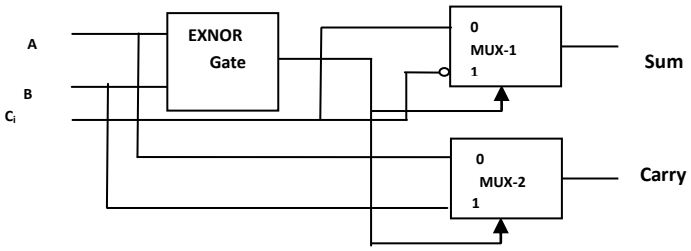

Figure 3: 1 XNM EXNOR & MUX based Full adder

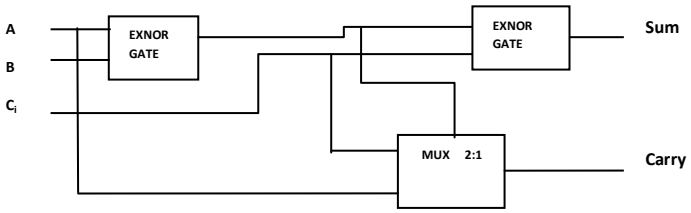

Figure 4: EXOR, AND & OR gate Full adder

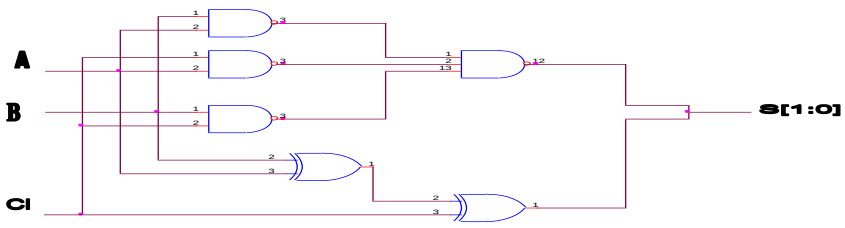

Figure 5: EXOR and Nand gates Full Adder

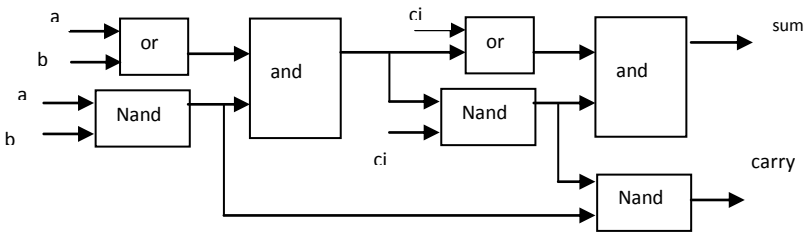

Figure 6: Proposed NAND, AND & OR gate full adder architecture

Out of the above five full adder architectures the proposed NAND, AND & OR gate architecture of full adder consumes low power, in this proposed architecture the carry generation is faster and the overall power consumption is made to below.

IV. ADDER EXPLORATION

The multi bit binary addition is the most important operation used in arithmetic operation on digital video / image processors. Hence multi bit adders are the most important blocks in building digital systems. The key challenge addressed in this work is the low power multi bit adders.

Various adder architectures have been proposed in the literature covering wide range of performance goals, but the suitability of the adder architectures for cell based design and hardware synthesis has been the very important for the low power addition, based upon the latency there are three adder architectures they are

4.1 Ripple Carry: It is the simplest architecture for an n-bit adder, intermediate carries are generated sequentially. It has smallest area, longest delay & consumes lowest power when two multi bit binary numbers are added. The ripple carry adder architecture is as shown in figure 7.

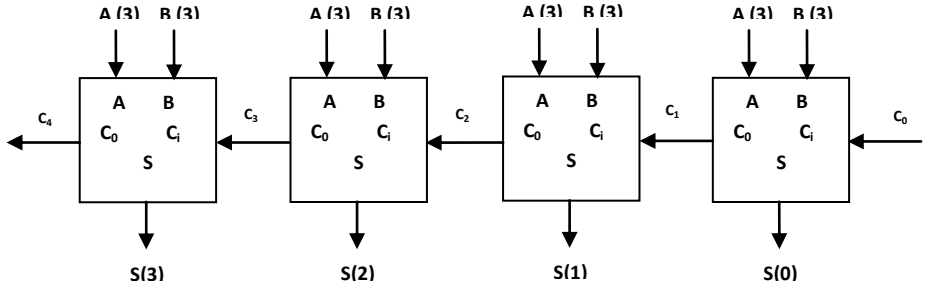

Figure 7: 4 bit ripple carry adder.

4.2 Carry Look Ahead: Here the carry is generated in parallel to reduce the processing delay. Hence it is faster than ripple carry architecture, and it consumes more area and power

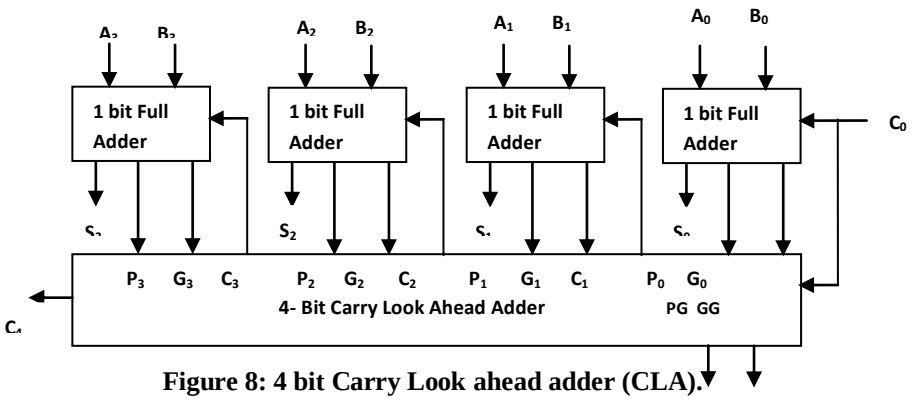

Figure 8: 4 bit Carry Look ahead adder (CLA).

4.3 Carry Save Addition: when multi bit addition is required then the low power adder called the Carry save adder is used which give very low power. The carry save adder circuit is as shown below

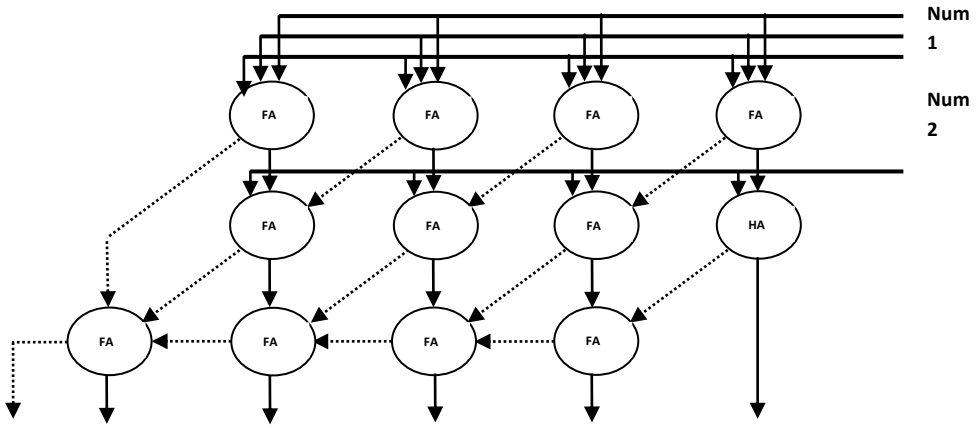

Figure 9: Carry Save Adder (CSA).

The multi bit binary addition is the most important operation used in arithmetic operation on digital video / image processors. Hence multi bit adders are the most important blocks in building digital systems. The key challenge addressed in this work is the low power multi bit adders.

V Sad Architectures

The sum of absolute differences (SAD) is the most repeated operation in block matching motion estimation subsystem. SAD algorithm is used for measuring the similarities between the images by calculating the absolute differences between the pixels of the image (Template image) and their corresponding ones (search image) in the macro block and then these differences are added up to result in the similarity block. It requires only two basic mathematical operations addition & shifting. The SAD algorithm is the simplest metric which considers all the pixels in the block for computation and also separately, which makes its implementation easier and parallel, due to its simplicity this algorithm is one of the fastest and can be used widely in block motion estimation and object recognition. This paper proposes the 4X4, 8x8 sum of absolute differences algorithm used in motion estimation of video compression. The architecture is able to perform a full motion search on integral multiples of 4X4 and 8x8 blocks sizes. The block and hierarchy diagrams of Sum of Absolute Difference are shown in figures 10 and 11 respectively.

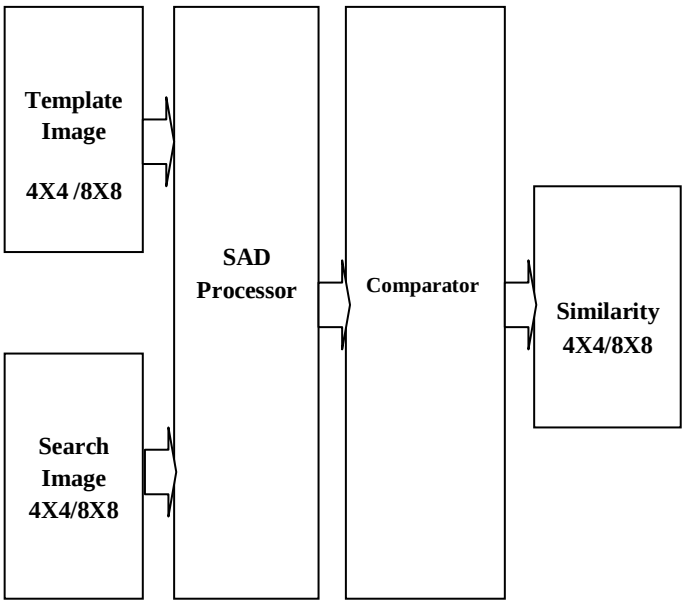

Figure 10: Block Diagram of 8X8 Sum of Absolute Difference block.

The sum of absolute difference architecture hierarchy is as shown below:

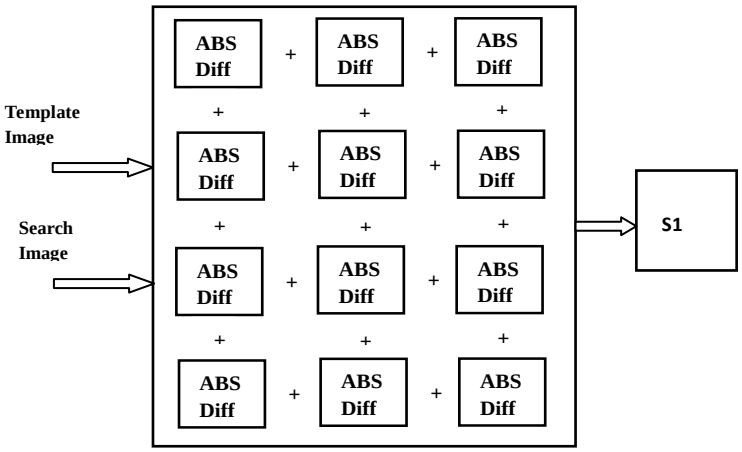

Figure 11: Hierarchy of sum of absolute difference block

Typical steps involved in fully parallel sum of absolute difference architecture are:

- ❖ Perform absolute difference of all the pixels (of a block of video).
- ❖ Perform sum of all the absolute differences.
- ❖ Select block with minimum difference value.

VI Results and Discussion

In this paper both 4X4 and 8X8 sum of absolute difference algorithms are implemented in three different ways they are

1. Implementation of SAD using normal existing ripple carry adder (which uses existing NAND and EXOR gates full adder).
2. Implementation of SAD using proposed ripple carry adder (which uses proposed NAND, AND & OR gate architecture for full adder).
3. Implementation of SAD using proposed carry save adder (which uses proposed NAND, AND & OR gate architecture for full adder).

The above SAD architectures were implemented in ASIC methodology. The architectures are modeled using verilog coding, functionally verified using modelsim and synthesized using RTL compiler. The results are tested using 180nm technology library of cadence EDA tools, the results are presented at 1 bit adder, 4X4 SAD and 8X8SAD levels as shown below:

Particulars	LP nW	DP nW	Total Power nW	Delay T in Ps	Area in Sq Microns
Full Adder using EXOR & Nand gates existing	96.144	492.446	588.590	157	24
proposed Full Adder using EXOR, AND & OR Gates	51.390	314.024	365.414	276	19

Table1: Full adder synthesis results Using 180 nano meter Technology

Particulars	LP µW	DP µW	Total Power µW	Delay T in Ps	Area in Sq microns
4X4 SAD using normal existing ripple carry adder	26.13	440.94	467.07	01561	17283
4X4 SAD using proposed ripple carry adder	18.55	162.13	180.68	02666	5492
4X4 SAD using proposed carry save adder	25.15	500.15	525.30	04490	6397

Table2: 4X4 SAD synthesis results Using 180 nano meter Technology.

Particulars	LP µW	DP µW	Total Power µW	Delay T in Ps	Area in Sq microns
8X8 SAD using normal existing ripple carry adder	119.61	1980.34	2099.95	5059	30643
8X8SAD using proposed ripple carry adder	85.23	1738.71	1823.94	5473	26080
8X8 SAD using proposed carry save adder	51.31	1066.23	1117.54	4954	12999

Table3: 8X8 SAD synthesis results Using 180 nano meter Technology.

Note: LP = Leakage Power; DP = Dynamic Power; T = Delay; A = Area;

The synthesis snap shot diagrams of both proposed 4X4 SAD and 8X8 SAD are as shown below

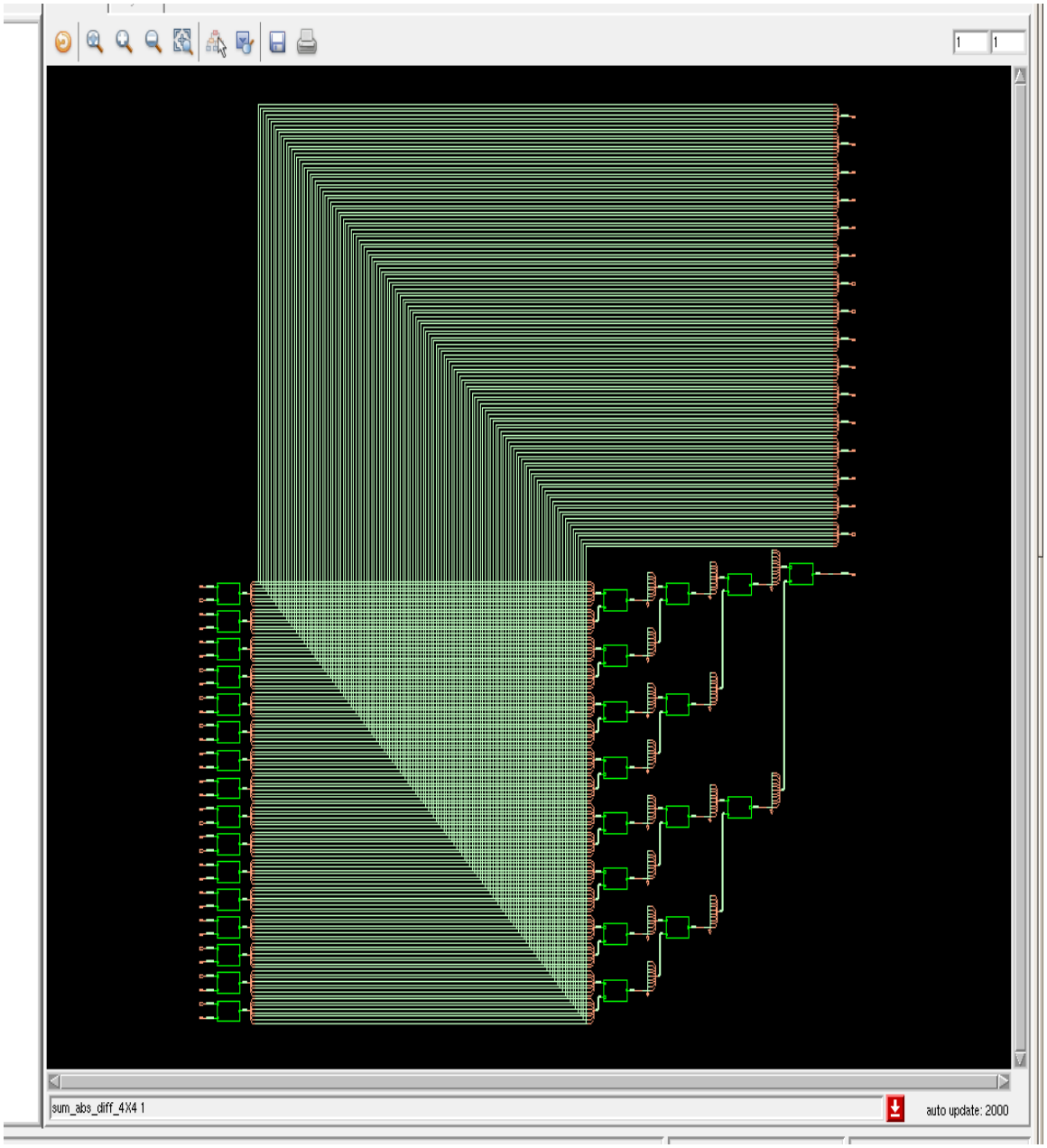

Figure12: Synthesis snapshot of proposed 4X4 Sum of Absolute Difference

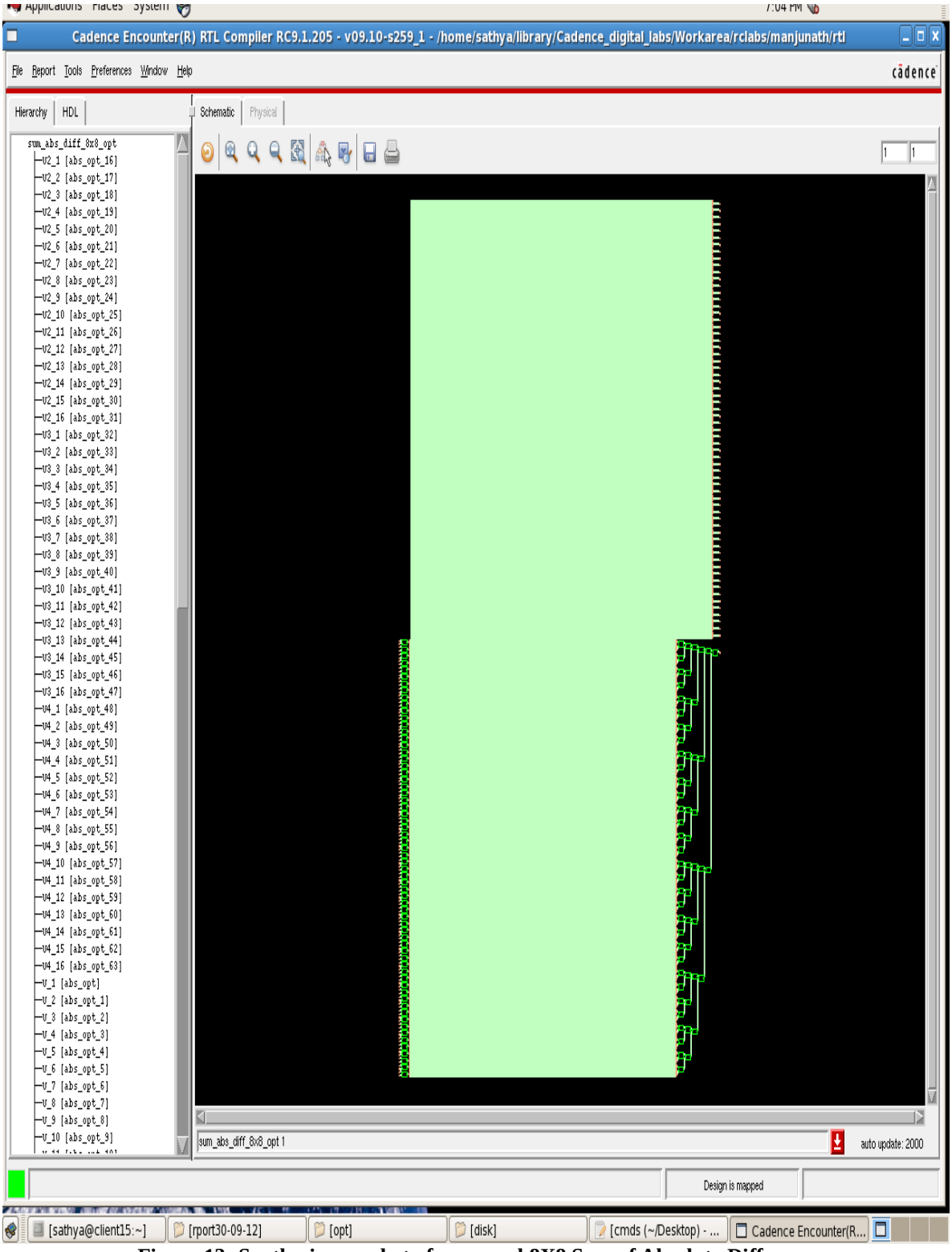

Figure 13: Synthesis snapshot of proposed 8X8 Sum of Absolute Difference

Looking at the synthesis results tabulated in the above tables, the following are the salient features of the paper.

1. The proposed 4X4 SAD using ripple carry adder structure proves that 29% improvement in leakage power dissipation, 63.23% improvement in dynamic power dissipation and 61.31% improvement in the total power dissipation as compared with existing 4X4 SAD using ripple carry adder at the gate level
2. In 8X8 SAD using proposed ripple carry adder about 28.70% improvement in leakage power dissipation and 12.20% improvement in dynamic power dissipation and 13.14% improvement in the total power dissipation as compared with 8X8 SAD using existing ripple carry adder.

3. In 8X8 SAD using proposed carry save adder about 39.79% improvement in leakage power dissipation and 38.73% improvement in dynamic power dissipation and 38.67% improvement in the total power dissipation as compared with 8X8 SAD using proposed ripple carry adder.
4. 8X8 SAD using proposed carry save adder proves that 57% improvement in leakage power dissipation and 46.16% improvement in dynamic power dissipation and 46.78% improvement in the total power dissipation as compared with 8X8 SAD using existing ripple carry adder.

VII Conclusion

In this paper we implemented the existing and the proposed 4X4 and 8X8 sum of absolute differences. Here the low power 1 bit Full adder Cell is proposed and is used in the design of sum of absolute difference algorithms. The SAD designs are implemented using ripple carry adder and carry save adder structures, the designs are implemented using 180 nm technology in ASIC flow, the simulations are done using modelsim and the synthesis is done using cadence-RC compiler, the implemented designs concludes that

(i) The 4X4 SAD using proposed ripple carry adder is the area and power efficient architecture and
(ii) The 8X8 SAD using proposed carry save adder is the area and the power efficient architecture as compared with both 8X8 SAD using existing ripple carry adder and the 8X8 SAD using proposed ripple carry adder structures.

At the gate level without optimization and if we try to optimize the same using power optimization techniques further improvement can be achieved.

Acknowledgement

The authors would like to thank Prof Venkatesvarlu and Prof. Siva Yellampalli of UTL technologies for their support in the lab, and especially the first author is thankful to the management of Don Bosco Institute of Technology, Bangalore for their constant encouragement and support.

REFERENCES

[1] Yankang Wang, Kuroda H, "Hilbert scanning search algorithm for motion estimation," *IEEE transactions on circuits and systems for video technology, vol. 9, issue 5 pp. 683-691, Aug. 1999.*

[2] Seongsoo Lee, Jeong-Min Kim, Suo-IK Chae, "New motion estimation algorithm using adaptively quantized low bit-resolution image and its VLSI architecture for MPEG2 video encoding**,"** *IEEE transactions on circuits and systems for video technology, vol. 8, issue 6, pp 734 -744, Oct. 1998.*

[3] Pickering M.R, Arnold J.F, Frater M.R, "An adaptive search length algorithm for block matching motion estimation," *IEEE transactions on circuits and systems for video technology, vol. 7, issue 6, pp 906-912, Dec. 1997.*

[4] Jo. Yew. Tham, Surendra Ranganath, Maitreya, Ashraf Ali Kassim, "A novel unrestricted centre biased diamond search algorithm for block motion estimation," *IEEE transactions on circuits and systems for video technology, vol. 8, issue 4, pp 369-377, Aug. 1998.*

[5] Huan-Sheng Wang, Mersereau R. M, "Fast algorithm for the estimation of motion vectors," *IEEE transactions on image processing, vol. 8, issue 3, pp 435-438, Mar. 1999.*

[6] Jon Wong Kim, Sang UK Lee, "Hierarchical variable block size motion estimation technique for motion sequence coding," optical *engineering, vol. 33, pp. 2553-2561, 1994.*

[7] H.264 AVC: 'Draft ITU-T recommendation and final draft international standard of joint video specification (ITUT Rec. H.264/ISO/IEC14496-10AVC', in *'Joint Video Team (JVT) of ISO/IECMPE Gland ITU-TVCEG', JVT G050, 2003.*

[8] Richardson I.E.G.: '*h.264 and mpeg-4 video compression: video coding for next-generation multimedia'* John Wiley & Sons, 2003.

[9] Tung-Chien Chen, Shao Yi Chien, Yu-Yeh Chen, To-Wei Chen, Liang-Gee Chen, "Analysis and architecture design of an HDTV720p 30 frames/s H.264/AVC encoder", *IEEE TCSVT, v. 16, no. 6, Jun. 2006, pp. 673-688.*

[10] Vanne J, Aho.E, Hamalainen T.D, Kuusilinna. K, "A high-performance sum of absolute difference implementation for motion estimation", *IEEE TCSVT, v. 16, n. 7, Jul. 2006, pp. 876-883.*

[11] Yufei. L, Feng Xiubo, Wang Qin, "A high-performance low cost SAD architecture for video coding". *IEEE TCE, v. 53, n. 2, May 2007. pp. 535-541.*

[12] Liu Zhenyu, Song Yang, Shao Ming, Li Shen, Li Lingfeng, Goto Satoshi, Ikenaga Takeshi, "32-Parallel SAD tree hardwired engine for variable block size motion estimation in HDTV 1080P real-time encoding application", *IEEE SiPS, 2007, pp. 675-680.*

[13] Stephan Wong, et al., "A sum of absolute differences implementation in FPGA hardware", *international journal of electrical and computer engineering 4:9 2009.*

[14] C Hisham, K Komal, Amith K Mishra, "Low power and less area architecture for integer motion estimation", *international journal of electrical and computer engineering 4:9 2009.*

[15] S. Kappagantula, et al. "Motion compensated predictive coding", *Proceedings of international symposium. SPIE, San Diego, CA, August 1983.*

[16] S. Vassiliadis, E.A Hakkennes, J.S.S.M Wong, G.G. Pechanek, "The sum-absolute-difference motion estimator accelerator", *Proceedings of the 24th Euromicro conference, 2000.*

IOSR Journal of VLSI and Signal Processing (IOSR-JVSP)
e-ISSN: 2319 – 4200, p-ISSN No. : 2319 – 4197 Volume 1, Issue 6 (Mar. – Apr. 2013), PP 19-26
www.iosrjournals.org

An Efficient Two's Complement Multiplier With FPGA Implementation

Kolathur Lakshmipathy [1], , Voruganti Santhosh Kumar [2,] Dr Vangala padmaja[3]
1(Department of ECE, VNR VJIET, Hyderabad, India)
2 (Department of ECE, AEC, Kodad, A.P, India)
3 (Department of ECE, VNR VJIET, Hyderabad, India)

Abstract: *The performance of multiplication is crucial for multimedia applications such as 3D graphics and signal processing systems which depend on extensive numbers of multiplications. Previously reported multiplication algorithms mainly focus on rapidly reducing the partial products rows down to final sums and carries used for the final accumulation. These techniques mostly rely on circuit optimization and minimization of the critical paths.*

In this paper, an algorithm to achieve fast multiplication in two's complement representation is presented. Indeed, our approach focuses on reducing the number of partial product rows. In turn, this directly influences the speed of the multiplication, even before applying partial products reduction techniques. Fewer partial products rows are produced, thereby lowering the overall operation time. This results in a true diamond-shape for the partial product tree which is more efficient in terms of implementation.

Keywords:— *MBE, PPR, PPRG, FPGA.*

I. INTRODUCTION

The performance of 3D graphics and signal processing systems strongly depends on the performance of multiplications because these applications need to support highly multiplication intensive operations. Therefore, there has been much work on advanced multiplication algorithms and designs [1, 22, 3, 23, 18, 14, 13, 6, 7, 16, 20, 24, 12].

There are three major steps to any multiplication. In the first step, the partial products are generated. In the second step, the partial products are reduced to one row of final sums and one row of carries. In the third step, the final sums and carries are added to generate the result. Most of the above mentioned approaches employ the Modified Booth Encoding (MBE) approach [6, 7, 13, 24, 4] for the first step because of its ability to cut the number of partial products rows in half. They then select some variation of any one of partial products reduction schemes such as the Wallace trees [22, 6] or the compressor trees [16, 13, 18, 14] in the second step to steeply reduce the number of partial product rows to the final two (sums and carries). In the third step, they use some kind of advanced adder approach such as carry-lookahead or carry-select adders [5, 17, 11] to add the final two rows, resulting in the final product. The main focus of recent multiplier papers [7, 16, 20, 24,4, 12] has been on rapidly reducing the partial product rows by using some kind of circuit optimization and identifying the critical paths and signal races. In other words, the goals have been to optimize the second step of the multiplication described above.

However, in this paper, we will focus on the first step which consists in forming the partial product array and we will strive to design a multiplication algorithm which will produce fewer partial product rows. By having fewer partial product rows, the reduction tree can be smaller in size and faster in speed. It should also be noted that 8 or16-bit words are the most commonly used word sizes in the kernels of most multimedia applications [19] and that the implementation of our overall algorithm is particularly well suited to such word sizes. In the next section, the conventional multiplication method is described in detail with an emphasis on its weaknesses. In section iii, a step-by-step procedure to prevent the adverse effects of some conventional multiplication algorithms is presented. In section iv, the effectiveness and usage of our method is presented by showing a detailed evaluation.

II. Multiplication Algorithms

There is no doubt that MBE is efficient when it comes to reducing the partial products. However, it is important to note that there are two unavoidable consequences when using MBE: sign extension prevention and negative encoding. The combination of these two unavoidable consequences results in the formation of one additional partial product row and of course, this additional partial product row requires more hardware but more importantly time

A. Modified Booth Encoding and the Overhead of Negative Encodings

This grouping of the multiplier bits of MBE is shown in Figure 1 and it is based on a window size of 3 bits and astride of 2. The multiplier (Y) is segmented into groups of three bits ($y2i+1$, $y2i$, $y2i-1$) and each such group of bits is associated with its own partial product row by using Table 1 [15]. In this grouping, $y-1 = 0$.By applying this encoding, the number of partial product rows to be accumulated is reduced from n to $n/2$. For example, for an 8 × 8 multiplication, a multiplier without MBE will generate eight partial product rows (because there is one partial product row for each bit of the multiplier).However, with MBE, only $n/2$ (= 4) partial products rows are generated as shown in the example of Figure 2.However, there are actually $n/2 + 1$ partial product rows anther than $n/2$, because of the last *neg* signal (*neg*3 in Figure2).

The *neg* signals (*neg*0, *neg*1, *neg*2, and *neg*3) are needed because MBE may generate a negative encoding ((-1) times the multiplicand or (-2) times the multiplicand).Consequently, one additional carry save adding stage is needed to perform the reduction. This is the overhead of implementing the negative encodings of MBE.

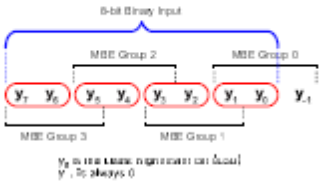

Figure 1: Multiplier bits grouping according to modified booth encoding for 8-bit input

Table 1: Modified Booth Encoding (radix-4)

Y_{2i+1}	Y_{2i}	Y_{2i-1}	Generated partial products
0	0	0	0×X
0	0	1	1×X
0	1	0	1×X
0	1	1	2×X
1	0	0	(-2)×X
1	0	1	(-1)×X
1	1	0	(-1)×X
1	1	1	0×X

B. Sign Extension and its Prevention

In signed multiplication, the sign bit of a partial product row would have to be extended all the way to the MSB position which would require the sign bit to drive that many output loads (each bit position until the MSB should have the same value as the sign). This makes the partial product rows unequal in length as shown in Figure : the first row spans 16 bits (*pp*00 to the leftmost *pp*80), the second row 14 bits (*pp*01 to the leftmost *pp*81), the third row 12bits (*pp*02 to the leftmost *pp*82), and the fourth row 10 bits(*pp*03 to the leftmost *pp*83). The sign extension prevention method shown in figure3.and arrives a newly formed partial product rows as in figure4[10]where the sign extension has been removed. We use this structure as the basis structure for our multiplier architecture.

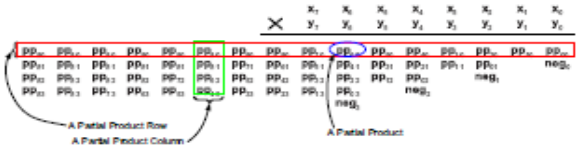

Figure 2. The Array of Partial Products for Signed Multiplication with MBE

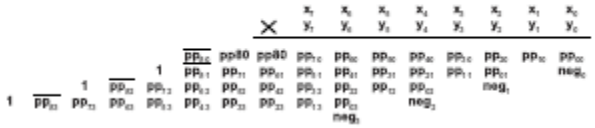

Figure. 3: Application of sign extension prevention measure on the partial product array of 8×8 multiplier

C. One Additional Partial Product Row

However, there is still the problem of having the last *neg* forming one additional partial product row (*neg*3 in Figure3) and this causes another carry save adder delay in order to generate the sums and carries before the final accumulation. This is because in any case, one more partial product means one additional 3-2 reduction. For example, Figure 4(a)[10] shows a 8-input reduction (16 bit × 16 bit multiplication for our architecture) using 4-2 compressors. If we have to reduce 9 inputs (16 bit × 16 bit multiplication for the conventional architecture), one additional carry save adder is required as in Figure 4(b)[10].

.

III . Stopping the Extra Partial Product Row

Therefore, our aim is to remove the last *neg* signal. This would prevent the extra partial product row, and thus save the time of one additional carry save adding stage and the hardware required for the additional carry save adding. We noticed that if we could somehow produce the two's complement of the multiplicand while the other partial products were produced, there would be no need for the last *neg* because this *neg* signal would have already been applied when generating the two's complement of the multiplicand.
Therefore, we "only" need to find a faster method to calculate the two's complement of a binary number.

A . A Quick Method to Find Two's Complements

Our method is an extension of well-known algorithm that two's complementation complements all the bits after the rightmost "1" in the word but keeps the other bits as they are. The two's complement of a binary number 0010102(1010) is 1101102 (−1010). For this number, the right most "1" happens in bit position 1 (the check mark position in Figure 4).

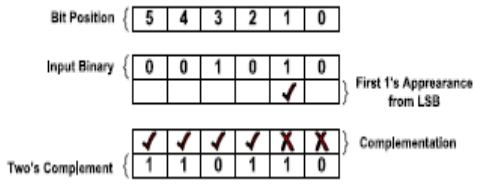

Figure 4:Two Complement Conversion Example

Therefore, values in bit positions 2 to5 can simply be complemented while values in bit positions0 and 1 are kept as they were. Therefore, two's complementation now comes down to finding the conversion signals that are used for selectively complementing some of the input bits. If the conversion signal at any position is "0" (the crosses in Figure 4), then the value is kept as it is and if the conversion signal is "1"(the checks in Figure 4), then the value is complemented. The conversion signals after the rightmost "1" are always1. They are 0 otherwise. Once a lower order bit has been detected to be a "1," the conversion signals for the higher order bits to the left of that bit position should all be "1."However, this searching for the rightmost "1" could as time consuming as rippling a carry through to the MSB since the previous bits information must be transferred to the MSB. Therefore, we must find a method to expedite this detection of the rightmost "1."As we will see, this search for the rightmost "1" can be achieved in logarithmic time using a binary search tree-like structure. We first find the conversion signals for a 2-bitgroup by grouping two consecutive bits (the grouping always starts from the LSB) from the input and finds the conversion signals in each group as shown in Figure 6(a)[10]. Then we find the conversion signals for a 4-bit group (formed by two consecutive 2-bit groups). Then we find the conversion

Signals for a 8-bit group (formed by two consecutive 4-bitgroup). This divide-and-conquer approach is pursued until the whole input has been covered. When grouping two 2*n*-bits groups, the leftmost conversion signals from the right group contain the accumulative information of its group about whether a "1" ever appeared in any bit position of its group, so that a conversion signal should force all the conversion signals from the left group all the way to the "1" if it is itself is a "1." For instance, as shown in Figure 6(b)[10], if *CS*1 (the leftmost conversion signal from the right group) = "1," the conversion signals from the left group (*CS*2 and *CS*3) should be forced to a"1," regardless of their previous values. If *CS*1 = "0," nothing happens to the conversion signals from the left group. This variable control is shown with a dashed arrow. Likewise,*CS*5 may affect conversion signals *CS*6 and *CS*7.The same goes for *CS*3' which may affect the conversion signals (*CS*7', *CS*6', *CS*5', and *CS*4').The inputs to the 2-bit group are bits from the original binary number. However, the inputs to the next level groups are conversion signals from the previous level. For instance, the inputs to the 4-bit group are the conversion signals generated from two 2-bit groups. Therefore, from the second level (4-bit grouping) on, the conversion signals are scanned in order to find the rightmost "1." One possible

implementation of our algorithm is shown in Figure7 (a). Figure 7(b)[10] shows another version of the design using NAND, NOR, and inverter. Once we have the complete conversion signals, these signals are shifted left 1 bit and EXOR-ed with the input to create the two's complement of the input. One complete example of two's complementation of "00101000_2"is shown in Figure 8[10]. Our approach is more general and shows better adaptability to any word size.

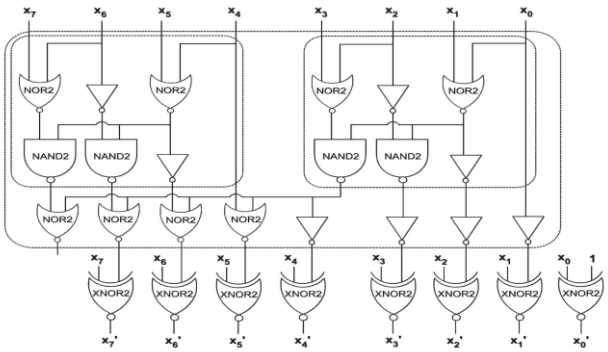

Figure 5: Two's complement computation

A. Putting it all together

By applying the method we just described for two's complementation, the last partial product row (in Figure 3) is correctly generated without the last *neg*(*neg*3 in Figure 3).Now, the multiplication can have a smaller critical path. This avoids having to include one extra carry saving adding stage. It also reduces the time to find the product and saves the hardware corresponding to the carry saving adding stage. Forming a truly parallelogram-shaped partial product array after removing the last *neg* requires undergoing the following steps:

Step a: Replace the last partial product row and *neg*3 in Figure 3 with signals *s*9 ~*s*0 as shown in Figure 6.
Step b: Replace the second to the last partial product row as in Figure 6.

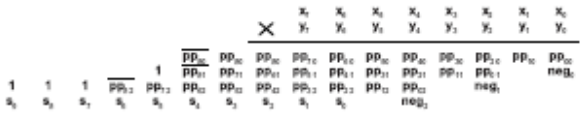

Figure 6: Replacing the last row and the Last *neg* with signals *s*9 -*s*0

Step c: Finally, the MSB of the last row can be complemented (*s*9) and the "1" directly above it can be removed as shown in Figure 7.

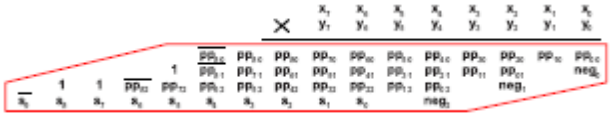

Figure 7: Partial Products After Removing the last *neg*

As can be seen, the critical path column with $n/2+1$ elements (6*th* bit position of Figure 3 ($n-2$)) now have only $n/2$ elements as shown in Figure 7(the *neg*3 is no longer there). This directly improves the speed of the multiplication. The multiplier architecture to generate the partial products is shown in Figure. The only Difference between our architecture and the conventional multiplier architectures is that for the last partial product row, our architecture has no partial product generation but partial product selection with a two's complement unit. The 3-5 decoder select the correct value from 5 possible inputs (2×X, 1×X, 0, -1×X,-2×X) which are either coming from the two's complement logic or the multiplicand itself and input into the row of 5-1selectors. Unlike the other rows which use PPRG (Partial Product Row Generator), the two's complement logic does not have to wait for MBE to finish. Two's complementation is performed in parallel with MBE and the 3-5 decoders.

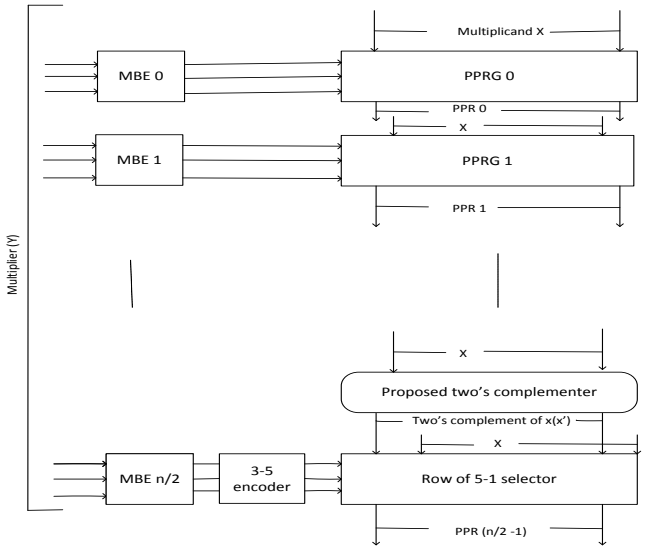

Figure 8. Proposed Multiplier Architecture

IV . Performance Evaluation and Results Discussion

The performance of our multiplier architecture clearly depends on the speed of the two's complementation step. If we can generate the last partial product row of our multiplier architecture within the exact time that the other partial product rows are generated, the performance will be improved as we have predicted because of the removal of the additional partial product row. Therefore, in this section, we evaluate the performance of our two's complement logic by comparing it to the delay of generating other partial products. Then, we investigate the overall impact (in terms of speed) of using our multiplier architecture as compared to previous methods.

The main tools required for this project is MODELSIM 6.4, XILINX 10.1i.By Using these tools we perform simulation and synthesis and get the simulation results and synthesis reports from a two's complement multiplier ppg module, and compare the ppg generation results with our method listed in Table 2.

Our proposed multiplier has generated partial product generation with estimated delay of 9.5 ns, 9.5ns, 9.5ns with corresponding 8×8, 16×16, 32×32 bit multipliers respectively. But the actual critical path delay for the partial product generation in proposed multiplier is 9.321ns; this one is obtained from synthesis report of ppg module. The figure shows the generation of partial product in our proposed multiplier. Hence we concluded here that our approach is reducing computation time in our proposed multiplier. The estimated critical path delay is slightly high when compared to actual critical path delay for generation of partial product in our method. This leads to reduce the maximum combinational path delay of our proposed multiplier.

Table 2: Estimated Critical Path Delay for the Partial Product Generation for various multipliers

Estimated Critical Path Delay for the Partial Product Generation (in Nano seconds)			
Technique	8×8	16×16	32×32
Standard multiplier (any row) (Gen MBE,Gen PPs)	9.8	9.8	9.8
Standard multiplier (first row) (Gen MBE +PPs)	4.8	4.8	4.8
Proposed multiplier (Gen PPs +last*neg)*	9.5	9.5	9.5
Two's complement (4× 1 mux +two's complement tree)	11.9	13.3	15.1

Figure 9 : simulation results for a partial product generation

The developed project is simulated and verified their functionality. Once the functional verification is done, the RTL model is taken to the synthesis process using the Xilinx ISE tool. In synthesis process, the RTL model will be converted to the gate level net list mapped to a specific technology library. Here in this Spartan 3E family, many different devices were available in the Xilinx ISE tool. In order to synthesis this design the device named as "XC3S500E" has been chosen and the package as "FG320" with the device speed such as "-4". There are four Partial product rows km1, km2, km3, km4 are generated. And simulation results for the top module show in figure 10.

We are compared our proposed multiplier with arry multiplier, booth's multiplier and conventional Vedic multiplier. From the table we concluded that our proposed multiplier is an efficient one among all. The Maximum combinational path delays are given table 3.

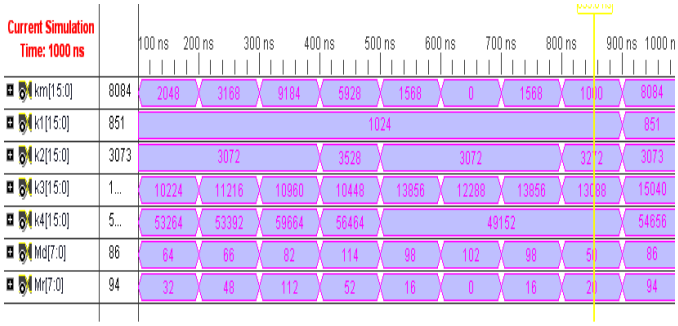

Figure 10: simulation results for top module

Table 3: Comparison of Maximum combinational Path Delay between different multipliers

Maximum Combinational Path Delay for Different Multipliers (in Nano seconds)			
Array Multiplier	Booth's Multiplier	Conventional Vedic Multiplier	Proposed Multiplier
32.01	29.549	23.679	21.995

.The RTL (Register Transfer Logic) can be viewed as black box after synthesize of design is made. It shows the inputs and outputs of the system. By double-clicking on the diagram we
can see gates, flip-flops and MUX

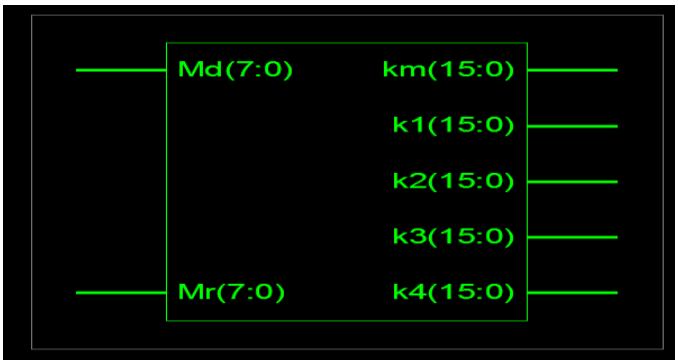

Figure 11 : RTL schematic diagram for test module

The figure shows the technical schematic of top module,

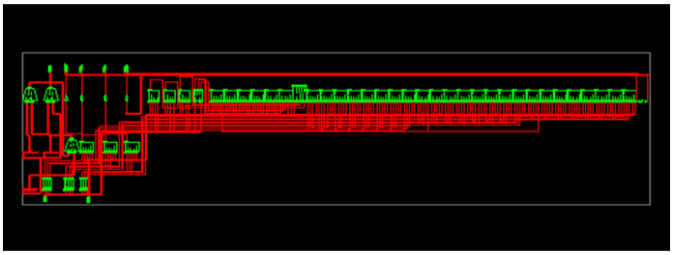

Figure 12 : technology schematic diagram for ppg module

which consists of iob's, lookup tables, functional blocks and flip-flops**.**

Figure 13 : Hardware implementation

The above FPGA implementation shows the multiplication operation, i.e. the multiplier value is 1 & the multiplicand value is 127. Hence the output lights glow from 1 to 7 continuously, which indicates the output value is 127

V . Conclusions

In this project an algorithm is presented to reduce from [*n*/2] +1 to [*n* /2] the number of partial product rows generated during the first step of a multiplication algorithm. By doing so, the structure of the partial product array becomes more regular and easier to implement. Even more importantly, the product is found faster. This can be achieved using less hardware. A detailed and step-by-step approach to prevent the occurrence of the additional row is shown. The proposed multiplication method is particularly efficient when executing the multiplications of the kernels of most common multimedia applications which are based on 8 to 16-bit operands & implemented by using Spartan 3(XC3S400) FPGA.

Compared our approach with a recent proposal with the same aim, considering results using a widely used industrial synthesis tool and concluded that our approach may improve both the performance and area requirements of square multiplier designs. The proposed approach also applies with small modifications to rectangular and to general radix-B Modified Booth Encoding multipliers.

References

[1] M.D. Ercegovac and T. Lang, Digital Arithmetic. Morgan Kaufmann Publishers, 2003.
[2] S.K. Hsu, S.K. Mathew, M.A. Anders, B.R. Zeydel, V.G.Oklobdzija, R.K. Krishnamurthy, and S.Y. Borkar, "A 110GOPS/W 16-Bit Multiplier and Reconfigurable PLA Loop in 90-nm CMOS," IEEE J. Solid State Circuits, vol. 41, no. 1, pp. 256-264, Jan.2006.
[3] H. Kaul, M.A. Anders, S.K. Mathew, S.K. Hsu, A. Agarwal, R.K.Krishnamurthy, and S. Borkar, "A 300 mV 494GOPS/W Reconfigurable Dual-Supply 4-Way SIMD Vector Processing Accelerator in 45 nm CMOS," IEEE J. Solid State Circuits, vol. 45, no. 1, pp. 95-101, Jan. 2010
[4] M.S. Schmookler, M. Putrino, A. Mather, J. Tyler, H.V. Nguyen, C.Roth, M. Sharma, M.N. Pham, and J. Lent, "A Low-Power, High-Speed Implementation of a PowerPC Microprocessor Vector Extension," Proc. 14th IEEE Symp. Computer Arithmetic, pp. 12-19,1999.
[5] O.L. MacSorley, "High Speed Arithmetic in Binary Computers," Proc. IRE, vol. 49, pp. 67-91, Jan. 1961.
[6] L. Dadda, "Some Schemes for Parallel Multipliers," Alta Frequenza, vol. 34, pp. 349-356, May 1965.
[7] C.S. Wallace, "A Suggestion for a Fast Multiplier," IEEE Trans.Electronic Computers, vol. EC-13, no. 1, pp. 14-17, Feb. 1964.
[8] D.E. Shaw, "Anton: A Specialized Machine for Millisecond-Scale Molecular Dynamics Simulations of Proteins," Proc. 19th IEEE Symp. Computer Arithmetic, p. 3, 2009.
[9] J.-Y. Kang and J.-L. Gaudiot, "A Simple High-Speed Multiplier Design," IEEE Trans. Computers, vol. 55, no. 10, pp. 1253-1258, Oct.2006.

[10] J.-Y. Kang and J.-L. Gaudiot, "A Fast and Well-Structured Multiplier," Proc. Euromicro Symp. Digital System Design, pp. 508-515, Sept. 2004.
[11] F. Lamberti, N. Andrikos, E. Antelo, and P. Montuschi,"Speeding-Up Booth Encoded Multipliers by Reducing the Size of Partial Product Array," internal report, http://arith.polito.it/ir_mbe.pdf, pp. 1-14, 2009.
[12] E.M. Schwarz, R.M. Averill III, and L.J. Sigal, "A Radix-8 CMOSS/390 Multiplier," Proc. 13th IEEE Symp. Computer Arithmetic,pp. 2-9, 1997.
[13] W.-C. Yeh and C.-W. Jen, "High-Speed Booth Encoded Parallel Multiplier Design," IEEE Trans. Computers, vol. 49, no. 7, pp. 692-701, July 2000.
[14] Z. Huang and M.D. Ercegovac, "High-Performance Low-Power Left-to-Right Array Multiplier Design," IEEE Trans. Computers,vol. 54, no. 3, pp. 272-283, Mar. 2005.
[15] R. Zimmermann and D.Q. Tran, "Optimized Synthesis of Sum-of-Products," Proc. Conf. Record of the 37th Asilomar Conf. Signals,Systems and Computers, vol. 1, pp. 867-872, 2003.
[16] V.G. Oklobdzija, D. Villeger, and S.S. Liu, "A Method for Speed Optimized Partial Product Reduction and Generation of Fast Parallel Multipliers Using an Algorithmic Approach," IEEE Trans.Computers, vol. 45, no. 3, pp. 294-306, Mar. 1996.
[17] P.F. Stelling, C.U. Martel, V.G. Oklobdzija, and R. Ravi, "Optimal Circuits for Parallel Multipliers," IEEE Trans. Computers, vol. 47, no. 3, pp. 273-285, Mar. 1998.
[18] J.-Y. Kang and J.-L. Gaudiot, "A Logarithmic Time Method for Two's Complementation," Proc. Int'l Conf. Computational Science, pp. 212-219, 2005.
[19] K. Hwang, Computer Arithmetic Principles, Architectures, and Design.Wiley, 1979.
[20] R. Hashemian and C.P. Chen, "A New Parallel Technique for Design of Decrement/Increment and Two's Complement Circuits,"Proc. 34th Midwest Symp. Circuits and Systems, vol. 2,pp. 887-890, 1991.
[21] D. Gajski, Principles of Digital Design. Prentice-Hall, 1997.
[22] STMicroelectronics, "130nm HCMOS9 Cell Library," http://www.st.com/stonline/products/technologies/soc/evol.htm, 2010.

Kolathur Lakshmipathy received the B.Tech. Degree in electronics and Communication engineering from SANA Engineering College, affiliated to Jawaharlal Nehru Technological University Hyderabad , AP, India, in 2007. He received M.Tech Degree in VLSI system design From VNR Vignana Jyothi Institute of Engineering & technology, Bachpally, Hyderabad, India,in 2012. His research interests include Digital design with FPGA and Low Power vlsi.

Voruganti Santhosh Kumar received the B.Tech. Degree in electronics and Communication engineering from SANA Engineering College, affiliated to Jawaharlal Nehru Technological University Hyderabad, AP, India, in 2007.he received M.Tech Degree in VLSI system design From Anurag Engineering college, kodad, AP, India. He is an assistant professor in Dept of ECE in Anurag College of engineering. His research interests include Digital design with FPGA.

Dr. V. Padmaja born in 1968. She received B.E Degree in Electronics and Communications Engineering, M.E Degree in Digital Systems Engineering from O.U in 1991 and 1999 respectively. She received Ph.D from J.N.T.U in 2009. She is an Professor in Dept. of ECE in VNRVJIET, her research of interest includes image processing and Embedded Systems. She has authored more than 5 Research papers in National and International Conferences and Journals

IOSR Journal of VLSI and Signal Processing (IOSR-JVSP)
e-ISSN: 2319 – 4200, p-ISSN No. : 2319 – 4197 Volume 1, Issue 6 (Mar. – Apr. 2013), PP 27-36
www.iosrjournals.org

A High Performance & Efficiently Designed IIR Filter Using Graphical Virtual Tool (LabVIEW)

Shikha Tiwari[1], Rajinder Tiwari[1], Amit Bajpai[2]
[1]*Department of Electrical & Electronics Engineering, Amity University Uttar Pradesh, Lucknow* [2]*Department of Physics, Indian Institute of Technology, Kanpur*

Abstract: *Designing of digital filters based on LABVIEW involves the concept of virtual instrumentation. In the recent years LABVIEW finds many applications in different fields for example industrial purpose like level sensor, temperature sensor pressure sensor etc. Virtual instruments are used in LABVIEW. Each VI has three parts a block diagram, a front panel and a connector panel. Connector panel is used to represent the VI in the block diagrams of other. Controls and indicators on the front panel allow an operator to input data into or extract data from a running virtual instrument. The front panel can also serve as a programmatic interface. A digital IIR filter system is developed using LABVIEW software. IIR filters possess certain properties which makes them preferred design choices in many situations over FIR filters. Following are the types of IIR filter Butterworth filters, Chebyshev filters, Inverse chebyshev filters, Elliptic filters. Virtual instrument reads the desired parameters of the filters entered by the user on the front panel and determines its magnitude response and filter coefficients.*
Keywords: ADC, DAC, DSP, Design Approach, Virtual instrument, LABVIEW, IIR filter.

I. INTRODUCTION TO BASICS OF THE FILTERS

The function of a filter is to remove unwanted parts of signal or to extract some useful parts of signal, such as the components lying within a certain frequency range.

Fig.1 Block diagram of basic filter

Infinite impulse response is a property of signal processing systems. IIR filters have impulse response function that is non zero over an infinite length of time. Simplest example of analog IIR filter is an RC filter made up of single resistor (R) feeding in to a node shared with single capacitor (C) . Impulse response of this filter is exponential characterized by RC time constant. The exponential function is asymptotic to a limit and thus never settles to a fixed value that's why response is considered infinite. Digital filters use digital processor to perform numerical calculations on sampled values of signal. Block diagram of digital filter is given below.

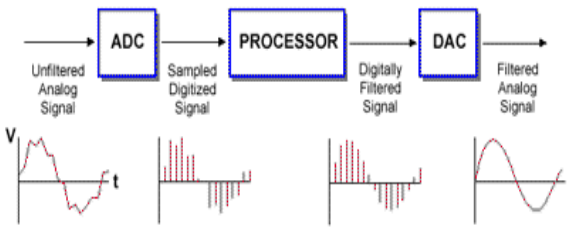

Fig.2 A block diagram of basic digital filter

Firstly the input signal must be sampled and digitized using an analog to digital converter. The result of converter is binary numbers, representing successive sampled values of the input signal, which are transferred to the processor and it performs numerical calculation on them. These calculations involve multiplying the input values by constants and adding the products together.

Following are the advantages of digital filters i.e.

- The principal advantage of digital filters is the flexibility available in their design.
- The ease of data storage is one of the main advantages of digital filters.
- Digital filters are programmable.
- Fast DSP processors can handle complex combinations of filters in parallel or cascade, making the hardware requirements relatively simple and compact.

II. FUNDAMENTALS OF THE OPERATION OF AN IDEAL FILTERS

Ideal filters pass specified frequency range while attenuate specified unwanted frequency range. Filters can be classified according to their frequency range characteristics. Following are the filter classifications based on frequency range a filter passes or attenuates.

- Low pass filters pass low frequencies and block high frequencies.
- High pass filters pass high frequencies and block low frequencies.
- Band pass filters pass a certain band of frequencies.
- Band stop filters attenuate a certain band of frequencies.

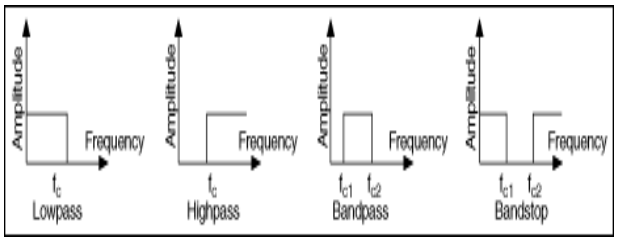

Fig. 3 Ideal frequency characteristics

The frequency points f_c, $f_{c1}$and f_{c2} specify the cut off frequencies for the different filters. An ideal filter has a gain of one (0 dB) in the passband so the amplitude of the signal neither increases nor decreases. Fig. 4 shows pass band and stop band for each filter type.

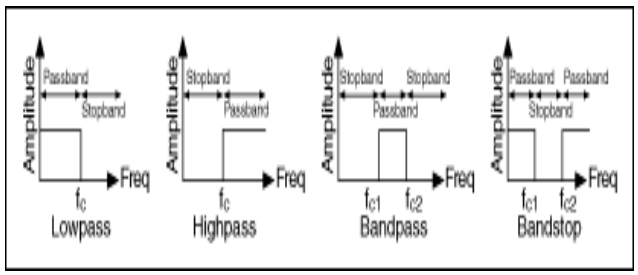

Fig.4 Pass band and stop band

III. PRACTICAL DESIGN OF A FILTER

In practical filters a transition band always exists between pass band and stop band. In this band the gain of filter changes gradually from one in the pass band to zero in the
stop band

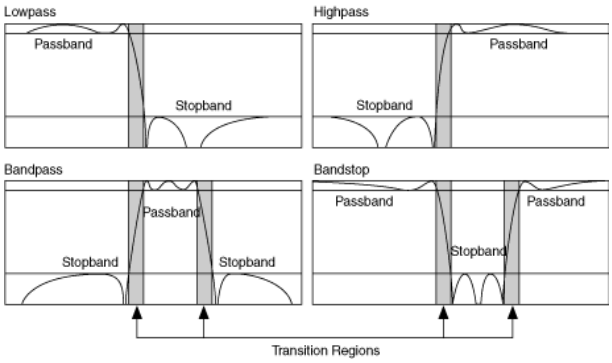

Fig.4 Response of non ideal filters

IV. DIGITAL FILTERS

Filters can be classified according to their impulse responses. There are mainly two types of digital filter i.e. Finite impulse response filters, which are also known as non recursive filters because they don't have feedback. These filters operate on current and past input values and Infinite impulse response filters, which are also known as recursive filters because they have feedback or recursive part of filter.

V. IMPULSE RESPONSE

An impulse is a short duration signal that goes from zero to a maximum value and back to zero again in a short time. The impulse response of a filter is the response of filter to an impulse and depends on the values upon which the filter operates. The Fourier transform of impulse response is frequency response of filter.

VI. BASICS OF A DIGITAL IIR FILTER

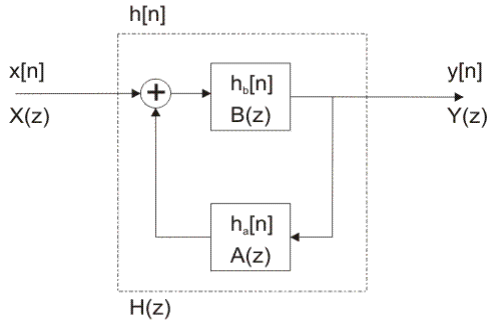

Fig.5 Block diagram of IIR filter

The design of digital filter depends on both values, past outputs and present input. If such a filter is subjected to an impulse then output of this filter need not necessarily become zero. The impulse response of such a filter can be infinite in duration. Such type of filter is called an infinite impulse response filter and indicates that the system is prone to feedback and instability. Following equation defines the direct form transfer function of an IIR filter

(1)

Where a_n and b_n are reverse and forward coefficients of the IIR filter. It can be written in the form of general difference equation as follows

(2)

Where

b_j, set of forward coefficients,
N_b, number of forward coefficients,
a_k, set of reverse coefficients,
N_a, number of reverse coefficients

Above equation describes a filter with an impulse response of theoretically infinite length for nonzero coefficients. In design of IIR filter with LABVIEW coefficient a_0 is 1. The IIR filters can be designed by any one of the following methods.

- Impulse invariance
- Bilinear transformation

1. Impulse invariance

Following are the steps of this method.

- Decide upon the desired frequency response
- Design an appropriate analog filter
- Calculate the impulse response of this analog filter
- Sample the impulse response of this analog filter
- Use the result as the filter coefficients

This method seems simple but it is complicated by all the problems inherent in dealing with sampled data systems. Particularly this method is subject to problems of aliasing and frequency resolution. IIR filters are very sensitive to quantization errors. It is a feature peculiar to digital systems. Its effects are nonlinear and signal dependent. In order to prevent severe distortion due to the band limiting this method is restricted to the design of lowpass and bandpass filters.

2. Bilinear transformation

This method overcomes the effect of aliasing that is caused due to analog frequency response containing components at or beyond the Nyquist frequency. This is also called frequency wrapping because this is a method of compressing the infinite, straight analog frequency axis to a finite one long enough to wrap around the unit circle once only.

VII. TYPES OF IIR FILTER

- Butterworth filters
- Chebyshev filters
- Inverse chebyshev filters
- Elliptic filters

The IIR filter designs differ in the sharpness of the transition between the pass band and stop band, where they exhibit various characteristics.

1. Butterworth filters

The frequency response of this filter has no ripples in the passband and the stopband therefore it is called maximally flat filter. Butterworth filter uses a Taylor series approximation to the ideal at both $\omega=0$ and $\omega=\infty$.

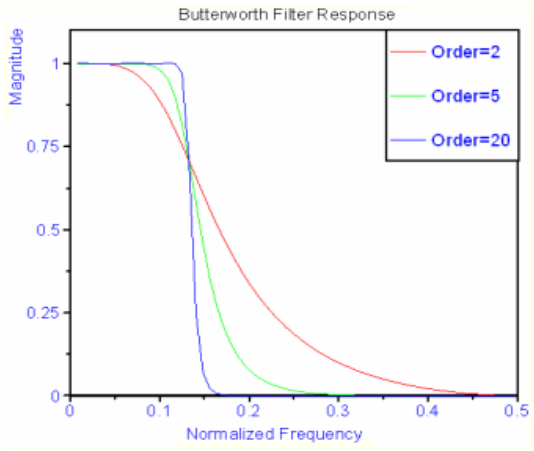

Fig.6 Response of Butterworth filter

We can see from above figure as order of filter increases response of filter closer to the ideal response. Butterworth filters have following characteristics:

- Smooth response at all frequencies.
- Monotonic decrease from the specified cut-off frequencies.
- Maximal flatness, with the ideal response of unity in the pass band and zero in the stop band.
- 3dB down frequency, that corresponds to the specified cut-off frequencies.

The transfer function of Butterworth filter is as follows

(3)

where n is the order of filter.

2. Chebyshev filters

This filter uses a chebyshev approximation across the passband and a Taylor series at ω=∞. Characteristics of this filter is as follows

- Minimization of peak error in the passband.
- Equiripple magnitude response in the passband.
- Monotonically decreasing magnitude response in the stopband.
- Sharper rolloff than Butterworth filters.

Chebyshev filter can achieve sharper transition between passband and stopband with lower order filter than Butterworth filter. This results in smaller absolute errors and faster execution speeds. Frequency response of this filter is given by

(4)

where ε is a parameter of the filter related to ripple present in the passband and $T_N(x)$ is the Nth order Chebyshev polynomial.

$$T_N = \cos(N \cos^{-1}x) \quad |x|\leq 1$$
$$= \cos(N \cosh^{-1}x) \quad |x|\geq 1 \qquad (5)$$

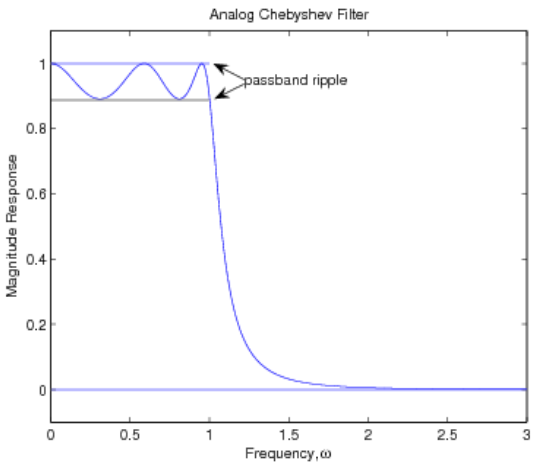

Fig.7 Response of Chebyshev filter

3. Inverse Chebyshev filters

Inverse Chebyshev filter uses a Taylor series approximation at ω=0 and a Chebyshev across the stopband. This filter differ from chebyshev filter in following ways

- These filters minimize peak error in stopband instead of passband.
- These filters have an equiripple magnitude response in the stopband instead of passband.
- These filters have a monotonically decreasing magnitude response in the passband instead of stopband.

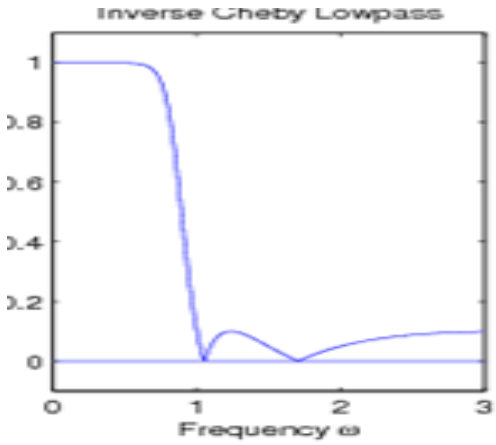

Fig.8 Response of Inverse Chebyshev filter

4. Elliptic filters

The elliptic function filter uses a Chebyshev approximation across both the passband and stopband. Elliptic filters have following characteristics

- Minimization of peak error in the passband and the stopband.
- Equiripples in the passband and stopband

Elliptic filters provide the sharpest transition between the passband and stopband, which accounts for their widespread use. Transfer function of Elliptic filters is given by

(6)

where $U_N(x)$ is the Jacobian elliptic function of order N and ε is a constant related to passband ripple.

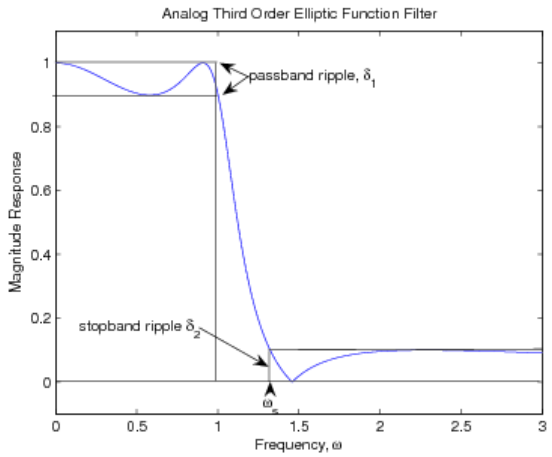

Fig.9 Response of Elliptic filter

VIII. SIMULATION AND DISCUSSION

IIR filters are used for applications where linear characteristics are not of concern. IIR filter is better for lower order tapping. IIR filters must have at least one pole. It is a recursive filter means it has feedback. IIR filters may be unstable depending on the location of poles where as FIR filter is always stable. Pole-Zero plots is an important tool. It can be used to determine stability.

We can distinguish from pole-zero plot whether the filter is low pass, high pass, band pass or band stop. Low pass filters have poles closer to the origin than zeros. They may not have zeros at all. High pass filters will have the zeros close the origin and will probably have at least one on the origin. Band pass filters

will have zeros close to the origin and some poles farther away. The transfer function of 3rd order elliptic low pass filter is given by

(7)

If both poles and zeros of a transfer function are all inside or on the unit circle of the z-plane, the filter is called minimum phase. Frequency responses of different IIR filters are shown in following figures under following parameters

Lower cutoff frequency-2K
Upper cutoff frequency-3.80K
Passband ripple-0.03
Stopband attenuation-90.00

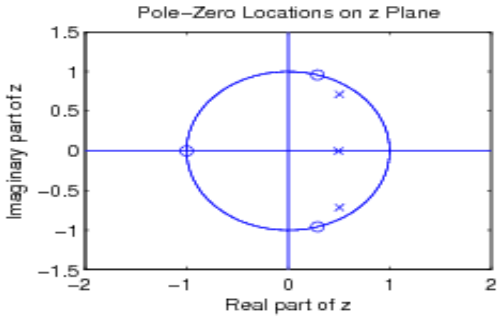

Fig.10 Pole-zero plot of 3rd order Elliptic filter

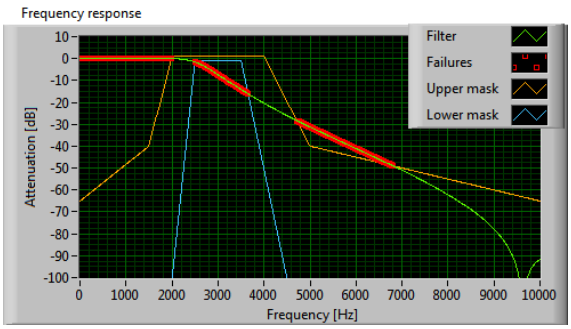

Fig.11 Frequency response of 4th order Butterworth filter

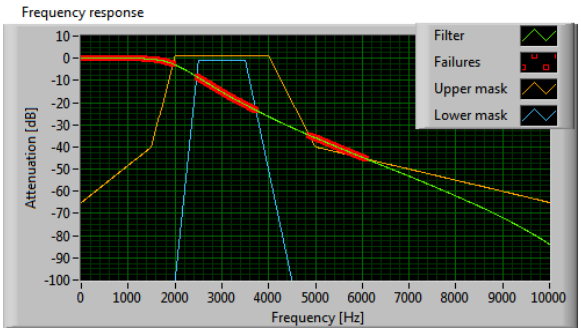

Fig.12 Frequency response of 4th order Chebyshev filter

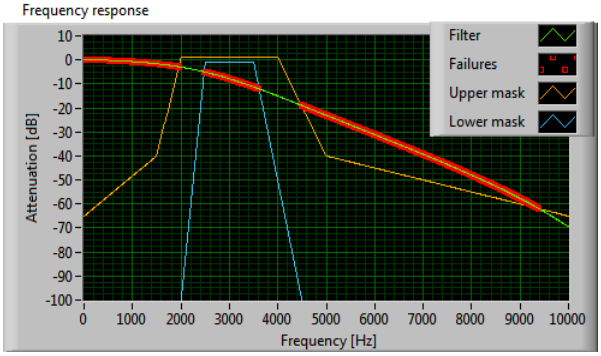

Fig.13 Frequency response of 4th order Inverse Chebyshev filter

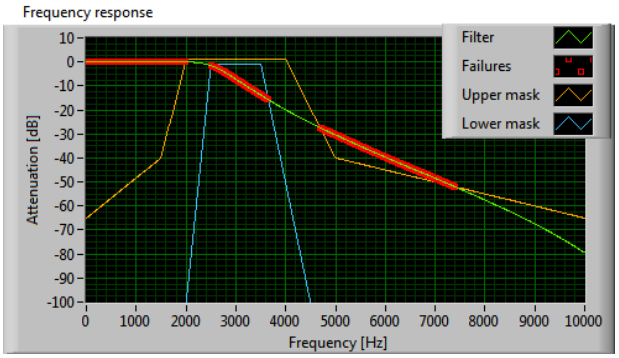

Fig.14 Frequency response of 4th order Elliptic filter

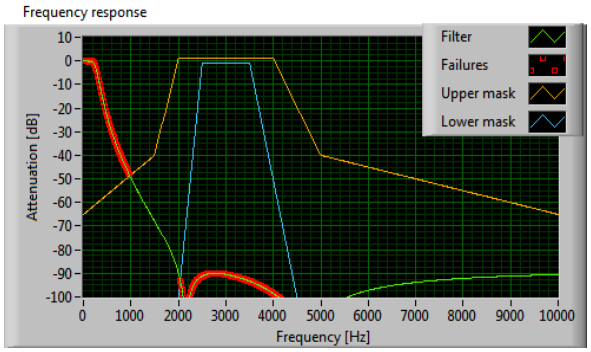

Fig.15 Frequency response of 4th order Bessel filter

ACKNOWLEDGEMENT

The authors are thankful to Mr. Aseem Chauhan (Additional President, RBEF and Chancellor AUR, Jaipur), Maj. General K. K. Ohri (AVSM, Retd.) Pro-VC & Director General, Amity University, Uttar Pradesh Lucknow, Prof. S. T. H. Abidi (Director ASET, Lucknow Campus), Brig. U. K. Chopra (Director AIIT & Dy. Director ASET), Prof O. P. Singh (HOD, Electrical & Electronics) and Prof. N. Ram (Dy. Director ASET) for their motivation, kind cooperation, and suggestions.

REFRENCES

[1] Aimin Jiang and Hon Keung Kwan,"IIR Digital Filter Design with Novel Stability Criterion Based on Argument Principle" Department of Electrical and Computer Engineering,University of Windsor , vol. 1, pp. 126-131, 2007

[2] Beyon, J. Y., *Hands-On Exercise Manual for LabVIEW Programming, Data Acquisition and Analysis*, Prentice Hall, Inc., New Jersey, 2001

[3] Chugani, M. L., *LabVIEW Signal Processing*, Prentice Hall, Inc., Upper Saddle River, New Jersey, 1998 [4] Clark C. L.,*LabVIEW Digital Signal Processing and Digital Communications*, Tata McGRAW-HILL, 2005

[4] Fahmy M.F., Abo-Zahhad M. and Shoby M.1., "Design of elective Linear Phase Switched-Capacitor Filters with Equiripple Passband Amplitude Responses", *IEEE Trans. On Circuits and Systems*, CAS-35, no. 10, pp. 1220-1229, 1988

[5] Jackson L. B., *Digital Filters and Signal Processing*, 3rd ed., Kluwer Academic Publishers, 1996

[6] Namjin Kim, "Digital Signal Processing System-Level Design Using LabVIEW", Elsevier Inc.,vol. 1, 122-127, 2005
[7] Oppenheim, A.V., R.W. Schafer, *Discrete Time Signal Processing*, 2nd ed., Pearson Education, 2005
[8] Proakis J.G., and D.G. Manolakis, *Digital Signal Processing, Principles Algorithms, and Applications*, 3rd ed., Pearson Education, Inc., 1996
[9] Wells, L. K. and Travis, J., *LabVIEW for Everyone Graphical Programming Made Even Easier*, Prentice Hall, Inc., Upper Saddle River, New Jersey, 1997
[10] FDS- Filter design system for SPW, Product data sheet, Comdisco, Inc., 1990. A. H Gray and J. D Markel, "A Computer Program for Designing Digital Elliptic Filters". IEEE Trans. Acous., Speech Signal Processing vol. ASSP-24, pp.529-538, 1973
[11] A.T. Chottera and G.A. Jullien, "A linear programming approach to recursive filter design with linear phase," *IEEE Trans. Circuits Syst.*, vol. CAS-29, pp.139-149, 1982
[12] V. Sreeram and P. Agathoklis, "Design of linear phase IIR filters via impulse response graminas," *IEEE Trans. Signal Processing*, vol. 40, pp.389-394, 1992
[13] Essik, J., *Advanced LabVIEW Labs*, Prentice Hall, Inc., Upper Saddle River, New Jersey, 1999
[14] Jackson L.B., *Digital filters and signal processing*, 3d ed., Kluwer Academic Publishers, 1996
[15] R.C. Eberhart, Kennedy J. A new optimizer using particle swarm theory, Proceedings of the Sixth International Symposium or Micromachine and Human Science, Nagoya, Japan. pp 39-43, 1995
[16] N. Kehtarnavaz and C. Gope, "DSP system design using LABVIEW and SIMULINK: A comparative evaluation", vol.4 pp. 165-169, 2006
[17] Later Mohammad Abo- Zahhad et.al., filter designer: A complete design and synthesis program for lumped, wave-digital, FIR and IIR filters, 1996
[18] L.R. Rabiner, N.Y.Graham, and H. D. Helms, "Linear programming design of IIR digital filters with arbitrary magnitude function", *IEEE Trans. Acoust., Speech Signal Processing*, vol. ASSP-22, pp.117-123, 1974
[19] M.F. Fahmy, M. Abo- Zahhad and M.I. Shoby, "Design of Odd degree Linear Phase Sampled- Data Bandpass Filters with Equiripple Amplitude Response" Inter. J. of Circuit Theory and Applications, vol. 17. pp. 87-101, 1989.
[20] M. Abo-Zahhad, Sabah M.A. and M.Yaseen, "Interactive Software Development for the Design and Synthesis of Lattice and Bireciprocal Wave – Digital filters", Proc. Of the 2nd Inter. Conf. on Engineering Research, ICER-95, Port Said, Egypt, pp. 199-216, 1995
[21] J.H. Mc.Clellan T.W. Parks and L.R. Rabiner, "A Computer Program for Designing Optimum FIR Linear Phase Digital Filters", *IEEE Trans. Audio Electroacoustic*, AU-21, pp. 506-526, 1973
[22] Thede Les, *Analog and Digital filter design using C*, Prentice Hall, Inc., Upper Saddle River, NJ, 1996
[23] M. Abo-Zahhad and T. Henk, "Design of Selective Low pass Sampled-Data and Digital Filters Exhibiting Equiripple Amplitude and Phase Error Characteristics", Inter. J. of Circuit theory and Applications, vol. 23. pp. 59-74, 1995
[24] W.S. Lu, S.C. Pei, and C.C. Tseng, "A weighted least squares method for the design of stable 1-D and 2-D IIR digital filters", IEEE Trans. Signal Processing, vol. 48, pp. 1-10, 1998
[25] S. Chen, "Minimum sensitivity IIR filter design using principle component approach", vol.8 pp. 342-347, 1991
[26] J. Kennedy, R.C. Eberhart, *Particle swarm optimization, Processing, Principles Algorithms, and Applications*, 3d ed., Pearson Education, Inc., 1996
[27] X. Zhang and Hiroshi Iwakura, "Design of IIR Digital Allpass filters Based on Eigenvalue Problem", vol.13, pp. 1333-1338, 1999
[28] C.C.T Seng and S.L. Lee, "Minimax design of stable IIR digital filter with prescribed magnitude and phase responses", IEEE Trans. Circuits Syst. I, vol. 49, pp. 547-551, 2002
[29] D.J. Krusienski, W.K. Jenkins, Particle swarm optimization for adaptive IIR filter structures, Evolutionary Computation, 2004, Congress on vol. 1, pp. 965-970, 2004
[30] Balbir Kumar and Ashwani Kumar, "Design of Efficient FIR filters for the Amplitude Response", vol. 16, pp. 122-125, 1999
[31] C.C. Tseng, "Design of stable IIR digital filter based on least power error criterion", *IEEE Trans. Circuits Syst.*, vol. 51, pp. 1879-1888, 2004
[32] Adam Slowik and Michal Bialko, "Design and Optimization of IIR Digital Filters with Non- Standard Characteristics Using Particle Swarm Optimization Algorithm", Department of Electronics and Computer Science, Technical University of Koszalin, vol. 1, pp. 276-282, 2007
[33] A. Slowik, M. Bialko, Evolutionary design of IIR digital filters with non- standard amplitude characteristics, 3rd- National Conference on Electronics, Kolobrzeg, pp. 345-350, 2004
[34] Chia- Nan Chang, Hui- Kang Teng, Jun- Yuan Chen, and Huang- Ten Chiu, Department of Electronic Engineering, National Taiwan University of Science and Technology, "Computerized
[35] W.S. Lu and T. Hinamoto, "Optimal design of IIR digital filters with robust stability using conic-quadratic- programming updates", *IEEE Trans. Signal Process.*, vol. 51, pp. 1581-1592, 2003
[36] S. Chen, R.H. Istepanian and B.L. Luk, Digital IIR filter design using adaptive simulated annealing, Digital Signal Processing, vol. 11, No. 3 pp. 241-251, 2001
[37] W.S. Lu, "Design of stable IIR digital filters with equiripple passbands and peak- constrained least- squares stopbands," *IEEE Trans. Circuits Syst. II*, vol. 46, pp. 1421-1426, 1999
[38] W. S. Lu, "Design of stable minimax IIR digital filters using semi definite programming", Proc. Int. Sym. Circuits and systems, vol. 1, pp. 355-358, 2000
[39] National Instruments Corporation, *LabVIEW: Measurements Manual*, July 2000

Author's Bibliography

Ms. Shikha Tiwari, She is completed M.Sc (Electronics) from CSJM University, Kanpur. Currently She is pursuing M.Tech (Electronics and Communication) from Amity University, Lucknow Campus. She has published a paper titled as "**A Novice Meta-Materials based Designing of an Highly Efficient Antenna & its Applications: An Overview"** in International Journal of Semiconductor Science and Technology.

Mr. Rajinder Tiwari, PhD (P), M.Tech, MIETE is a member of academic staff of Department of Electronics & Electrical Engineering (ASET), Amity University Uttar Pradesh, Lucknow, where he is serving in the capacity of Asstt. Professor in the Department of Electronics Engineering (ASET). He has done M.Tech (I&CE) and M.Sc (Electronics) from NIT, Kurukshetra and University of Jammu, respectively. Presently, he is pursuing Ph.D. (ECE) from Department of Electronics Engineering, Kumaon Engineering College, Dawarahat (Almora) under Uttarakhand Technical University. Mr. Tiwari has given his contribution to the area of Microelectronics (Modeling & Simulation of the Analog CMOS Circuits for ASP Applications), Embedded System Design, Digital System Design and Process Industries Automation and Control System Design (using Graphical Programming Language with dedicated Hardware). He has published several research papers in International/National Journals/Seminar/Conference. He is associated with several technical institutions and bodies as a life member. Before taking the assignment of Amity University, Uttar Pradesh, Lucknow, he had worked in Electronics for Societal Group, CEERI, Pilani, as a Project Scientist and a Multi – National Company as a Sr. Software Engineer (Bridge Instrumentation Division). He is also associated with the successfully implementation of the Hardware and Software for number of projects undertaken by him and in organizing number of International/National Conferences and Seminars.

Mr. Amit K Bajpai, completed M.Sc (Electronics) from CSJM University Kanpur. He is also associated as a life time member of Indian Association of Physics Teachers (IAPT). He is working for Science propagation in all over India mainly for rural areas. He is a Senior Resource Person (SRP), SRP group is coordinated by very great Physicist Prof H. C. Verma, Department of Physics, IIT Kanpur. He is also associated with an NGO called Shiksha Soapn, IIT Kanpur. He has attended many more workshops from different places in India as a SRP member; He has visited BITS pilani, CEERI, Pilani, Rajasthan Homi Bhabha Research Center, Mumbai. He organizes workshops related with Physics for teachers as well as students in different states of India. He developed a CD named as "Fun with Physics" with Vigyan Prasar, Noida.

IOSR Journal of VLSI and Signal Processing (IOSR-JVSP)
e-ISSN: 2319 – 4200, p-ISSN No. : 2319 – 4197 Volume 1, Issue 6 (Mar. – Apr. 2013), PP 37-41
www.iosrjournals.org

Removal of High Density Impulse Noise Using Cloud Model Filter

Easwara.M IV Sem, M.Tech, Guide: Satish Babu. J Asst. Professor
SJCIT, Chickballapur

Abstract: *The fact that makes image denoising a difficult task is uncertainties in the impulse noise. The most knowledge in dayflies is uncertainty and erratic, unfortunately it is similar to impulse noise. The mathematic implements for handling uncertainty mostly are probability theory and fuzzy mathematics. That means, among the uncertainties involved in impulse noise, the randomness and the fuzziness are the two most important features. In this paper we use a detail-preserving filter based on the Cloud Model (CM) to remove severe impulse noise. CM is an uncertain conversion model, between qualitative and quantitative description that integrates the concept of randomness and fuzziness. The normal random number generation method in normal cloud generator algorithm overcomes the insufficiency of common method to generate random numbers. It can produce random numbers which can be predictable and replicated, and this random numbers present to be a random sequence as a whole. The digital features of the normal cloud characterized by three values with the expectation Ex, entropy En and Hyper entropy He and are good enough to represent a normal cloud. First, an uncertainty-based detector, normal cloud generator, identifies the pixels corrupted by impulse noise. Then, the identified noise pixels are replaced by a fuzzy mean estimation of the processed noise free pixels within the detection window. Compared with the traditional switching filters, the CM filter makes a great improvement in image denoising. Especially, at high density noise level. Thus, the cloud model filter can remove severe impulse noise while preserving the image details.*
Key words*—uncertainty, fuzzy median, normal cloud generator, cloud drops.*

I. Introduction

Digital images are often corrupted by impulsive noise during data acquisition, transmission, and processing**.** The main sources of noise are malfunctioning pixel sensors, faulty memory units, imperfection encountered in transmission channels, external disturbances in a transmission channels, electro-magnetic interferences, timing errors in ADC, etc. The noise may seriously affect the performance of image processing techniques. Hence, an efficient de-noising technique becomes a very important issue in image processing. Impulse noise produces small dark and bright spots on an image. Grasping the noise characteristics is helpful to remove the noise. Noise reductions are basically classified into two types: linear and non-linear techniques. Mean filters are linear filters. Their estimation alter the good pixels, thus produce image blurring. Non-linear noise reduction is a two step process: 1) noise detection and 2) noise replacement. Median filters and its variants [3], [4], [5], [8] have an effective noise suppression and high computational efficiency at low noise density (< 50%), but they fail to account local features such as thin lines, edges at high noise density. Also, they think about only the randomness. The randomness mainly shows in two aspects: 1) the pixels are randomly corrupted by the noise and 2) the noise pixels are randomly set to the maximum or minimum value.
Some decision based filters [7] are good even at high noise density (80%), however, many jagged edges appear in the restored images. It requires more processing time since it uses 21 x 21 window. Sorting fixed window filter [6] uses the median values or the left neighborhood values to replace the noise pixels. This filter creates mainly stripe regions, because it often replaces the corrupted pixel by the left neighborhood pixel. It smears the image details seriously and also sharply decreases the qualities of restored images.

This reveals that the early de-noising techniques fail to understand the uncertainties of noise completely. The better solution is that the pixels those identified as good ones would remain unchanged, while those identified as noisy are replaced with an appropriate estimation. Since, most knowledge in dayflies is uncertainty and erratic, unfortunately it is similar to impulse noise. Among the uncertainties involved in impulse noise, the randomness and the fuzziness are the two most important features. On the other hand, the fuzziness focuses on the pixels with the extreme values whether they belong to the noise or not. Not all of the pixels, which are set to the extreme values, will be the noise pixels [1]. The mathematic implements for handling uncertainty mostly are probability theory and fuzzy mathematics. In fact, CM is an uncertain conversion model, between qualitative and quantitative description that integrates the concept of randomness from probability theory and fuzziness from fuzzy set theory [2]. To represent the uncertainties better and resolve the afore mentioned problems, this paper presents a novel effective filter based on the CM for impulse noise removal. It is compared with the traditional switching filters, the CM filter has the better performance in image

de-noising across a wide range of noise levels with good detail preservation. The outline of the paper is as follows. The cloud model and noise detection-estimation illustrations are reviewed in Section II and III. Simulation results and conclusions are presented in Sections IV and V, respectively.

II. Cloud Model And Its Parameters

Cloud is model described by linguistic values for representation of uncertain relationships between a specific qualitative concept and its quantitative expression. Cloud integrates the concept of randomness and fuzziness. The normal random number generation method in normal cloud generator overcomes the insufficiency of common method to generate random numbers. It can produce random numbers which can be predictable and replicated, and this random numbers present to be a random sequence as a whole. CM is defined as :

Let U be a universal set expressed by exact numbers, and C be the qualitative concept associated with U. If number $x \in U$ exists, which is the random realization of concept, and the certainty degree of x for C, i.e., $\mu(x) \in [0,1]$, is a random value with stabilization tendency, $\mu : U \rightarrow [0,1] \; \forall x \in U \rightarrow \mu(x)$ (1)

then the distribution of x on U is called the cloud, and each x is called a drop. The cloud can be characterized by three parameters, the expected value Ex, entropy En, and hyper entropy He. Ex is the expectation of the cloud drops' distribution in the domain, it points out which drops can best represent the concept and reflects the distinguished feature of the concept. En is the uncertainty measurement of the qualitative concept, which is determined by both the randomness and the fuzziness of the concept. It represents the value region in which the drop is acceptable by the concept, while reflecting the correlation of the randomness and the fuzziness of the concept [1]. The greater the En is, the range of values represented by the concept is the greater, the more vague the concept is. Hyper entropy He, is entropy En of entropy, reflecting the degree of dispersion of the cloud droplets [2]. En is derived from Mean Deviation about the mean for n independent random variables x_i. $i=1,2,3,...n,$ with mean X. The cloud employs its three parameters to represent the qualitative concept as shown in Fig. 1.

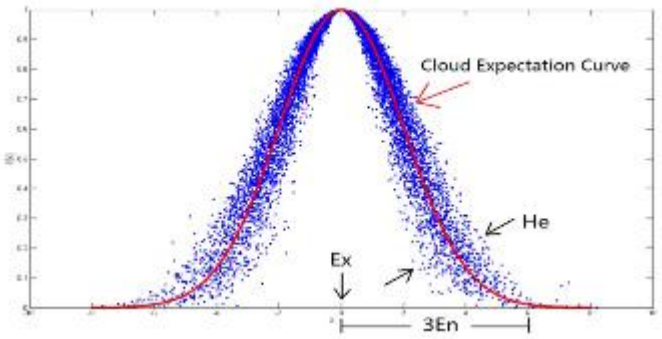

Fig 1. Illustration of three digital cloud parameters

The distribution of pixel values on domain is called cloud and each pixel in the domain is called cloud drop. According to the normal cloud generator [2], the certainty degree of each drop is a probability distribution rather than a fixed value. It means that the certainty degree of each drop is a random value in a dynamic range. If He of the cloud is 0, then the certainty degree of each drop will change to be a fixed value. The fixed value is the expectation value of the certainty degree. In fact, the value is also the unbiased estimation for the average value of the certainty degrees in the range. All the drops and their expectations of certainty degrees can compose a curve, and the curve is the Cloud Expectation Curve (CEC) [1]. All drops located within [Ex+3En, Ex-3En] take up to 99.99% of the whole quantity and contribute 99.74% to the concept. Thus, the drops are located out of domain [Ex+3En, Ex-3En], and then, their contributions to the concept can be neglected. The certainty degree of each pixel is calculated through the CEC, given by,

$$\mu=\exp(-(x_i-Ex)^2/2En^2) \quad (2)$$

Where x_i is cloud drops, Ex is their expectation value and En is entropy.

Noise Model:

Due to faulty switching devices, pixels are randomly corrupted by the two extreme values. Thus, the noise pixels are usually set to the maximum and minimum values in the dynamic range. Let $x(i,j)$ for $(i,j) \in \mathcal{A}$ be the gray value of image X at pixel location (i,j) and $[S_{min}, S_{max}]$ be the dynamic range of X, i.e., $S_{min} \leq x(i,j) \leq S_{max}$ for all (i,j). Denote **y** by a noisy image. In the salt and pepper impulse noise model, the observed gray level at location (i,j) is

$$Y(i,j) = \begin{cases} S_{min}, & \text{with probability } p \quad ; \text{for } (i,j) = 0 \\ S_{max}, & \text{with probability } q \; ; \text{for } (i,j) = 255 \\ x\,(i,j) & \text{with probability } 1-(p+q) \; ; \text{for } 0 < (i,j) < 255 \end{cases} \quad \text{where } p+q = \text{noise level} \qquad (3)$$

III. Noise Detection And Estimation

We consider all the pixels in the window as a set and use CM to represent it. Let each pixel of image X_{MxN} be a cloud drop and input them into Backward Cloud Generator (BCG). It generates three parameters of the cloud C. These Ex, En and He, will be inputs to Forward Cloud Generator (FCG), which generates cloud drops (random numbers). It is as shown in fig.2. This is basis for uncertainty reasoning.

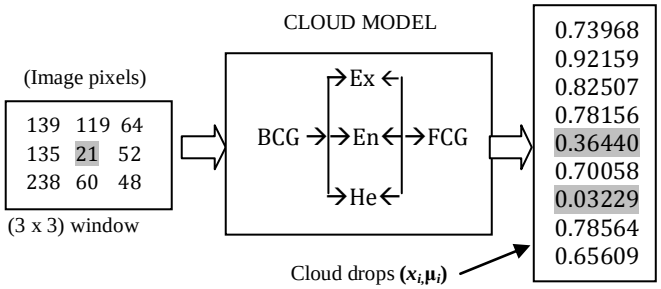

Fig 2. Calculated the cloud drop (x_i, μ_i) for a (3 x 3) window using normal cloud generator.

It is seen that in the fig. 2 at the output of FCG, the certainty degrees of the noise pixels (shaded figures) are far less than that of the uncorrupted pixels. Also, the noise pixels are usually distributed on the both sides of the cloud, and the uncorrupted pixels are located near the central region of the cloud. The CM uses all the pixels in the window to detect the noise pixel and the certainty degrees of each pixels in the proposed detector are "soft" values between [0,1]. Hence, cloud model filter is capable to overcome the drawbacks of existing filters. According to "the 3En rule," the drops out of domain [Ex±3En] can be neglected, which is helpful to identify the noise. Based on this idea, this section presents a novel impulse noise detector using only a fixed 3x3 window, and its details shown as follows. Let w (i,j) be a window of size (2N+1) x (2N+1) centered at location (i,j). w (i,j) = x (i+p, j+q) $\forall$ p,q$\in$ (-N, N) where N = 1.

Step 1: Impose 3x3 window with N = 1 for $w(i,j)^{(2N+1)\,x\,(2N+1)}$ on image X.

Step 2: Compute expectation Ex:

$$Ex = 1/n \sum_{x\,(i+p,\,j+q)\; \in w\,(i,j)3x3} x\,(i+p, j+q) \qquad (4)$$

Step 3: Compute entropy En

$$En = \sqrt{\frac{\pi}{2}} * \frac{1}{n} \sum_{x\,(i+p,\,j+q)\; \in w\,(i,j)3x3} | x\,(i+p, j+q) - x(i,j) | \qquad (5)$$

Step 4: Calculate w_{min} and w_{max} in $w(i,j)^{(3x3)}$ which are extreme operations to recover the smallest and the largest of two values, respectively. i.e., w_{max} = min ($S_{max,}$ Ex+3En) and

w_{min} = max ($S_{mim,}$ Ex -3En)

Step 5: If $w_{min} < x(i,j) < w_{max}$, $x(i,j)$ is uncorrupted pixel (it has to remain unchanged). Then, $y(i,j) = x(i,j)$. Otherwise, $x(i,j)$ is a corrupted pixel. Go to step 6.

Step 6: Noisy pixel $x(i,j)$ is replaced by weighted mean of already processed previous four uncorrepted pixel values , X_{nbp}, within the $w(i,j)^{(3x3)}$. i.e., $X_{nbp} = [x(i-1,j-1), x(i,j-1), x(i+1,j+1), x(i-1,j),]$

Step 7: Calculate the weights for X_{nbp} within the $w(i,j)^{(3x3)}$ $\mu_{nbp} = \exp[-(X_{nbp} - Ex)^2 / 2En^2]$. (6)

Step 8: Then, calculate the weighted mean, $y(i,j) = 1/m \sum X_{nbp} * \mu_{nbp}$. (7)

The CM filter replaces the noise pixel by using the weighted mean of the neighborhood pixels, and their weights are the certainty degrees of them. For understanding of the above steps, a 3x3 windowed sub-image, shown in fig. 2, as an example, is illustrated as follows: Assume that the central pixel **21** lies at an edge of the image. Since, the certainty degrees of each pixels in the proposed detector are "soft" values between [0,1], the noisy pixel values will be replaced by an appropriate pixel values.

*The pixel under test is $x(i,j) = 21$; Expectation, Ex = 97; Entropy, En = 53.7; $S_{min} = 21$; $S_{max} = 238$.
*Computing $w_{max} = \min(238, 258.4) = 238$; $w_{min} = \max(21, -63.8) = 21$.
*If $w_{min} < x(i,j) < w_{max}$; $21 < 21 < 238$; hence, $x(i,j) = 21$, is a noisy pixel.
*To replace the noisy pixel, $x(i,j)$, collect already processed previous four good pixel values, X_{nbp} = [139, 119, 64, 135] and compute the weights of X_{nbp} using equation (5).
i.e., μ_{nbp} = [0.73968, 0.92159, 0.82507, 0.78156].
Then, noisy pixel value 21 is replaced by equation (6).
i.e., $y(i,j) = 92$, is an appropriate pixel value, this provides higher correlation between the corrupted pixel and neighborhood pixel. Higher correlation gives rise to better edge preservation. to preserve the edge of the given image [6].
The CM detector has three major differences with the traditional detectors. First, the proposed detector uses all the pixels in the window to detect the pixel. Second, the traditional filters usually discard the extreme values in the detection window. However, not all of the pixels that are set to the maximum or minimum values will be the noise pixels, the CM does not. Third, the proposed detector identifies if the detected pixel is a noise pixel or not and replacel the noise candidate in $w(i,j)^{(3x3)}$ at the same time. It is a pretreatment to increase the computational efficiency of the post-processing, because those pixels with lower contribution degrees play a small role in the post-filtering.

IV. Simulation Results

An 8-bit gray scale image Lena of 512 x 512 size, has been used to test the performance of the CM filter with dynamic range of values. Image will be corrupted by salt-and-pepper noise at different noise densities, 10% to 80%. The restoration performances are quantitatively measured by peak signal-to-noise ratio (PSNR),

$$\text{PSNR} = 20 \log_{10} \frac{255}{MSE} \text{ dB} \quad (8)$$

$$\text{MSE} = \frac{1}{MN} \sum_{ij}^{mn} (y(i,j) - x(i,j))^2 \quad (9)$$

Where $y(i,j)$ and $x(i,j)$ denote the pixel values of the restored image and the original image, respectively.

The experiment aims to study the detail-preserving abilities of the filter when the images are affected by a severe noise. In this case, since, an effective result would be obtained the window size of the CM filter is limited to 3x3, this causes to increase the computational efficiency. It removes a pixel immediately after the pixel has been identified as a corrupted candidate. Therefore, in the CM filter, the noise detector and the postfilter (replacing noisy pixel) use the same windows.

For comparison, the boundary discriminative noise detection (BDND) filter [7], and the fast median (FM) filter [6] are used. When the noise level is lower than 60%, the performance of the CM filter is similar to the BDND filter, at high noise densities the CM filter proves that having good detail preserving ability. For the FM filter, the decrease in the PSNR is more pronounced than the others and it creates many stripe regions, because it often replaces the corrupted pixel by the left neighborhood pixel. However, the CM filter is a switching fuzzy mean filter, which restores the images and preserves the details well without any jagged edges. To study the detail-preserving abilities of two filters CM and BDND filter, they are tested by the noise image with the noise level 90% (see Figs. 3). Although the BDND filter restores the images without noise, however, many jagged edges appear in the image details at the high noise levels, particularly in the Lena hat region.

(a) (b)
(a) Lena with the noise level of 90% (b) Original image.


(b) CM filter (26.85 dB). d) BDND filter (25.45 dB)

Fig. 3. Restoration results of different filters.

All these are because theBDND filter is a switching median filter, which makes the filter often smear the image details. Obviously, in those regions, the images restored by the CM filter basically keep the same gray levels with the original images. Table-I lists comparison of restored images in PSNR (in decibels)

Table-I (comparison of restored images in PSNR) (in dB)

.	Noise Density(%)				
Filter	**10**	**30**	**50**	**70**	**80**
CM	42.23	37.13	33.26	30.61	28.36
BDND	41.91	35.95	32.62	29.53	27.08
FM	41.64	34.01	29.83	25.82	23.08

To make a reliable comparison, each filter is run 20 times in the same running environment; it is MATLAB 7.0.1 on a personal computer equipped with the 3.2-GHz CPU and 2 GB RAM. Table-II lists the average runtimes in milliseconds for each filter operating on the Lena.

Table-II (average runtimes in milliseconds)

	Noise Density(%)				
Filter	**10**	**30**	**50**	**70**	**80**
CM	440	439	439	440	441
BDND	12324	11390	12074	11509	11341
FM	186	187	186	187	187

V. Conclusion

There are three important aspects in image denoising: First, the accuracy of the noise detection, it will directly influence the results of the image denoising. Second, the computational efficiency, for the real-time work, the filters with lower computational efficiency may not obtain the satisfactory results. Finally, large uncertainties exist in the noise. Thus, understanding the uncertainties can completely help to improve the qualities of the restored images. In this paper, a novel filter with uncertainty for impulse noise removal has been proposed. It represents the uncertainties of the noise perfectly by using the CM, which is helpful in detecting and removing the noise. In addition, the proposed filter identifies the noise pixel without needing to sort the pixel gray values, using 3x3 window, which immensely increases the computational efficiency in noise detection. No matter whether, in noise detection, the image details preservation or computational complexity, the CM filter makes a great improvement and has the higher performances. In sum, the CM filter is a moderately fast denoising filter with good detail preservation.

References:

[1]. Zhe Zhou, "Cognition and Removal of Impulse Noise With Uncertainty", IEEE *Transactions on image processing*, vol. 21, no. 7, pp. 3157-3167, July 2012.

[2]. Zhaohong Wang, Cloud Theory and Fractal Application in Virtual Plants *I.J. Intelligent Systems and Applications*, 2, 17-23 **,** MECS (http://www.mecs- press.org/) March 2011.

[3]. S.-J. Ko and S.-J. Lee, "Center weighted median filters and their applications to image enhancement," *IEEE Trans. Circuits.*,vol.38, no. 9, pp. 984–993, Sep. 1991.

[4]. H. Hwang and R. A. Haddad, "Adaptive median filters: New algorithms and results," *IEEE Trans. ImageProcess.*, vol. 4, no. 4, pp. 499–502, Apr. 1995.

[5]. Z. Wang and D. Zhang, "Progressive switching median filter for the removal of impulse noise from highly corrupted images," *IEEE Trans. Circuits Syst. II, Analog Digit. Signal Process.*, vol. 46, no. 1, pp. 78–80,Jan. 1999.

[6]. K. S. Srinivasan and D. Ebenezer, "A new fast and efficient decisionbased algorithm for removal of high- density impulse noises," *IEEE Signal Process. Letters*, vol. 14, no. 3, pp. 189–192, Mar. 2007.

[7]. P.-E. Ng and K.-K. Ma, "A switching median filter with boundary discriminative noise detection for extremely corrupted images," *IEEE Trans. Image Process.*, vol. 15, no. 6, pp 1506–1516, Jun. 2006.

[8]. T. Chen, K.-K. Ma, and L.-H. Chen, "Tri-state median filter for image denoising," *IEEE Trans. Image Process.*, vol. 8, no. 12, pp. 1834–1838, Dec. 1999.

IOSR Journal of VLSI and Signal Processing (IOSR-JVSP)
e-ISSN: 2319 – 4200, p-ISSN No. : 2319 – 4197 Volume 1, Issue 6 (Mar. – Apr. 2013), PP 42-48
www.iosrjournals.org

Survey on Different Image Fusion Techniques

Miss. Suvarna A. Wakure[1], Mr. S.R. Todmal[2]
[1]*M.E.(E&TC- Signal Processing) ,* [2]*HOD(IT Department) University of Pune*
[1,2]*JSPM's, ICOER, Pune, India*

Abstract: *In medical imaging and remote sensing, image fusion technique is a useful tool used to fuse high spatial resolution panchromatic images (PAN) with lower spatial resolution multispectral images (MS) to create a high spatial resolution multispectral of image fusion while preserving the spectral information in the multispectral image (MS).Image fusion is the process that combines information from multiple images of the samescene. The result of image fusion is a new image that retains the most desirable informationand characteristics of each input image. Now-a-days, almost all areas of medical diagnosis are impacted by the digital image processing. When an image is processed for visual interpretation, the human eye is the judge of how well a particular method works. Clinical application demanding Radiotherapy plan, for instance, often benefits from the complementary information in images of different modalities. For medical diagnosis, Magnetic Resonance Image (MRI) is a medical imaging technique used in radiology to visualize internal structures of the body in detail. MRI provides better information on soft tissue with more distortion. Whereas, Computed Tomography (CT) provides the best information on denser tissue with less distortion. Wavelet transform fusion is more formally defined by considering the wavelet transforms of the two registered input images together with the fusion rule .Then, the inverse wavelet transform is computed, and the fused image is reconstructed. The wavelets used in image fusion can be classified into three categories Orthogonal, Bi-orthogonal and A'trous' wavelet. Although these wavelets share some common properties, each wavelet has a unique image decompression and reconstruction characteristics that lead to different fusion results. Since medical images have several objects and curved shapes, it is expected that the curvelet transform would be better in their fusion. In this paper the fusion results are compared visually and statistically. The simulation results show the superiority of the curvelet transform to the wavelet transform in the fusion of digital image and MR and CT images from entropy, difference entropy, quality measure, standard deviation, PSNR.*

Keywords*- Fusion, Wavelet transform, Curvelet Transform*

I. Introduction

Image fusion has become a common term used within medical diagnostics and treatment. The term is used when multiple patient images are registered and overlaid or merged to provide additional information. Fused images may be created from multiple images from the same imaging modality,[1] or by combining information from multiple modalities,[2] such as magnetic resonance image (MRI), computed tomography (CT).CT images are used more often to ascertain differences in tissue density while MRI images are typically used to diagnose brain tumors.

Multisensor data fusion has become a discipline which demands more general formal solutions to a number of application cases. Several situations in image processing require both high spatial and high spectral information in a single image. This is important in remote sensing. However, the instruments are not capable of providing such information either by design or because of observational constraints. One possible solution for this is data fusion.Image fusion is the process of merging two images of the same scene to form a single image with as much information as possible. Image fusion is important in many different image processing fields such as satellite imaging, remote sensing and medical imaging [2].Image fusion methods can be broadly classified into two groups - spatial domain fusion and transform domain fusion.The disadvantage of spatial domain approaches is that they produce spatial distortion in the fused image. Spectral distortion becomes a negative factor while we go for further processing, such as classification problem. Spatial distortion can be very well handled by frequency domain approaches on image fusion.The multiresolution analysis has become a very useful tool for analyzing remote sensing images. The discrete wavelet transform and curvelet transform based image fusion has become a very useful tool for medical and remote sensing images. These methods show a better performance in spatial and spectral quality of the fused image compared to other spatial methods of fusion. The images used in image fusion should already be registered.

Wavelet Transform has good time frequency characteristics. It was applied successfully in image processing field [3]. Nevertheless, itsexcellent characteristic in one-dimension can't be extended to two dimensions or multi-dimension simply. Separable wavelet which was spanning by onedimensional wavelet has limited directivity [4].

Aiming at these limitation, E. J. Candes and D. L. Donoho put forward Curvelet Transform theory in 2000 [5]. Curvelet Transform consisted of special filtering process and multi-scale Ridgelet Transform. It could fit image properties well. However, Curvelet Transform had complicated digital realization, includes sub-band division, smoothing block, normalization, Ridgelet analysis and so on. Curvelets pyramid decomposition brought immense data redundancy [6]. Then E. J. Candes put forward Fast Curvelet Transform(FCT) that was the Second Generation Curvelet Transform which was more simple and easily understanding in 2005[7]. Its fast algorithm was easily understood. Li Huihui's researched multi-focus image fusion based on the Second Generation Curvelet Transform [8]. This paper introduces the Second Generation Curvelet Transform and uses it to fuse images, different kinds of fusion methods are compared at last. The experiments show that the method could extract useful information from source images to fused images so that clear images are obtained.

II. Image Fusion Based On Wavelet Transform

The most common form of transform type image fusion algorithms is the wavelet fusion algorithm due to its simplicity and its ability to preserve the time and frequency details of the images to be fused.

Some generic requirements can be imposed on the fusion result. a) the fused image should preserve as closelyas possible all relevant information contained in the input images. b)The fusion process should not introduce any artefacts or in consistencies which can distract or mislead the human observer or any subsequent image processing steps. c) in the fused image irrelevant features and noise should be suppressed to a maximum extent. When fusion is done at pixel level the input images are combined withoutany pre-processing.

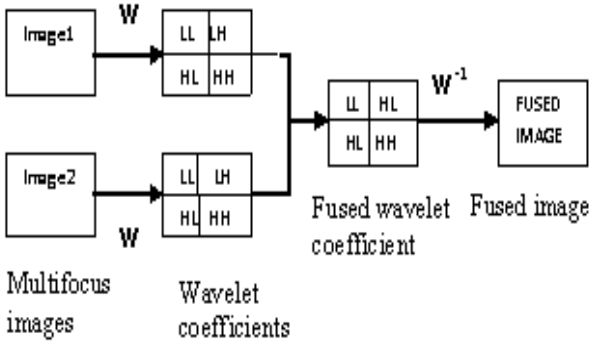

Fig.1 Block diagram of Discrete Wavelet transform

A schematic diagram of the wavelet fusion algorithm of two registered images $I_1(X_1, X_2)$ and $I_2(X_1, X_2)$ is depicted in fig.1. It can be represented by the following equation,

$$I(X_1,X_2)=W^{-1}\{\Psi[W(I_1(X_1, X_2)),W(I_2(X_1, X_2))]\}$$

Where W, $W^{-1}$and ψ are the wavelet transformoperator, the inverse wavelet transform operator andthe fusion rule, respectively. There are several waveletfusion rules that can be used for the selection ofwavelet coefficients from the wavelet transforms of theimages to be fused. The most frequently used rule isthe maximum frequency rule which selects thecoefficients that have the maximum absolute values.The wavelet transform concentrates on representingthe image in multi-scale and it is appropriate torepresent linear edges. For curved edges, the accuracyof edge localization in the wavelet transform is low.So, there is a need for an alternative approach whichhas a high accuracy of curve localization such as thecurvelet transform.

III. Types Of Wavelet Transforms

A] Orthogonal Wavelet Transform

The dilations and translation of the scaling function $\phi j, k(x)$constitute a basis for Vj, andSimilarly $\Psi j, k(x)$ for Wj, if the $\phi j, k(x)$ and $\Psi j, k(x)$ are orthonormal, they include the following property [1].

$$Vj \perp Wj$$

These results in a representation of a single image, containing multiscale detail information from all component images involved. This representation leads to multiple applications ranging from multispectral image fusion to color and multi-valued image enhancement, denoising and segmentation [9].

B] Bi-orthogonal Wavelet Transform

For biorthogonal transform, perfect reconstruction is available. Orthogonal wavelets give orthogonal matrices andunitary transforms; biorthogonal wavelets give invertiblematrices and perfect reconstruction. For biorthogonal wavelet filter, the Low-pass and high-pass filters do notthe same length. The low pass and high pass filters do nothave the same length. The low-pass filter is alwaysSymmetrical, while high pass filter could

be eithersymmetric or anti-symmetric.The method allows unusual flexibility in choosinga filter for any task involving the multiresolution analysis and synthesis.Using our method, one can choose any low-pass filter forthe multiresolution filtering [1].

C]A'trous (Non-orthogonal) Wavelet Transform

A'trous is a kind of non – orthogonal wavelet that is different from orthogonal and biorthogonal. It is astationary or redundant transform, i.e. decimation is notimplemented during the process of wavelet transform, whilethe orthogonal or biorthogonal wavelet can be carried out using either decimation or undecimation mode [1].The enhancement of the spatial information often leadsto the distortion of the information in the spectral domain. Inthis paper, a spectral preserve fusion method is developed by introducing àtrous wavelet transform [10].

IV. Wavelet Transform Algorithm Steps

The process can be divided into four steps.

a) Histogram match

Apply the histogram match process between panchromatic image and differentbands of the multispectral imagerespectively, and obtain three newpanchromatic images PANR, PANG,PANB

b) Wavelet decomposition

Use the wavelet transform to decomposenew panchromatic images and differentbands of multispectral image twice,respectively.

c) Details information combination

Add the detail images of the decomposed panchromatic images at different levels tothe corresponding details of differentbands in the multispectral image andobtain the new details component in thedifferent bands of the multispectral imageand obtain the new details component inthe different bands of the multispectralimage.

d) Inverse wavelet transform

Perform the wavelet transform on thebands of multispectral images,respectively and obtain the fused image.

V. Image Fusion Based On Curvelet Transform

The curvelet transform is a multiscale directional transform thatallows an almost optimal nonadaptive sparse representationof objects with edges. It hasgenerated increasing interestin the community of applied mathematics and signal processing over the years. Most natural images/signals exhibit line-like edges, i.e., discontinuities across curves (so-called line or curve singularities). Although applications of wavelets have become increasingly popular in scientific and engineering fields, traditional wavelets perform well only at representing point singularities since they ignore the geometric properties of structures and do not exploit the regularity of edges.

The curvelet transform has evolved as atool for the representation of curved shapes ingraphical applications. Then, it was extended to thefields of edge detection and image denoising. Recently, curvelet transform used in image fusion. Thealgorithm of the curvelet transform of an image P can be summarized in the following steps:

A) The image P is split up into three subbands Δ1,Δ2and P3 using the additive wavelet transform.

B) Tiling is performed on the subbands Δ1 and Δ2.

C) The discrete Ridgelet transform is performed oneach tile of the subbands Δ1 and Δ2.

A schematic diagram of the curvelet transform isshown in Fig.2

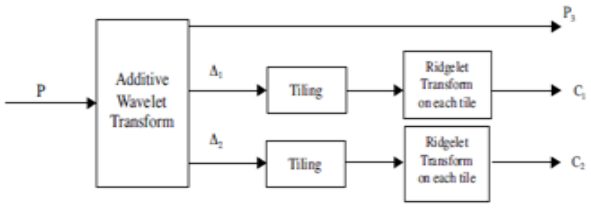

Figure 2. Discrete curvelet transform of an image *P*.

1. Subband Filtering:

The purpose of this step is to decompose the image into additive components; each of which is a subband of that image. This step isolates the different frequency components of the image into different planes without down sampling as in the traditional wavelet transform. Given an image P, it is possible to construct the sequence of approximations: $F_1(P)=P_1$, $F_2(P)=P_2$, ……$F_N(P)=P_N$. Where n is an integer which is preferred to be equal to 3. To construct this sequence, successive convolutions with a certain low pass kernel are performed. The

functions f1, f2, f3, and fn mean convolutions with this kernel. The wavelet planes are computed as the differences between two consecutive approximations P_{1-1} and P_1 i.e. $\Delta 1=P_{1-1}-P_1$

Thus, the curvelet reconstruction formula is given by:

$$P=\sum_{l=1}^{n-1} \Delta 1+P_1$$

2. Tiling:

Tiling is the process by which the image is divided into overlapping tiles. These tiles are small in dimensions to transform curved lines into small straight lines in the subbands $\Delta 1$ and $\Delta 2$. The tiling improves the ability of the curvelet transform to handle curved edges.

3. Ridgelet Transform:

The ridgelet transform belongs to the family of discrete transforms employing basis functions. Tofacilitate its mathematical representation, it can beviewed as a wavelet analysis in the Radon domain.The Radon transform itself is a tool of shape detection.So, the ridgelet transform is primarily a tool of ridgedetection or shape detection of the objects in an image.The ridgelet basis function is given by,

$$\Psi_{a,b,\theta}(x_1,x_2)= a^{-1/2}\Psi [(x_1\cos\theta+ x_2\sin\theta-b)/a]$$

for each $a>0$, each [$b \varepsilon R$] and each ($b \varepsilon [0, 2\pi]$) this function constant along with lines $X_1\cos\theta+X_2\sin\theta$=constant. Thus the ridgelet coefficients of an image $f(x_1,x_2)$ are represented by:

$$R_f(a,b,\theta)= \int_{-\infty}^{\infty}\int_{-\infty}^{\infty}\Psi_{a,b,\theta} (x_1,x_2)\, f(x_1,x_2)dx_1dx_2$$

This transform is invertible and the reconstruction formula is given by:

$$f(x_1,x_2)=\int_0^{2\pi}\int_{-\infty}^{\infty}\int_0^{\infty} R_f(a,b,\theta)\Psi_{a,b,\theta}(x_1,x_2)\,da\,db\,d\theta \,/\, 4\pi a$$

The radon transform for an object F is the collection of line integrals indexed by $(\theta, t) \varepsilon [0, 2\pi] \times R$ and is given by:

$$R_f(\theta, t)= \int_{-\infty}^{\infty}\int_{-\infty}^{\infty} f(x_1,x_2)\delta(x_1\cos\theta+ x_2\sin\theta-t)dx1dx2$$

Thus for ridgelet transform can be represented in terms of the randon transform as follows:

$$R_f(a,b,\theta)= \int_{-\infty}^{\infty} R_f(\theta, t)a^{-1/2}[(t-b)/a]dt$$

Hence, the ridgelet transform is the application of the1-D wavelet transform to the slices of the Radontransform where the angular variable θ is constant and it is varying.To make the ridgelet transform discrete,both the Radon transform and the wavelet transformhave to be discrete.It is known that different imaging modalities areemployed to depict different anatomical morphologies.CT images are mainly employed to visualize densestructures such as bones. So, they give the generalshapes of objects and few details. On the other hand,MR images are used to depict the morphology of softtissues. So, they are rich in details. Since these twomodalities are of a complementary nature, ourobjective is to merge both images to obtain as muchinformation as possible.

VI. Wavelet And Curvelet Based Image Fusion Algorithm

1. First, we need pre-processing, and then cut the same scale from awaiting fused images according to selected region. Subsequently, we divide images into sub-images which are different scales by WaveletTransform. Afterwards, local Curvelet Transform of every sub-image should be taken. Its sub-blocks aredifferent from each others on account of scales' change.

2. Resample and registration of original images, we can correct original images and distortion so that bothof them have similar probability distribution.Then Wavelet coefficient of similar component will stay in the same magnitude.

3. Using Wavelet Transform to decompose original images into proper levels. One low-frequency approximate component and three high-frequency detail components will be acquired in each level.

4. Curvelet Transform of individual acquired low frequency approximate component and high frequencydetail components from both of images, neighborhood interpolation method is used and the details of graycan't be changed.

5. According to definite standard to fuse images, local area variance is chose to measure definition for low frequency component. First, divide low-frequency coefficients C jo(k1,k2) into individual four square

subblocks which are N1X M2 (3×3 or 5× 5), then calculate Standard deviation(STD) of the current sub-block and other statistical parameters.

VII. Results

In medicine, CT and MRI image both are tomography scanning images. They have different features. Fig. 3 shows CT image, in which image brightness related to tissue density, brightness of bones is higher, and some soft tissue can't be seen images. Fig. 4 shows MRI image, here image brightness related to an amount of hydrogen atom in tissue, thus brightness of soft tissue is higher, and bones can't be seen. There is complementary information in these images.

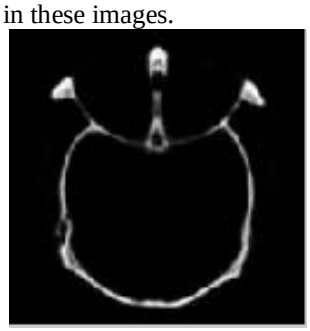

Fig. 3 CT Image of brain

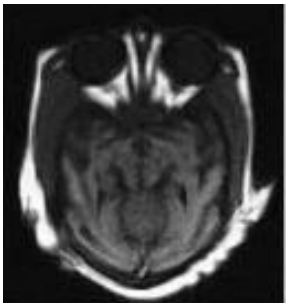

Fig. 4 MRI Image of brain

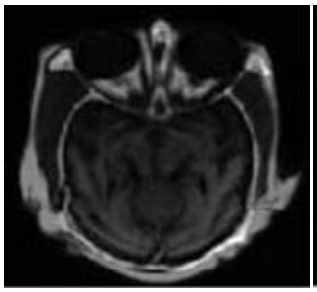

Fig.5a) Orthogonal Fused Image

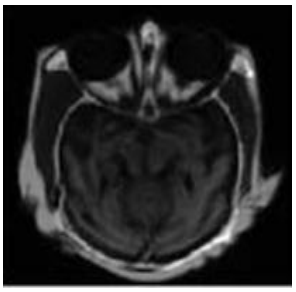

Fig.5b) Biorthogonal Fused Image

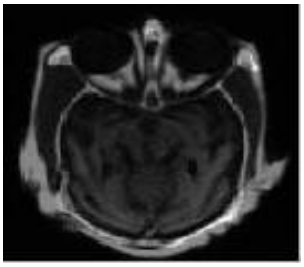

Fig. 5c)A'trous fused image

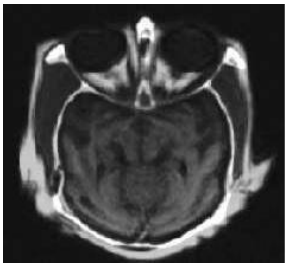

Fig.6 Fused Image of Wavelet Transform

Fig. 3 and fig. 4 represents the MRI and CT images of brain of same person respectively.In the MRI image theinner contour missing but it provides better information onsoft tissue. In the CT image it provides the best informationon denser tissue with less distortion, but it misses the softtissue information. The fig. 5a image is the result of orthogonal waveletfusion technique which is by combining of MRI and CT images .The orthogonal wavelet fused image haveinformation of both images but have more aliasing effect.The fig. 5b image is the result of Biorthogonal wavelet fusion technique. When compare Biorthogonal wavelet withorthogonal wavelet it shows soft tissues information whichare not shown in above figure i.e at the left and right side ofthe inner part. The fig. 5c image is the result of 'A trous' wavelet(non-orthogonal wavelet) based fusion. The fusion results of non-orthogonal wavelet have information on soft tissues anddenser tissues.

Fig.7 Fused Image of
Curvelet Transform

Since the curvelet transform is well-adapted to represent panchromatic image containing edges as shown in fig.7 and the wavelet transform preservesspectral information of original multispectral images as shown in fig.6, the fusedimage has high spatial and spectral resolution simultaneously. In addition to the visual analysis, we extended our investigationto a quantitative analysis. The experimental result was analyzedbased on the combination entropy, standard deviation, quality measure as shown in table 1.

VIII. Quantitative Analysis

In order to compare the wavelet and curvelet based approaches; apart from visual appearancequantitative analysis is done over the fused images. For the visual evaluation, the followingcriterion is considered: natural appearance, brilliance contrast, presence of complementaryfeatures, enhancement of common features etc. The quantitative criterion [11] includes three parameters namely Entropy, DifferenceEntropy and Standard deviation. Each has its importance in evaluating the image quality.

1. Entropy: The entropy of an image is a measure of information content .The estimate assumes a statistically independent source characterized by the relative frequency of occurrence of the elements in X, which is its histogram. For a better fused image, the entropy should have a larger value.

2. Difference Entropy: It is calculated from taking the entropy of the image obtained from subtracting a source image from the fused image and the input source image.

Example: Fused image –CT Image=MRI ImageEntropy [obtained MRI Image –Input MRI] gives Difference Entropy. The difference entropy between two images reflects the difference between the average amounts of information they contained. Minimum difference is expected for a better fusion.

3. Standard deviation: The standard deviation (SD), which is the square root of variance, reflects the spread in the data. Thus, a high contrast image will have a larger variance, and a low contrast image will have a low variance.

Table 1: Statistical parameters of Wavelet and Curvelet transform

FUSION METHODS	WAVELET TRANSFOM	CURVELET TRANSFORM
Entropy	5.05	5.823
Difference entropy	5.40	5.361
Standard deviation	62.03	69.29
Quality measure Q	0.891	0.90
RMSE	2.392	1.530

Quantitative analysis of the fused images indicates better results for curvelet transform based fusion with greater entropy, larger standard deviation and lower difference entropy than their wavelet equivalents. And among the curvelets, addition gives a better result.Moreover, compared withthe fused results obtained by the wavelet and the curvelet, the curveletbasedfusion result has a better visual effect, such as contrastenhancement.

IX. Conclusion

A comparison study has been made between the traditional wavelet fusion algorithm and the proposed curvelet fusion algorithm. The experimental study shows that the application of the curvelet transform in the fusion of MR and CT images is superior to the application of the traditional wavelet transform.In many important imaging applications, images exhibit edges anddiscontinuities across curves. In biologicalimagery, this occurs whenever two organs ortissue structures meet. Especially in image fusionthe edge preservation is important in obtainingthe complementary details of the input images.As edge representation in Curvelet is better,Curvelet based image fusion is best suited formedical images.

References

[1] A. Soma Sekhar, Dr.M.N.Giri Prasad , A Novel Approach of Image Fusion on MR and CT Images Using Wavelet Transforms, 2011 IEEE

[2] Smt.G. Mamatha(Phd) , L.Gayatri, An Image Fusion Using Wavelet And Curvelet TransformGlobal Journal of Advanced Engineering Technologies, Vol1, Issue-2, 2012 , ISSN: 2277-6370

[3] Abhijit Somnathe, Ujwal Harode, A Novel Approach of Image Fusion based on Wavelet Transform and Curvelet Transform,International Conference & Workshop on Recent Trendsin Technology, (TCET) 2012

[4] Rafael c. Gonzalez,richard E.woods Digital image processing, Addison-wesley.an imprint of pearson education, 1st edition

[5] E. J. Candes, D. L. Donoho. Curvelets: A surprisingly effective nonadaptive representation for objects with edges[J]. In:C. Rabut A. Cohen , L. L. Schumaker. Curves and Surfaces. Nashville , TN: Vanderbilt University Press ,2000. 105-120.

[6] E. J. Candes, D. L. Donoho. New tight frames of curvelets and optimal representations of objects with singularities[J]. Commun. On Pure and Appl. Math.2004, 57(2):219-266.

[7] E. J. Candes , L. Demanet D. L. Donoho et al.. Fast Discrete Curvelet Transforms[R].Applied and Computational Mathematics. California Institute of Technology , 2005.1.

[8] LiHui-hu,i GuoLe,i LiuHang. Research on image fusion based on the second generation curvelet transform [J]. Acta Optica Sinica, 2006,26(5): 657 ~662.

[9] Paul Scheunders, Member, IEEE. An Orthogonal Wavelet Representation ofMultivalued Images. IEEE Transactions on Image Processing, Vol. 12, no. 6, June 2003

[10] Shaohui Chen, Renhua Zhang, Hongbo Su, *Senior Member, IEEE*, Jing Tian, and Jun Xia,SAR and Multispectral Image Fusion Using Generalized IHS Transform Based on à Trous Wavelet and EMD Decompositions. IEEE SENSORS JOURNAL, VOL. 10, NO. 3, MARCH 2010

[11] Y.Kiran Kumar Technical Specialist- Philips HealthCare, Comparison Of Fusion Techniques Applied To Preclinical Images: Fast Discrete Curvelet Transform Using Wrapping Technique & Wavelet Transform.Journal of Theoretical and Applied Information Technology

IOSR Journal of VLSI and Signal Processing (IOSR-JVSP)
e-ISSN: 2319 – 4200, p-ISSN No. : 2319 – 4197 Volume 1, Issue 6 (Mar. – Apr. 2013), PP 49-53
www.iosrjournals.org

Image Steganography using Polynomial key and Covert Communications in Open Systems Environment

Babbala Sundeep[1], Bhusam Gnanaprakash[1,] Alapati Harivanditha[2], Bobbu Yaswanth[1], Dr.A. Sivasankar[3]
[1](Department of ECE ,Priyadarshini College of Engineering , India)
[2](Department of ECE ,Priyadarshini College of Engineering , India)
[3](Head of the Department, Department of ECE ,Priyadarshini College of Engineering , India)

Abstract : *Steganography, the art of hiding secrete messages inside other messages, innocuous wrapper, as until recently had been the poor cousin of cryptography, to communicate privately in an open channel. This area of study got widespread popularity after its alleged use by many extremist groups while hatching and executing their plans remotely. Because of this, in the recent past, many law enforcement and government agencies have also shown keen interest in it. There are many other reasons like Digital Rights Management applications (Watermarking and Finger Printing), which acted as catalyst too. This paper proposes a new steganographic encoding scheme which separates the colour channels of the windows bitmap images and then hides messages Randomly using polynomials in the LSB of one colour component of a chosen pixel where the colour components of the other two are found to be equal to the key selected.*

Keywords :*Steganography, Data Hiding, LSB, Polynomials.*

I. INTRODUCTION

Digital Rights Management is a method of controlling access to copyrighted material. Communication and the flow of free thought, is regarded by many as a unique virtue that is greatly attributed to the overall development of human being. Moreover it was instrumental in overall growth of the human fraternity. According to Oxford Advanced Dictionary [1], communication is defined as the activity or process of expressing ideas and feelings or of giving people information; also communications is defined as methods of sending information. Communication has many divisions, and two of the most predominant ones are interpersonal and intrapersonal. Interpersonal communication can further be divided into two, namely public and private. One problem with the public communication channel is that it may have many eavesdroppers; eavesdroppers of passive, or active nature. A Passive eavesdropper may be one who just listens and an active one will listen and modify the message. Hence we could conclude that at times public communication demands the need of covert communications; a mechanism to communicate privately in a public environment.

Throughout history, people have tried to find methods to hide information. History of Steganography, which is the original method of information concealment, dates back to ancient times. One of the earliest example of information hiding is the ATBASH code (2000-1500 BC) [2] used in Jewish mysticism, a cipher that substitutes the first letter of the Hebrew alphabet with the last, the second letter with the one before last, and so on. A book named Steganographia explaining many techniques for covert communication was explained by Johannes Trithemius around 500 BC and because of its very nature, the authorities never permitted him to publish the same and the book saw the light only in the mid 16th century, long after his demise [3]. The rapid growth of interest in this subject, over the last few years, is attributed to many reasons and some of the major reasons are discussed in the following paragraphs: Firstly, it got widespread popularity after the alleged use of it by many extremist groups while hatching and executing their plans, without bothering much about the geographical distance. This prompted various governments across the world to restrict the availability of covert services to the general public. This was causing inconvenience to many, which in turn has motivated open minded people to study methods by which secret messages can be embedded in seemingly innocuous cover messages through an open systems environment. The ease with which this can be done was thought by many as a potential argument against imposing restrictions. Secondly, the publishing and broadcasting industries have become interested in techniques for hiding copyright marks andserial numbers in digital images, audio and video recordings, books, multimedia products etc. The fearful fact is that it is too easy to copy a digital work, which only requires a right click. A proactive measure in this direction is the need of the hour and the industry demands one.

Thirdly the volume of communication lines are increasing exponentially and in fast developing countries like India, there is a high chance of covert communication going unnoticed in this bedlam. According to the Telecom Regulatory Authority of India (TRAI), Indians owned 429.72 million phones, 391.76 mobiles and 37.96 million landlines, at the end of March 2009. Total Broadband subscribers' base has reached 6.22 million by the end of March 2009 growing at a staggering 59.48 % during March 2008 to March 2009 and both the mobile and the broadband subscribers' are ever growing [4]. It is an enormous task for the law enforcement and intelligence agencies to monitor this entire 435.94million plus phones and broadband connections - deciding which communication to intercept and which one to leave, because of the huge volume of traffic.

II. Information Hiding In Bitmap Images Using Lsb Based Chromatic Steganography Using Polynomial

Redundancy is one of the major aspects of creation. A close inspection reveals that redundancy does exist, and exists in abundance. Computer files are not an exception to this fact. For e.g. an image on a computer is represented by tons and tons of pixels, which in turn have many redundant information's. The simplest technique here is to fabricate the redundant bits so as to do the covert communication. For e.g. each pixel of an image consists of a variation of all three primary colors, red, green and blue, in a standard 24-bit bitmap, requiring 8 bits each for these three colors. i.e.there are 256 different variations, ranging from 00000000 to 11111111, for each colour in a pixel. So, to represent the colour white, the code would look like 11111111 11111111 11111111. Keeping in mind that, the human eye cannot distinguish the difference between too many colours, the colour 11111110 11111110 11111110 would look exactly the same as white, which means that the last digit in every bit in every pixel could be changed without much visual degradation of quality. This is the basis of the Least Significant Bit Insertion technique. We require 8 bits to represent an ASCII text and there are three potential slots extra in every pixel of a picture. Therefore, in a conducive environment, with every three pixels, one ASCII text could be concealed. In order to make this practical to the user, a computer program would be needed. After typing in the secret message and determining a suitable cover message, the program would go through every pixel to find the potential candidate pixels and will change the least significant bit to represent each bit of the message. The image could then be sent to the recipient who in turn runs his program to take off the least significant bits to form the secret message.

The current study took windows bit map image file format with loss less compression in to consideration. The proposed algorithm would require secret message (M), a wrapper (W) and a pseudorandom seed Generated by polynomial (S) as input. In Windows bit map format, every image will have three separate colour channels; a channel dedicated for the red component (rCom), another one for the green component (gCom), and a third one for the blue component (bCom). After separating the colour channels, the program would go through each pixel to find all those pixels where the value of the rCom and gCom is equal to that of the supplied R and G values. Spatial details of every such pixel will be stored in an array named Candidate Pixel (CP) and the total numbers of such potential candidate pixels are calculated. If the length of the message (in bits) is more than the length of CP then a message will be displayed prompting the unsuitability of the wrapper under consideration. If the wrapper is found to be suitable then a pseudorandom number will be generated from a pre-decidedpolynomial, by making use of the seed, which was agreed beforehand by both the parties. The pseudorandom number will be mapped to the Target Pixel index (TP) of CP by using the polynomial, with the length of the CP. This will enable us to insert the secret data bit randomly across the wrapper thereby increasing the stealth of the system. Once embedded, all the colour channels will be concatenated to form the innocuous Stego Image. Here in the algorithm, we have embedded data in bCom where the colour coefficients of the rCom and gCom were found to be equal to that of the chosen key; but the combinations may be changed so as to increase the stealth of the system. The algorithm performing the above said concept is shown below:

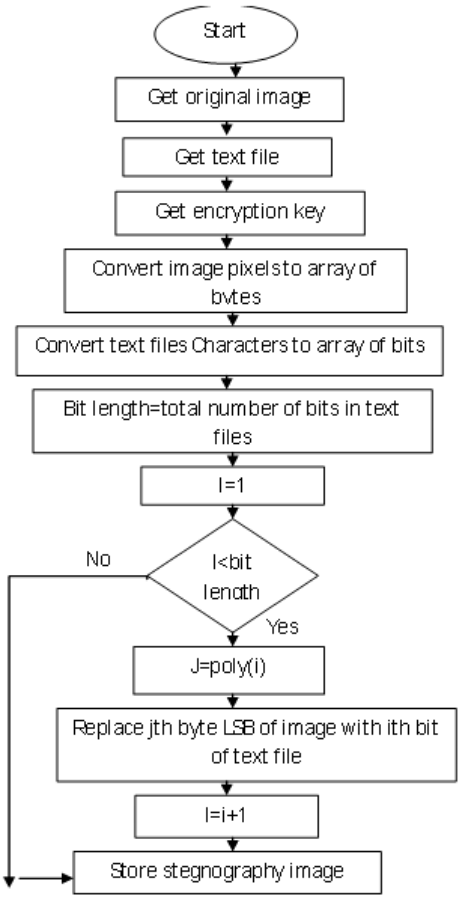

LSB Encoding Method

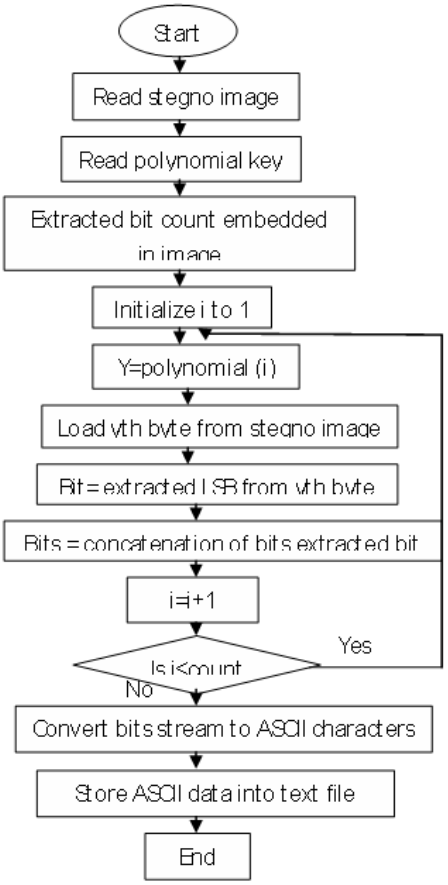

LSB Decoding Method

The Stego Image could then be send to the recipient through open systems environment, who in turn runs his program to extract those randomly stored least significant bits of bCom component where the colour coefficients of the rCom and gCom are found to be equal to that of selected keys i.e. R and G. Thus the secret message could be communicated covertly[10]. The algorithm implementing the decoding procedure is shown above:

If we compress the secret message before embedding, using any available text compression algorithm, like Run length encoding scheme, we may further reduce the message length, thus reducing the entropy and in turn enhancing the robustness of the system. Also the great thing about this insertion technique is that because the secret message is encoded into the color channels, the message is not lost even if the file is compressed.

III. RESULTS

Figure 1 and 2 are images with a resolution of 2272 × 1704 with 24-bit color depth. The sizes of the two windows bitmap images shown are 11.0 MB (11,614,464 bytes). Fig. 1 is unmodified where as Fig. 2 the modified one and an encrypted secrete message is also shown. It is impossible for the human eye to find a visual difference between two of the above shown images. Since the visual difference test was unable to find any positive results, some statistical tests were exercised with the intention to prove that the image was tampered. If the image happen to be modified then at least some of image's statistical properties may deviate from a norm. Here also no significant difference in the quality of the cover and stego image were found. We therefore conclude from the basic statistical test that there is no evidence from the current experiment to suggest that the proposed system deteriorate the quality of the image. The different tests conducted and there results are tabulated in table 1

Figure1: Original Image

Figure2: Stego Image

qANQR1DBwU4D/TlT68XXuiUQCADf
j2o4b4aFYBcWumA7hR1Wvz9rbv2BR6
WbEUsyZBIEFtjyqCd96qF38sp9IQiJIK1Na
Zfx2GLRWikPZwchUXxB+AA5+1qsG/ELB

Secret Message

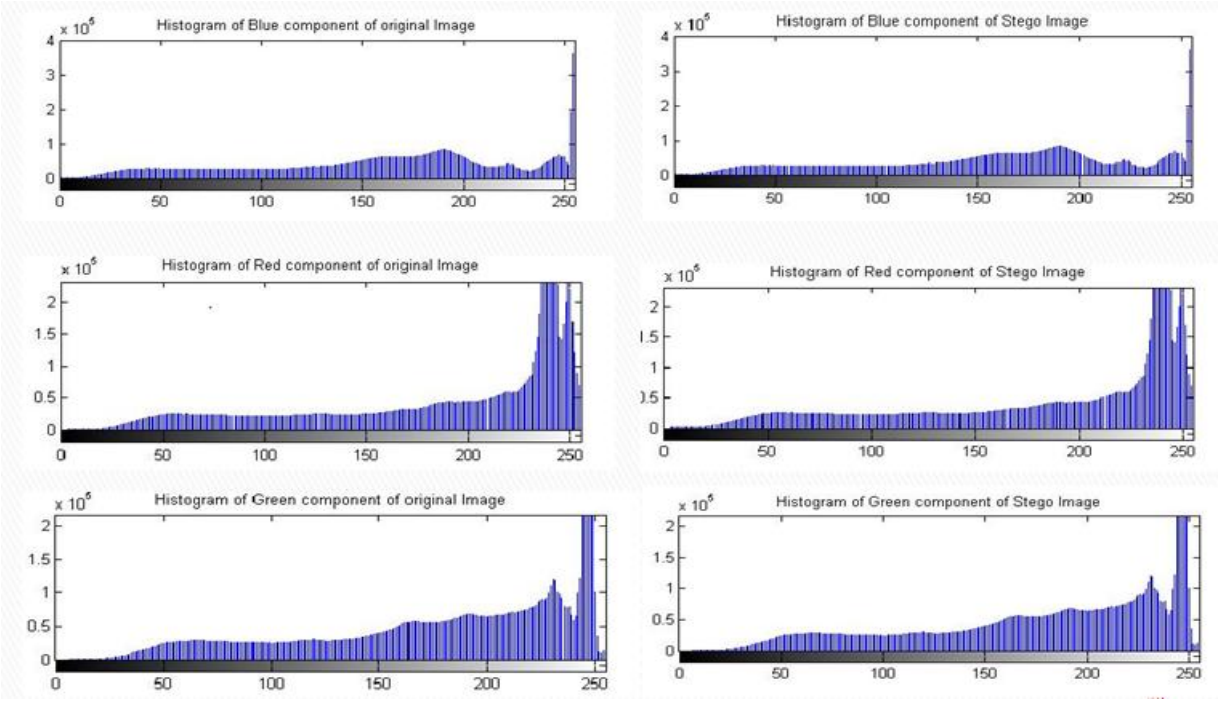

Figure 3 : Histogram results

Test name	Original image	Stego image
Mean	117.231369	117.231369
Standard deviation	93.502419	93.502411
Median	205.000000	205.000000
Size	36636672.0000000	36636672.000000

Table 1 : Statistical results

IV. Conclusion

In the paper, the authors have introduced a new steganographic encoding scheme which separates the colour channels of the windows bitmap images and then randomly hide messages in the LSB of one component of the chosen pixel using polynomial where the colour coefficients of the other two are found to be equal to the keys selected.

References

[1]. Murray, A.H., and R.W Burchfiled (eds.), The Oxford English Dictionary, Oxford, England: Clarendon Press, 1933.
[2]. J. Bright, Jeremiah (AB; New York 1965) 209; R.K. Harrison, Jeremiah and Lamentations (Winona Lake 1973)
[3]. D. Kahn, 'The History of Steganography' in Anderson, pp. 1-5.
[4]. http://www.trai.gov.in/WriteReadData/trai/upload/PressReleases/ 671/pr21apr09no38.pdf
[5]. Oosterwijk, Herman and Paul T. Gihring; DICOM Basics, 3rd ed.; OTech, Inc., Aubrey, TX;2002
[6]. D. Kahn, 'The Codebreakers - The Story of Secret Writing', Scribner, New York, New York, U.S.A., 1996. ISBN 0-684-83130-9.
[7]. G.J. Simmons , "The prisoners' problem and the subliminal channel" , Advances in Cryptology : Proceedings of CRYPTO 83, (ed. D. Chaum), Plenum , New York , 1984,pp.51-67.
[8]. NF Maxemchuk, Electronic Document Distribution", AT & T Technical Journal v 73 no 5 (Sep/Oct 94) pp 73 - 80
[9]. A. Westfeld and A. Pfitzmann, "Attacks on Steganographic System", Proc. Information Hiding-3 Int'l Workshop in Information Hiding, Springer- Verlag, 1999, pp. 61-76.
[10]. JijjuA.Mathew& Prof. Gurmit Singh, "Stegnography and Covert Communications in open systemsenvironment", 2009 IEEE, pp.847-849.
[11]. K.Sukumar, et.al., " Multi-Image –Watermarking Scheme based on Framelet and SVD", 2009 IEEE, pp. 379-388

IOSR Journal of VLSI and Signal Processing (IOSR-JVSP)
e-ISSN: 2319 – 4200, p-ISSN No. : 2319 – 4197 Volume 1, Issue 6 (Mar. – Apr. 2013), PP 54-67
www.iosrjournals.org

Application of Segmentation Techniques on Atherosclerosis Images

Patel Janakkumar Baldevbhai[1], R.S. Anand[2]
[1](*Research Scholar, Electrical Engineering Department, Indian Institute of Technology Roorkee, India)*
[2](*Professor, Electrical Engineering Department, Indian Institute of Technology Roorkee, India)*

Abstract : *This paper presents application of segmentation techniques on atherosclerosis images using various segmentation methods like Otsu thresholding, fuzzy C means, clustering algorithm and marker controlled watershed segmentation algorithm. Atherosclerosis is one of the causes of coronary heart disease (CHD). The proposed marker controlled watershed algorithm for medical image segmentation and analysis is very important because of its advantages, such as always being able to construct an entire division of the color image and prevent over segmentation as compared to conventional watershed algorithm. Paper finds Region of Interest (ROI) values of segmented image with proposed technique for coronary atherosclerosis.*

Keywords - *Coronary heart disease (CHD), Clustering Image Segmentation Technique, Medical Image Segmentation, Fuzzy C means algorithm, Marker based Watershed Image Segmentation Technique.*

I. Introduction

Image segmentation is a vital method for most medical image analysis tasks. Segmentation is an important process to extract information from complex medical images. Image segmentation is a necessary preliminary step for any image analysis task. This process partitions an image into a number of constituting regions. Each partition region is homogeneous with respect to a given property, while the set including any two adjacent regions is not homogeneous. Watershed transformation (WT) [1] is a basic tool for image segmentation exploiting both region-based and edge-detection-based methodologies. Segmentation is accomplished by using the watershed [2] transformation, which provides a partition of the image into regions whose contours closely fit. The watershed transformation considers the gradient magnitude of an image as a topographic surface. Pixels having the highest gradient magnitude intensities (GMIs) correspond to watershed lines, which represent the region boundaries. Water placed on any pixel enclosed by a common watershed line flows downhill to a common local intensity minimum (LIM). Pixels draining to a common minimum form a catch basin, which represents a segment. Luc Vincent [3] presented a morphological grayscale reconstruction algorithm for image analysis. Serge Beucher [4] redefined hierarchical segmentation by means of a new algorithm called the waterfall algorithm. V. Grau [5] et al. presented an improvement to the watershed transform that enables the introduction of prior information in its calculation with the information via the use of a previous probability calculation. Hardening of the arteries, also called atherosclerosis, is a common disorder. It occurs when fat, cholesterol, and other substances build up in the walls of arteries and form hard structures called plaques. Over the course of years and decades, plaque build-up narrows patient's arteries and makes them stiffer. These changes make it harder for blood to flow through them. Coronary heart disease (CHD) is a narrowing of the small blood vessels that supply blood and oxygen to the heart. CHD is also called coronary artery disease. Coronary heart disease (CHD) is the leading cause of death in the United States for men and women. Coronary heart disease is caused by the build-up of plaque in the arteries to patient's heart. This may also be called hardening of the arteries. Atherosclerosis is a disease characterized by a deposit of plaque in an arterial wall over time. The disruption of an atherosclerotic plaque is considered to be the most frequent cause of heart attack and sudden cardiac death. Studying vulnerable plaques constitutes a major research area in the field of clinical and medical imaging. In order to track progression and regression during therapy of the atherosclerosis, the inner and outer borders of the arterial wall are extracted and the plaque area is identified in the region between these two borders. Atherosclerosis is an underlying cause of cardiovascular disease, which impacts the health of more than 30% of the U.S. population. Valerie Pazos et al. [6] presented research on mechanical characterization of atherosclerotic arteries. Carotid atherosclerosis is a primary cause of transient ischemic attack and stroke. Accumulating evidence suggests that it is most likely not the size of the carotid atherosclerotic plaque nor the per cent stenosis of the carotid lumen that determines the risk for stroke. Rather plaque composition and activity are now thought to play central roles in determining the severity of the disease and the probability for plaque rupture [7]. Danijela *et al.* presented a method for carotid artery vessel wall segmentation in computed tomography angiography (CTA) data [8]. Gozde Unal *et al.* presented a shape-driven approach to segmentation of the arterial wall from intravascular ultrasound images in the rectangular domain [9]. Simon *et*

al. [10] presented a research paper on vulnerable atherosclerotic plaque elasticity reconstruction based on a segmentation-driven optimization procedure using strain measurements a theoretical framework approach.

Definition: Atherosclerosis is defined by the WHO as variable combination of focal accumulation of lipids, complex carbohydrates, blood and its constituents, fibrous tissue and calcium deposits combined with its changes of the media.

Atherosclerosis is thus a patchy, nodular type of arteriosclerosis. It is a process of hardening of the arteries [41]. A catheter is inserted (figure 5) through the patient's groin into an artery and pushed toward the distal end of the coronary arteries. Thereafter, the ultrasound transducer in the catheter is pulled back with constant speed. During the pullback, sequences of images are acquired. The lumen is the interior of the vessel, through which the blood flows. The intima is the innermost layer of an artery. It is made up of one layer of endothelial cells and is supported by an internal elastic intima. The endothelial cells are in direct contact with the blood flow. It is a fine, transparent, colorless structure that is highly elastic. The media is the middle layer of an artery, which is made up of smooth muscle cells and elastic tissue. The adventitia is the outermost layer of the blood vessel, surrounding the media. It is mainly composed of collagen. Extraction of the boundaries of the coronary arterial wall by segmenting the lumen and media adventitia contours is a first step in measuring quantities such as lumen diameter and plaque dimensions, and assessment of the atherosclerotic plaque. Manual segmentation and processing of the lumen contour and the media-adventitia contour is tedious, time-consuming, and susceptible to intra- and interobserver variability. Due to the high number of images, typically in the order of hundreds, automated segmentation of the arterial contours is an essential task.

Image segmentation algorithms are classified into two types, supervised and unsupervised. Unsupervised algorithms are fully automatic and partition the regions in feature space with high density. The different unsupervised algorithms are Feature-Space Based Techniques, Clustering (K-means algorithm, C-means algorithm), Histogram thresholding, Image-Domain or Region Based Techniques (Split-and-merge techniques, Region growing techniques, Neural network based techniques, Edge Detection Technique), Fuzzy Techniques. The watershed segmentation technique has been widely used in medical image segmentation. Watershed transform is used to segment medical images. The method originated from mathematical morphology that deals with the topographic representation of an image. Neural Network based algorithm like Pulse Coupled Neural Network (PCNN) can be utilized as a supervised algorithm for image segmentation.

Segmentation is often a critical step in image analysis. Microscope image components show great variability of shapes, sizes, intensities and textures. An inaccurate segmentation conditions the ulterior quantification and parameter measurement. The Watershed Transform is able to distinguish extremely complex objects and is easily adaptable to various kinds of images. The success of the Watershed Transform depends essentially on the existence of unequivocal markers for each of the objects of interest. The standard methods of marker detection are highly specific, they have a high computational cost and they determine markers in an effective but not automatic way when processing highly textured images. This paper implements segmentation techniques using Otsu thresholding method, Fuzzy C means level 0 and level 1 method, color clustering technique and proposed marker controlled watershed segmentation technique on atherosclerosis images. This proposed marker controlled watershed algorithm for medical image segmentation and analysis is very important and useful because of its advantages, such as always being able to construct an entire division of the color image and prevent over segmentation as compared to conventional watershed algorithm.

Watersheds are one of the typical regions in the field of topography. A drop of the water falling it flows down until it reaches the bottom of the region. Monochrome image is considered to be a height surface in which high-altitude pixels correspond to ridges and low altitude pixels correspond to valleys. This suggestion says if we have a minima point, by falling water, region and the frontier can be achieved. Watershed uses image gradient to initial point and region can get by region growing. The accretion of water in the neighbourhood of local minima is called a catchment basin. Watershed refers to a ridge that divides areas shattered by different river systems. A catchment basin is the environmental area draining into a river or reservoir. If we consider that bright areas are high and dark areas are low, then it might look like the plane. With planes, it is natural to think in terms of catchment basins and watershed lines.

An intangible water drop is placed at each untagged pixel. The drop moves to low amplitude neighbour until it reaches a tagged pixel and it assumes tag value. In flooding approach, intangible pixel holes are pierced at each local minima. The water enters the holes and takings to fill each catchment basin. If the basin is about to overflow, a dam is built on its neighbouring ridge line to the height of high altitude ridge point. These dam borders correspond to the watershed lines. Advantages of the watershed transform include the fact that it is a fast, simple and intuitive method. More importantly, it is able to produce an entire division of the image in separated regions even if the contrast is poor, thus there is no need to carry out any post processing work, such as contour joining. Its limitations will include over-segmentation and sensitivity to noise. There has also been an increasing interest in applying soft segmentation algorithms, where a pixel may be classified partially into multiple classes, for medical images segmentation. Clustering is a method of grouping a set of patterns into a

number of clusters such that similar patterns are assigned to one cluster. Each pattern can be represented by a vector having many attributes. Clustering technique is based on the computation of a measure of similarity or distance between the respective patterns. A cluster is a collection of objects which are similar between them and are dissimilar to the objects belonging to other clusters. Unlike classification, in which objects are assigned to predefined classes, clustering does not have any predefined classes. The main advantage of clustering is that interesting patterns and structures can be found directly from very large data sets with little or none of the background knowledge. The cluster results are subjective and implementation dependent. K-means clustering is a simple clustering method with low computational complexity. The clusters produced by K means clustering do not overlap. The Fuzzy C-means clustering algorithm is a soft segmentation method that has been used extensively for segmentation of medical images. In this work, we use K-means clustering and Fuzzy C-means Clustering methods exclusively to produce a segmentation of the image. In this research paper we implemented color clustering algorithm, Fuzzy C Means clustering as well as marker controlled watershed segmentation algorithm separately for medical image segmentation. The Clustering algorithms are unsupervised learning algorithms, while the marker controlled watershed segmentation algorithm makes use of automated thresholding on the gradient magnitude map and post-segmentation merging on the initial partitions to reduce the number of false edges and over-segmentation.

Segmentation has wide application in medical field [11-15]. Having good segmentations will help clinicians and patients as they provide vital information for 3-D visualization, surgical planning and early disease recognition. Microscope image components show great variability of shapes, sizes, intensities and textures [16]. Moreover, during acquisition, it is necessary to establish a high number of parameters that result in the presence of noise, non-homogeneous illumination, fuzzy contours and low contrast. This characteristic results in an incorrect segmentation when applying conventional segmentation methods. Watershed Transform (WT) is a powerful morphological tool to segment texture images into regions of interest. This transform is adaptable to different types of images and capable of distinguishing extremely complex objects. The WT is a segmentation method based on regions, which classifies pixels according to their spatial proximity, the gradient of their gray levels and the homogeneity of their textures. To avoid over segmentation a single marker for each object of interest has to be selected [17].The selection of adequate markers on these kinds of images is a painful and sometimes fruitless task. Hence, the experienced observer defines markers in a semiautomatic way [18] [19] [20]. The automatic determination of markers is still a difficult goal to achieve. The current determination algorithms are highly dependent on the structure to be segmented [21] [22]. Moreover, they have a high computational cost and they determine markers in an effective but not automatic way when processing images [23].

The proposed algorithm uses, characteristics determined from the regions resulting from the over-segmentation produced by the watershed transform (WT) through regional minima. WT markers are selected as the cluster that represents the objects of interest. Finally WT is applied again over these new markers allowing an effective and robust segmentation of images. In this way two stage marker controlled watershed method is implemented.

II. Inputs, Methods And Results

2.1. Input Images

For this work, microscope images were used in order to evaluate the proposed algorithms due to the great difficulty that their segmentation presents. Cardiovascular microscopic images having atherosclerosis were used. In these images we need to segment the microscopic images in order to make a diagnosis. Image resolution is 3150 x 1446 pixels, 24 bpp. Figure 2(a) and 3(a) top original image is severe atherosclerosis of the aorta in which the atheromatous plaques have undergone ulceration along with formation of overlying mural thrombus. Figure 2(a) and 3(a) middle original image is coronary atherosclerosis with the complication of hemorrhage into atheromatous plaque, seen here in the center of the photograph. Such hemorrhage acutely may narrow the arterial lumen. Figure 2(a) and 3(a) bottom original image is Berkeley dataset image no. 317080, which is used here for algorithm validation.

2.2 Inputs and Methods

The proposed methodology is a two stage process. The first process uses WS to produce a primary segmentation of the input image, while the second process applies the marker controlled watershed segmentation algorithm to the primary segmentation to obtain the final segmentation map. Figure 1 describes block diagram of the proposed method.

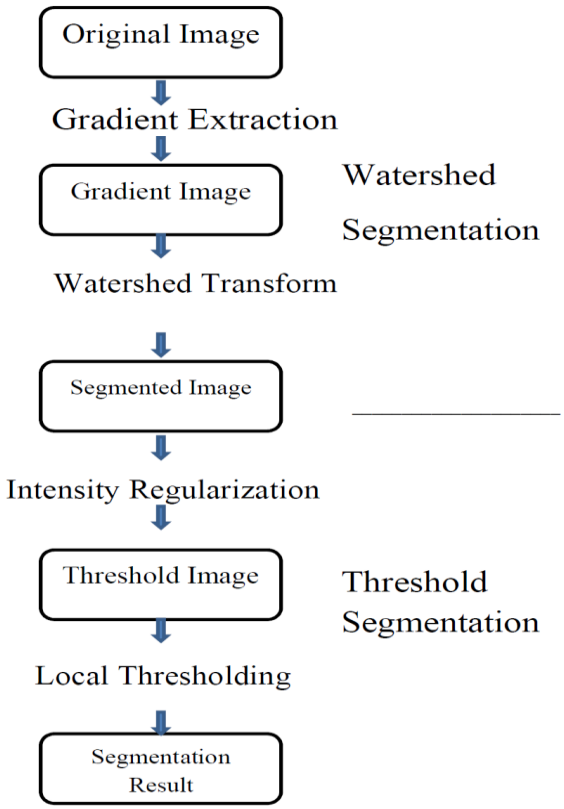

Fig.1 Block diagram of proposed segmentation procedure

2.2.1 Watershed Transformation Based Segmentation

1) Watershed Segmentation

Detecting Touching Objects is a challenging problem. Using Watershed Segmentation this problem can be solved. Here we used various morphological functions to perform marker-control watershed segmentation. A potent and flexible method for segmentation of objects with closed contours, where the extremities are expressed as ridges is the Marker-Controlled Watershed Segmentation. In Watershed Segmentation, the Marker Image used is a binary Image comprising of either single marker points or larger marker regions. In this, each connected marker is allocated inside an object of interest. Every specific watershed region has a one-to-one relation with each initial marker; hence the final number of watershed regions determines the number of markers. Post Segmentation, each object is separated from its neighbours as the boundaries of the watershed regions are arranged on the desired ridges. The markers can be manually or automatically selected, automatically generated markers being generally preferred. A solution to limit the number of regional minima is to use markers to specify the only allowed regional minima. The watershed transformation is a powerful tool for image segmentation. The segmentation of images by means of the watershed transform and the use of markers have many advantages: **1]** the watershed transform provides closed contours by construction. **2]** It avoids severe over-segmentation. In watershed segmentation topographic interpretation, there are 3 types of points: **1)** Points belonging to a regional minimum **2)** Points at which a drop of water would fall to a single minimum (The *catchment basin* or *watershed* of that minimum.) **3)** Points at which a drop of water would be equally likely to fall to more than one minimum. (The *divide lines* or *watershed lines*.) The elements labelled 1 belong to the first watershed region, the elements labelled 2 belong to the second watershed region, and so on. If the elements labelled 0 do not belong to a unique watershed region. These are called watershed pixels. 8-connected neighbourhoods are used for watershed implementation.

A gray scale image can be interpreted as the topographic image of land relief. It can be indicated that the gray intensities of higher amplitude correspond to plains and mountains and the lower intensity ones correspond to valleys and rivers [24] [25]. Using the characteristics of these images we define a technique of digital image processing called Watershed Transform (WT), which through the flooding of the valleys, is capable of recognizing similar topographical areas, surrounded by mountain ridges. The WT is a segmentation method based on regions, which classifies pixels according to their spatial proximity, the gradient of their gray levels and the homogeneity of their textures [26] [27]. With the objective of segmenting an image in gray levels, prior to the application of the WT, a gradient image must be obtained, where the levels of the contours of the

objects to be segmented represent an area of elevated gray intensity. The areas of low intensity give way to the basins where the water would flow and flood the topography of the image. The elevations in gray levels generated by the contours would remain and give way to the segmentation of the image through the resulting watershed lines [17] [26]. Mathematical morphology allows us to obtain a gradient which is highly adaptable to different kinds of images with a higher precision than conventional algorithms. In this paper we used the morphological gradient to obtain the intermediate image before applying the WT [28] [29].

The classic WT floods the gradient image from its regional minima. In non-homogeneous or noise embedded images there is not a one to one relation between regional minima and objects of interest. This results in an over segmentation in the majority of images, in other words, after WT each of the objects is represented by more than one region [17-19] [26] [30]. To avoid this over segmentation we resort to the selection of a single marker for each object of interest. Theses markers or seeds initiate the flooding algorithms indicating the sector that gives rise to the basins. Based on these characteristics we can conclude that the success of the WT depends mainly upon the characteristics of the markers.

2.2.2 Fuzzy C-means algorithm

Fuzzy C-M clustering [31] (FCM), also called as ISODATA, is a data clustering method in which each data point belongs to a cluster to a degree specified by a membership value. FCM is used in many applications like pattern recognition, classification, and image segmentation. FCM [32] divides a collection of n vectors c fuzzy groups and finds a cluster centre in each group such that a cost function of dissimilarity measure is minimized. FCM [33] uses fuzzy partitioning such that a given data point can belong to several groups with the degree of belongingness specified by membership values between 0 and 1. This algorithm is simply an iterated procedure. The algorithm is given below:

1] Initialize the membership matrix U with random values between 0 and 1.

2] Calculates C fuzzy cluster center C_i , i = 1, 2,… C ., using the following equation:

$$C_i = \frac{\sum_{j=1}^{n} u_{ij}^m x_j}{\sum_{j=1}^{n} u_{ij}^m} \tag{1}$$

3] Compute the cost by following equation. Stop when it is below a certain threshold or it improves over previous iteration.

$$J(U, C_{1,\ldots,} C_c) = \sum_{i=1}^{c} J_i = \sum_{i=1}^{c} \sum_{j}^{n} u_{ij}^m d_{ij}^2 \tag{2}$$

4] Compute a new U by the equation. Go to step 2.

$$u_{ij} = \frac{1}{\sum_{k=1}^{c} \left(\frac{d_{ij}}{d_{kj}} \right)^{\frac{2}{(m-1)}}} \tag{3}$$

5]

There is no guarantee ensures that FCM [34] converges to an optimum solution. The performance is based on the initial cluster centers. FCM also suffers from the presence of outliers and noise and it is difficult to identify the initial partitions.

2.2.3 Color Cluster segmentation

We also implemented color cluster segmentation algorithm. Features extracted from over segmentation resulting regions, after applying WT from its regional minima, are used as input to a clustering algorithm [23] [35]. There are different methods that group these regions to segment images; however none uses them to obtain the markers for the WT [36]. The basis for the development of this algorithm was to reduce the sensitivity of the algorithm to noise and irrelevant objects and to increase its robustness to process medical images with different features. We used two clustering algorithms. First the k means algorithm was used [22] [25] [37]. This unsupervised algorithm requires the specification of the number of classes in which the data set is going to be partitioned. To each class there is a corresponding cluster centre so that the distance of each pattern to its center

is minimal. The partition is done by measuring, in an iterative process, the distance between each pattern to its cluster center, and computing again the centres until there is no change. In a second stage the fuzzy k-means algorithm was used [21] [25]. This algorithm is based on fuzzy logic and assigns to each pattern a level of belonging to each class instead of offering a unique aggrupation of them.

Different regions are obtained by applying the WT to the original image. The mean and standard deviation of each region characterize different components in the images. The k-means algorithm applied to the features in those regions determined effectively the internal markers of the objects. The fuzzy k-means did not classify correctly the markers of any kind of regions. We applied morphological operators to the class that represents the objects to generate the internal markers. The markers of the background, external markers, were obtained eroding the internal markers complements. This procedure resulted in adequate segmentations when internal markers sizes are similar to the size of the objects. The gradient of the medical images does not have a visible contrast, making it difficult to apply the flooding algorithms. The method based on clustering is malleable and can be applied to all kinds of images. Consequently, by obtaining internal and external markers of a considerable size the results were improved. These properties of the markers were attained due to the use of the algorithm developed from the over segmentation.

2.2.4 K-means algorithm

K-means algorithm [31] is under the category of Squared Error-Based Clustering (Vector Quantization) and it is also under the category of crisp clustering or hard clustering. K-means algorithm is very simple and can be easily implemented in solving many practical problems. K-Means is ideally suitable for biomedical image segmentation since the number of clusters (k) is usually known for images of particular regions of human anatomy. Steps of the K-means algorithm are given below:

1) Choose k cluster centers to coincide with k randomly chosen patterns inside the hyper volume containing the pattern set (C).

2) Assign each pattern to the closest cluster center. i.e. (C_i , i=1, 2…C)

3) Recomputed the cluster centers using the current cluster memberships. (U):

$$u_{ij} = \left\{ \begin{array}{c} 1, if \left\| X_j - C_i \right\|^2 \le \left\| X_j - C_k \right\|^2 , foreach k \ne i \\ 0, otherwise \end{array} \right\} \quad (4)$$

4)

5) If convergence criterion is not met, go to step 2 with new cluster centers by the following equation, i.e. minimal decrease in squared error:

$$c_i = \frac{i}{G_i} \sum_{k, X_k \in G_i} X_k \quad (5)$$

6)

Where, $|G_i|$ is the size of G_i or $|G_i| = \sum_{j=1}^{n} u_{ij}$

The performance of the K-means algorithm depends on the initial positions of the cluster centers.

This is an inherently iterative algorithm. And also there is no guarantee about the convergence towards an optimum solution. The convergence centroids vary with different initial points. It is also sensitive to noise and outliers. It is only based on numerical variables. Coronary atherosclerosis images were processed with a clustering algorithm. Figure 2(e) shows the images resulting from the application of the clustering algorithm and figure 3(e) shows corresponding cluster plots. The Atherosclerosis images successful segmentation can be seen.

2.2.5 Watershed Transform based algorithm:

Step 1 Application of the WT using the regional minima as markers. The result is a matrix that assigns a label to each pixel indicating the regional minima to which it belongs.

Step 2 The regions resulting from the WT are analysed to obtain features from each one of them to distinguish the objects of interest based on their texture. Mean and standard deviation are computed from the intensities that are found inside the regions.

Step 3 The features vectors are used as input for the k-means algorithm.

Step 4 An image is obtained with only the class that distinguishes the objects of interest.

Step 5 Application of the morphological opening and closing operators on the markers to obtain the object markers, or internal markers [28] [29]. These operators join adjacent regions because they correspond

to the same object and eliminate regions that do not belong to the wanted objects. The previous result is slightly eroded to eliminate the regions that belong to the possible borders of the objects. As a final result we obtain the image that is to be used as the internal marker for the WT.

Step 6 Application of the morphological erosion to the complement of the internal markers, to obtain the background markers, or external markers.

Step 7 Application of WT using the internal and external markers computed in the previous steps, over the morphological gradient of the original image.

2.2.6 Proposed Marker Controlled Watershed Segmentation algorithm:

Segmentation using the watershed transforms works well if you can identify, or mark, foreground objects and background locations. The gradient magnitude of the primary segmentation is obtained by applying the Sobel operator. The Canny edge detector was also experimented on, but it was found that the results obtained by both methods are comparable. Hence, we decided on the Sobel filter as the Canny edge detector has higher complexity. In addition, the Sobel filter has the advantage of providing both a differencing and smoothing effect. Marker controlled watershed segmentation follows this basic procedure:

1) Compute a segmentation function. This is an image whose dark regions are the objects we are trying to segment.
2) Compute foreground markers. These are connected blobs of pixels within each of the objects.
3) Compute background markers. These are pixels that are not part of any object.
4) Modify the segmentation function so that it only has minima at the foreground and background marker locations.
5) Compute the watershed transform of the modified segmentation function. Finally the WT was applied to the gradient image of the original image using the markers obtained in the previous steps. It was not possible to obtain this result with other conventional methods of image segmentation.

Openings with structuring elements of 3x3 pixels were applied, obtaining unequivocal and homogeneous internal markers for each one of the objects of interest. To apply the WT it is necessary to mark not only the objects but also the background. We need to define the internal markers for the objects of interest as well as the external markers. The latter ones were obtained through the morphological erosion of the complement of the internal markers. To obtain the object markers, or internal markers, morphological opening and closing operators are applied. These unite the adjacent regions that correspond to the same object and eliminate the regions that do not belong to the wanted objects. Then the result is eroded to eliminate the regions that belong to the possible borders of the objects. As a result the internal markers for the WT are obtained. The background markers or external markers are obtained eroding the complement to the internal markers. Finally, the WT is again calculated with the internal and external markers previously determined and the morphological gradient of the original image. Figure 3(c) shows the resulting segmentation. Medical images were successfully segmented. It was possible to analyse atherosclerosis images that could not be segmented with other algorithms of marker detection. The morphological operations and WT have a minimal computational cost. The error of the algorithms can be determined by a parameter μ based on the symmetrical distance and the Hausdorff distance [38].

Segmentation using the watershed transforms works well if we can identify, or "mark," foreground objects and background locations. Marker-controlled watershed segmentation (figure 6) follows this basic procedure:

Step 1: Read in the original color microscopic images of coronary artery and convert it to grayscale.

Step 2: Use the gradient magnitude as the segmentation function. Compute a segmentation function. Input various microscopic images whose regions are the objects to be segmented. The gradient is high at the borders of the objects and low (mostly) inside the objects. Gradient can be computed by $Gradmag = \sqrt{I_x^2 + I_y^2}$. The watershed transform directly on the gradient magnitude will generate “over segmentation”, so markers are introduced in the image.

Step 3: Mark the foreground objects. These are connected blobs of pixels within each of the objects. The foreground markers, which must be connected blobs of pixels inside each of the foreground objects. Here we used morphological techniques called "opening-by-reconstruction" and "closing-by-reconstruction". These operations will create flat maxima inside each object. Opening is erosion followed by dilation, while opening-by-reconstruction is erosion followed by a morphological reconstruction. To obtain good foreground markers, reconstruction-based opening and closing are more effective than standard opening and closing at removing small imperfections without affecting the overall shapes of the objects, for that compute the regional maxima. Ideally we don't want the background markers to be too close to the edges of the objects we are trying to segment. We'll "thin" the background by computing the "skeleton by influence zones". This can be done by

computing the watershed transform of the distance transform of black and white image, and then looking for the watershed ridge lines (ideally zero) of the result.

Step 4: Compute background markers. These are pixels that are not part of any object. The markers of the background or external markers were obtained by morphological erosion of the internal markers complements. This procedure resulted in adequate segmentations when the internal markers and the objects of interest are of similar size. Perform minima imposition through morphological reconstruction by erosion of $(f_g + 1) \wedge f_m)$ from f_m which can be written by $f_{g\min} = R^E_{(f_g+1)\wedge f_m}(f_m)$ so that markers are only at the single minima (figure 1(a)). Thus we obtain automatic selection of markers. Where, f_g = gradient image having many local minima; f_m = marker image; R^E = Region created through morphological reconstruction by erosion; $f_{g\min}$ = single global minimum morphological reconstruction.

Step 5: Modify the segmentation function so that it only has minima at the foreground and background marker locations. Here, modify the gradient magnitude image, so that its only regional minima occur at foreground and background marker pixels.

Step 6: Compute the watershed transform (second time) of the modified segmentation function. In this application on microscopic images of coronary arteries, we have applied two stage watershed algorithms to take care for over segmentation.

Step 7: Obtained threshold image. Here threshold selected for the skeleton of the image.

Step 8: Representation and Visualization of the results in form of color watershed. For better interpretation of results, one visualization technique is to superimpose the foreground markers, background markers, and segmented object boundaries on the original image.

Step 9: To help interpret the result, superimpose the color segmented image on the original image.

The intuitive idea underlying the notion of watershed comes from the field of topography: a drop of water falling down on a topographic surface follows a descending path and reaches a regional minimum area. The watershed may be thought of as the separating lines of the domain of attraction of drops of water.

The regions of a watershed, also called catchment basins, are associated with the regional minima of the map. In other words, each catchment basin contains a unique regional minimum, and conversely, each regional minimum is included in a unique catchment basin: the regions of the watershed are the connected components of an extension relative to the minima. They are separated by a set of edges from which a drop of water can flow down towards different minima.

2.2.7 Assessment parameters:

A] The structural similarity (SSIM) index [39] is a method for measuring the similarity between two images. The SSIM index is a full reference metric, in other words, the measuring of image quality based on an initial uncompressed or distortion-free image as reference. SSIM is designed to improve on traditional methods like peak signal-to-noise ratio (PSNR) and mean squared error (MSE), which have proved to be inconsistent with human eye perception.

The SSIM metric is calculated on various windows of an image. The measure between two windows *x* and *y* of common size *N*×*N* is:

$$SSIM(x,y) = \frac{(2\mu_x\mu_y + c_1)(2\sigma_{xy} + c_2)}{\mu_x^2 + \mu_y^2 + c_1)(\sigma_x^2 + \sigma_y^2 + c_2)} \tag{6}$$

With

μ_x The average of x;

μ_y The average of y;

σ_x^2 The variance of x;

σ_y^2 The variance of y;

σ_{xy} The covariance of x and y;

$c_1 = (k_1 L)^2$, $c_2 = (k_2 L)^2$ two variables to stabilize the division with weak denominator;

L The dynamic range of the pixel-values (typically this is $2^{\#bitsperpixel}-1$);
$k_1 = 0.01$ and $k_2 = 0.03$ by default.

In order to evaluate the image quality this formula is applied only on luma. The resultant SSIM index is a decimal value between -1 and 1, and value 1 is only reachable in the case of two identical sets of data.

B] The universal image quality index (UIQI or Q) which measures the distortion between two images. The dynamic range of Q is between -1 and 1, the best value of Q = 1 is achieved if and only if the two images are equal. Higher the Q values, the less will be the distortion between the original and the processed image.

III. Results and Discussion

We implemented these algorithms on a 64 bit operating system Window 7(Ultimate), Mat Lab 7.11.0 (R2010b) [40] (Intel Core i5 3.6 GHz and 4GB RAM). In this research paper, we compared results of Otsu thresholding, Fuzzy C-means clustering, K-means clustering and marker controlled watershed algorithm. And also we showed that our proposed method produced segmentation maps which gave fewer partitions than the segmentation maps produced by the conservative watershed algorithm.

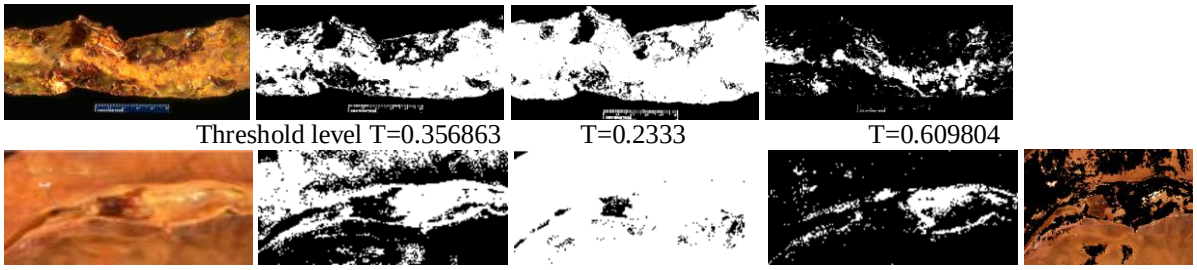

Fig. 2 Results of Otsu, FCM0 level, FCM1 level and Color Clustering (CC) Segmentation Techniques (a) Original images of Atherosclerosis, Coronary Atherosclerosis (b) Results of Otsu Thresholding method (c) Results of Fuzzy C Means level 0 method (d) Results of Fuzzy C Means level 1 method (e) Segmentation result of CC technique.

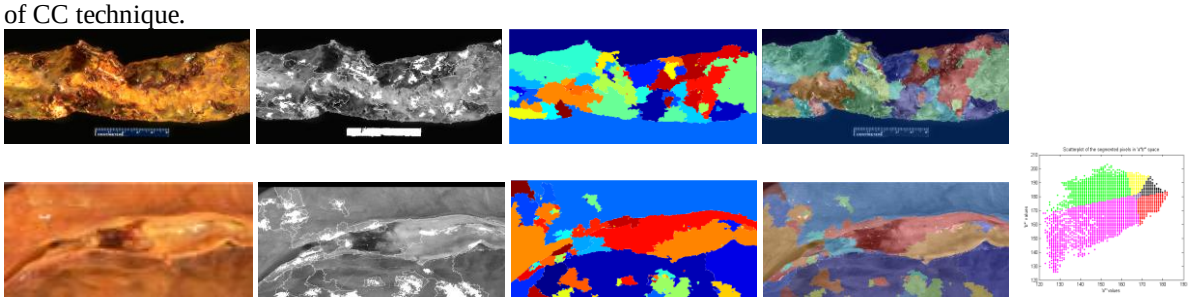

Fig. 3 Results of proposed marker control Watershed (MCWS) Segmentation Technique (a) Original images of Atherosclerosis, Coronary Atherosclerosis (b) Gradient magnitude of original image of figure 3(a) with MCWS (c) Colored segmentation using MCWS (d) Colored segmentation superimposed on original image of figure 3(a) (e) Graph using CC technique.

TABLE 1: Formulas for assessment parameters

Name of Parameters	**Formulas**	**Ideal or Desired Value**
Mean Square Error	$MSE = \frac{1}{MN}\sum_{m=1}^{M}\sum_{n=1}^{N}(x_{m,n} - \bar{x}_{m,n})^2$	Lower

Peak Signal to Noise Ratio	$PSNR = 10\log\frac{(2^n-1)^2}{MSE} = 10\log\frac{255^2}{MSE}$	Higher
Normalized Absolute Error	$NAE = \sum_{m=1}^{M}\sum_{n=1}^{N}\left\|x_{m,n} - \bar{x}_{m,n}\right\| \Big/ \sum_{m=1}^{M}\sum_{n=1}^{N}\left\|x_{m,n}\right\|$	Lower

TABLE 2: Results of segmented image of Atherosclerosis figure 3(c) upper with assessment parameters

Sr. No.	Methods	MSE	PSNR	NAE	STD	CoV	UIQI	Corr Coeff	SSIM
1	MCWS	**5709.3**	**10.5650**	0.8573	**71.0361**	**2207.9**	0.4539	0.4876	0.4570
2	Otsu	6204.9	10.2034	0.8135	120.7704	6764.3	**0.6770**	**0.8792**	**0.6778**
3	FCM0	15290	6.2867	1.3402	119.8344	5236	0.4299	0.6859	0.4309
4	FCM1	**5549**	**10.6887**	**0.7784**	79.2966	3187.4	0.4607	0.6310	0.4624

TABLE 3: Results of segmented image of Coronary atherosclerosis figure 3(c) lower with assessment parameters

Sr. No.	Methods	MSE	PSNR	NAE	STD	CoV	UIQI	Corr Coeff	SSIM
1	MCWS	**4253.4**	**11.8434**	**0.4389**	**53.8765**	537.5480	0.2683	0.3435	0.2785
2	CCT	9632.1	8.2936	0.5338	58.7586	-430.4538	-0.1560	-0.2522	-0.1435
3	Otsu	9363.1	8.4166	0.7129	114.3957	2430.9	**0.3455**	**0.7324**	**0.3482**
4	FCM0	15604	6.1984	0.9415	**42.7048**	**346.7194**	0.2139	0.2798	0.2269
5	FCM1	14703	6.4567	0.9037	71.2572	602.0788	0.0860	0.2912	0.0894

Abbreviations: MCWS=Marker Control Watershed Segmentation method; Otsu= Otsu Thresholding method; CCT=Color Clustering Technique; FCM0=FCM 0 level method; FCM1=FCM 1 level method; MSE=Mean Square Error; PSNR=Peak Signal to Noise Ratio; NCC=Normalized Cross Correlation; AD= Average Difference; SC=Structural Content; NAE= Normalized Absolute Error; STD=Standard Deviation; CoV= Covariance; UIQI=Universal Image Quality Index; Corr Coeff = Correlation Coefficient; SSI=Structural Similarity Index Matrix.

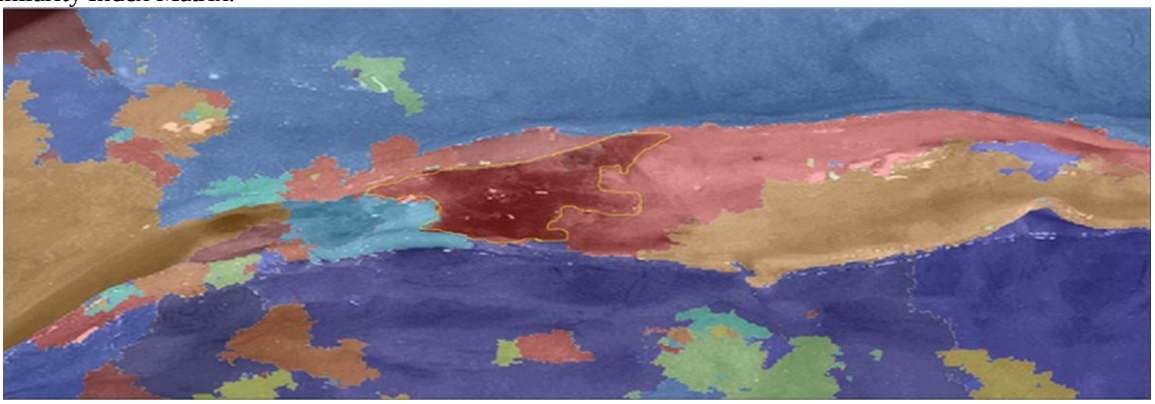

Figure 4 Region of interest of segmented image with proposed technique for coronary atherosclerosis with the complication of hemorrhage into atheromatous plaque.

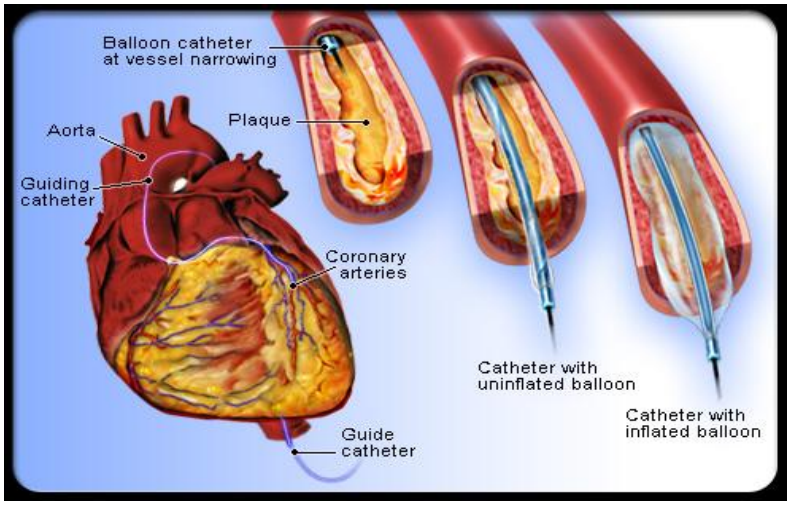

Figure 5: Insertion of Catheter in coronary arteries to remove plaque [41].

We applied our proposed methodologies of K Means clustering, Fuzzy C-means clustering and marker controlled watershed algorithm to medical images of the atherosclerosis images and obtained general segmentation maps of them. Fig. 2 shows the results of Otsu, FCM0 level, FCM1 level and Color Clustering (CC) Segmentation Techniques. Fig. 2 (a) is the original images of Atherosclerosis of aorta and Coronary Atherosclerosis. Fig. 2 (b-e) shows the results of Otsu thresholding method, results of fuzzy C means level 0 methods, and results of fuzzy C means level 1 method and segmentation result of CC technique respectively. Otsu, FCM0 level, FCM1 level and Color Clustering (CC) Segmentation Techniques are considered for comparisons because those methods provide segmentation results which are visually and quantitative way comparable with our proposed segmentation technique MCWS.

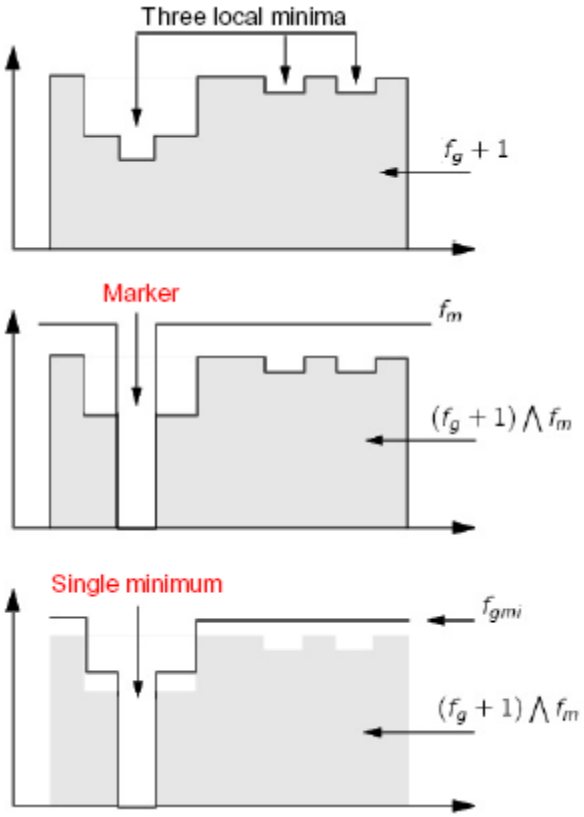

Figure 6: Representation of proposed watershed transformation in two dimensions

TABLE 4: Values for Region of Interest of segmented image of figure 4

Image	Area	Mean	StdDev	Perim.	Circ.	Feret	IntDen	Skew	Kurt
Fig 3(d) lower	1.766	86.677	25.313	8.524	0.305	2.938	153.077	0.652	1.175

Abbreviations: StdDev=Standard Deviation; Perim. =Perimeter; Circ=Circularity; IntDen=Integrated Density; Skew=Skewness; Kurt= Kurtosis.

Fig. 3 shows the results of proposed marker control Watershed (MCWS) Segmentation Technique. Fig. 3 (a) is the original images of Atherosclerosis of aorta and Coronary Atherosclerosis. Fig. 3 (b-e) represent the gradient magnitude of original image of figure 3(a) with MCWS , colored segmentation using MCWS , colored segmentation superimposed on original image of figure 3(a) and Graph using CC technique respectively. Table 1 represents the formulas for assessment parameters and mention about what should be their ideal values.

Table 2, 3 and 4 show the segmentation results. Ideally error should be small. So MSE and NAE values should be smaller, which are obtained through proposed MCWS algorithm. A higher value of PSNR is better, which is also obtained by proposed algorithm. Standard deviation and Co variance should be lower value, which is also good for proposed algorithm. As seen from table 2, for Atherosclerosis image using marker controlled WS(MCWS) method, the values of MSE=5709.3, PSNR=10.5650, STD=71.0361 and CoV=2207.9 which are best as compared to Otsu method and Fuzzy C means. It can be observed in table 2, that the values of UIQI= 0.6770, Corr Coeff = 0.8792 and SSI= 0.6778 parameters are best for atherosclerosis image using Otsu method among all methods. As seen from table 3, for Coronary Atherosclerosis image using marker controlled WS(MCWS) method, the values of MSE=4253.4, PSNR=11.8434, NAE=0.4389 and STD=53.8765, which are best as compared to Otsu method and Fuzzy C means. Results of Coronary atherosclerosis of FCM0 method for STD = 42.7048 which is on gray image, while MCWS results are on color images. As seen from table 2 and table 3, the values of UIQI (range -1 to 1) and SSI(range -1 to 1) are better for Otsu thresholding technique for all images i.e. atherosclerosis, coronary atherosclerosis, which proves the consistency of all algorithms. Values toward 1 are better. Here, it is observed that MCWS algorithm gives results in form of color segmentation and provides better results for majority of assessment parameters. TABLE 4 represents the values for Region of Interest (ROI) of segmented image of figure 3(d) lower image, which is coronary atherosclerosis with the complication of hemorrhage into atheromatous plaque. We evaluated the performance of our proposed methodologies by comparing them with conservative watershed algorithm. The use of marker controlled watershed segmentation algorithm had achieved the objective of reducing the problem of over segmentation when applied to atherosclerosis images.

IV. Conclusion

This paper presents, application of Segmentation Techniques on Atherosclerosis Images using Otsu thresholding method, Fuzzy C means level 0, Fuzzy C means level 1, color clustering algorithm and with marker controlled watershed algorithm. Marker controlled watershed algorithm gave better segmentation than all other algorithms. By reducing the amount of over segmentation, we obtained a segmentation map which is more diplomats of the several anatomies in the medical images. It addressed the limitations of the conservative watershed algorithm, which included over segmentation. Comparing with the algorithm based on fuzzy logic, clustering is not only automatic but it is also able to segment the atherosclerosis images with a lower error. The marker controlled watershed algorithm presents smaller computational costs than the algorithm based on clustering. With our proposed algorithm we obtained desired values for various assessment parameters. Here with proposed algorithm, we obtained MSE and NAE values lower, PSNR values higher. Deviation and Variance of pixels for segmentation results are less. UIQI and SSIM values are sufficiently moderate. Finally, values for Region of Interest of resultant segmented image using proposed MCWS method are computed and presented in table 4 from which severity of atherosclerosis can be determine.

References

[1] Milan Sonka, Vaclav Hlavac, Roger Boyle, Image Processing, Analysis and Machine Vision, 2nd ed., Bangalore , by Thomson Asia Pte Ltd., Singapore, first reprint 2001, pp-186.
[2] Anil k. Jain, Fundamentals of Digital Image Processing, Delhi, Published by Pearson Education, 3rd Impression, 2008, pp-370.
[3] J. L. Vincent, "Morphological grayscale reconstruction in image analysis: Application and efficient algorithms," IEEE Trans. Image Proc., vol. 2, pp. 176-201, 1993.
[4] S. Beucher, "Watershed, hierarchical segmentation and waterfall algorithm," Mathematical Morphology and Its Applications to Image Processing, Dordrecht, and The Netherlands: Kluwer pp. 69-76, 1994.
[5] V. Grau, A. U. J. Mewes, M. Alcaniz, R. Kikinis and S. K. Warfield, "Improved Watershed Transform for Medical Image Segmentation Using Prior Information," IEEE Trans. Medical imaging, vol. 23, No. 4, pp. 447-458, April 2004.
[6] Valerie Pazos, Rosaire Mongrain, and Jean-Claude Tardif, "Mechanical Characterization of Atherosclerotic Arteries Using Finite-Element Modeling: Feasibility Study on Mock Arteries," IEEE Trans. on biomedical Eng., vol. 57, no. 6, June 2010.

[7] Christof Karmonik, Pamela Basto, Kasey Vickers, Kirt Martin, Micheal J. Reardon, Gerald M. Lawrie, and Joel D. Morrisett, "Quantitative Segmentation of Principal Carotid Atherosclerotic Lesion Components by Feature Space Analysis Based on Multicontrast MRI at 1.5 T," IEEE Transactions on biomedical engineering, vol. 56, no. 2, February 2009.

[8] Danijela Vukadinovic, Theo van Walsum, Rashindra Manniesing, Sietske Rozie, Reinhard Hameeteman, Thomas T. de Weert, Aad van der Lugt, and Wiro J. Niessen, "Segmentation of the Outer Vessel Wall of the Common Carotid Artery in CTA," IEEE Transactions on medical imaging, vol. 29, no. 1, January 2010

[9] Gozde Unal, Susann Bucher, Stephane Carlier, Greg Slabaugh, Tong Fang, and Kaoru Tanaka, "Shape-Driven Segmentation of the Arterial Wall in Intravascular Ultrasound Images," IEEE Trans. on info. Tech. in biomedicine, vol. 12, no. 3, May 2008

[10] Simon Le Floch, Jacques Ohayon, Philippe Tracqui, Gerard Finet, Ahmed M. Gharib, Roch L. Maurice, Guy Cloutier, and Roderic I. Pettigrew, "Vulnerable Atherosclerotic Plaque Elasticity Reconstruction Based on a Segmentation-Driven Optimization Procedure Using Strain Measurements: Theoretical Framework," IEEE Trans. on medical imaging, vol. 28, no. 7, July 2009.

[11] Gonzalez, R.C., R.E. Woods and S.L. Eddins, 2004.Digital Image Processing using MATLAB. 1st Edn., Pearson Education India, India, and ISBN: 9788177588989, pp.: 620.

[12] Jayaraman, S., 2009. 'Digital Image Processing', 1st Edn., Tata McGraw Hill Education, New Delhi, and ISBN: 780070144798, pp: 723.

[13] Murugavalli, S. and V. Rajamani, "An improved implementation of brain tumor detection using segmentation based on neuro fuzzy technique," J. Comput. Sci., 3: 841-846. DOI: 10.3844/jcssp.2007.841.846, 2007.

[14] Shanmugam, N., A.B. Suryanarayana, D. Chandrashekar and C.N. Manjunath, 2011, "A novel approach to medical image segmentation," J. Comput. Sci., 7: 657-663. DOI: 10.3844/jcssp.2011.657.663

[15] Velmurugan, T. and T. Santhanam, "Computational complexity between k-means and kmedoids clustering algorithms for normal and uniform distributions of data points" J. Comput. Sci., 6: 363-368. DOI: 10.3844/jcssp.2010.363.368

[16] C. A. Glasbey and G W Horgan, "Image analysis for the biological science," Statistics in Practice, Series Editor Vic Barnett, Jonh Wiley and Sons 1994.

[17] L Vincent and P. Soille, "Watersheds in digital spaces: An efficient algorithm based on immersion simulations," *IEEE trans. Pattern Anal,* Machine Intell 1991, 13:583-598.

[18] J. M. Gauch, "Image segmentation and analysis via multiscale gradient watershed hierarchies," *IEEE Trans. on Image Processing* 1999, 8 (1):69-79

[19] P. Jackway, "Gradient Watersheds in morphological scalespace," IEEE *trans. Image Processing,* Machine Intell., 1996, 5:913-921

[20] D. Wang, "A multiscale gradient algorithm for Image Segmentation using Watersheds," *Pattern Reconition,* 1997, 30:2043-2052

[21] P. V. Gorsevski, P. E. Gessler and P. Jankowski, "Integrating a fuzzy k-means classification and bayesian approach for spatial prediction of landslide hazard," *J. of Geographical Systems,* 2003, 5:5930-5949.

[22] X. Li and G. Harnarneh, "Modeling prior shape and appearance knowledge in watershed segmentation*," Image Vision Comput,* 2007.

[23] M. A. Gonzalez and V. L. Ballarin, "Determinación automática de marcadores para la Transformada Watershed mediante técnicas de clasificación de patrones," *9vo Simposio Argentino de Informática y Salud (SIS),* 2006

[24] K.Castleman, Digital Image Processing. Ch. 15, Prentice Hall 1979

[25] R. González and R. Woods, Addison Wesley 1996.

[26] S. Beucher and F. Meyer, "The morphological approach to segmentation: The Watershed Transformation," Mathematical Morphology and its application to image processing, optical engineering. TT16 1994

[27] M. Couprie and G. Bertrant, "Topological grayscale Watershed Transform," SPIE *Vision Geometry Proceedings* 1997, 3168:136-146

[28] E. R. Dougherty J. and Astola, "An introduction to nonlinear image processing," Ed. New York: Marcel Decker 1993, 433-481

[29] Mariela A. Gonzalez, Teresita R. Cuadrado, Virginia L. Ballarin, "Comparing marker definition algorithms for Watershed segmentation in microscopy images," JCS&T Vol. 8 No. 3 October 2008

[30] L. S. Stanislav and S. Wolfgang, "Extracting regions of interest applying a local watershed transformation," *Proc. of IEEE Visualization* 2000

[31] M.C. Jobin Christ and R.M.S. Parvathi, "Segmentation of Medical Image using Clustering and Watershed Algorithms," American Journal of Applied Sciences 8 (12): 1349-1352, 2011 ISSN 1546-9239

[32] M. Ceccarelli, F. Musacchia and A. Petrosino, "A fuzzy scale-space approach to feature-based image representation and retrieval," Brain Vision and Artificial Intelligence 2006, 377-385

[33] Ceccarelli M and Petrosino A, "A parallel fuzzy scale-space approach to the unsupervised texture separation," Pattern Recognition Letters 2002, 5: 557-567.

[34] Cheng H D, Chen Y H and Sun Y, "A novel fuzzy entropy approach to image enhancement and thresholding," Signal Processing, 1999, 75:277-301.

[35] Gonzalez M A and Ballarin V L, "Segmentación de imagines mediante la Transformada Watershed: Obtención de marcadores mediante Morfología Matemática," *9vo Simposio Argentino de Informática y Salud (SIS),* 2006

[36] S. E. Hernandez and K. E. Barner, "Joint region merging criteria for Watershed-Based image segmentation," *IEEE Trans on Image Processing,* 2000

[37] J. B. Mc Queen, "Some Methods for Classification and Analysis of Multivariate Observation," Proceedings of the 5th *Berkeley Symposium on Mathematical Statistics and Probability* 1967, Berkeley University of California Press, 281-297.

[38] J.Pastore, E.Moler and V.Ballarin, "Comparison of segmentation techniques by means of non-Euclidean distances," *Digital Signal Processing* (revision) 2006.

[39] http://en.wikipedia.org/wiki/Structural_similarity.

[40] http://www.mathworks.in

[41] http://saintlukeshealthsystem.adam.com/content.aspx?productId=108&pid=1&gid=000171

Janak B. Patel (born in 1971) received B.E. (Electronics & Communication Engg from L.D. College of Engg. Ahmedabad, affiliated with Gujarat University and M.E. (Electronics Communication & System Engg.) in 2000 from Dharmsinh Desai Institute of Technology, Nadiad, affiliated *with* Gujarat University. He is Asst. Prof. & H.O.D. at L.D.R.P. Institute of Technology & Research, Gandhinagar, and Gujarat. He has submitted his Ph.D. thesis at Indian

Institute of Technology, Roorkee under quality improvement program of AICTE, India. His research interest includes digital signal processing, image processing, bio-medical signal and image processing. He has 7 years of industrial and 12 years of teaching experience at Engineering College. He taught many subjects in EC, CS and IT disciplines. He is a life member of CSI, ISTE & IETE.

R.S. Anand received B.E., M.E. and Ph.D. in Electrical Engg. from University of Roorkee (Indian Institute of Technology, Roorkee) in 1985, 1987 and 1992, respectively. He is a professor at Indian Institute of Technology, Roorkee. He has published more than 100 research papers in the area of image processing and signal processing. He has also supervised 10 PhDs, 60 M.Tech.s and also organized conferences and workshops. His research areas are biomedical signals and image processing and ultrasonic application in non-destructive evaluation and medical diagnosis. He is a life member of Ultrasonic Society of India.

IOSR Journal of VLSI and Signal Processing (IOSR-JVSP)
e-ISSN: 2319 – 4200, p-ISSN No. : 2319 – 4197 Volume 1, Issue 6 (Mar. – Apr. 2013), PP 68-75
www.iosrjournals.org

Low Power R4SDC Pipelined FFT Processor Architecture

Anjana R[1], Krunal Gandhi[2], Vaishali lad[3]
Assistant professor [1],Lecturer [2,3], Laxmi Institute of technology,Gujarat

***Abstract**: When the real-time signal processing is required pipelined FFT is the suitable option because of its high throughput and low power demands. A number of FFT architectures are there. Radix-4 single delay commutator (R4SDC) architecture is researched in this paper. R4SDC is the most popular pipeline FFT architectures, because of its efficient use of butterflies and multipliers.*

In this a low power technique for the pipeline FFT architecture is discussed. In this, Conventional R4SDC architecture, complex multiplier, and multiplier-less architecture based on common sub-expression technique are implemented and compared for 16, 64 and 256-point FFT architectures. A new type of multiplier algorithm called Multiplier-less architecture is implemented and compared with the carry save array, Wallace and Conventional complex multiplier (NBW).

I. Conventional R4SDC FFT Architecture

R4SDC was first proposed in [1], a brief introduction is given in Chapter-4. Each stage in R4SDC includes a complex multipliers and a full radix-4 butterfly. The R4SDC architecture can be directly interfaced to a sequential word input without the requirement for input buffers. [1]. A 16-point pipeline FFT processor is shown in Figure 1. Equation 1 defines computation for the first stage [*1*].

$$x_1(q_1,m_1) = W_N^{Q_1 m_1} \sum_{p=0}^{r_1-1} W_{N1}^{pm_1} x_1(N_1p+q_1) \quad (1)$$

Equation 5.2 defines the computation for the final stage.

$$X(r_1r_2\ldots r_{v-1}m_v + \ldots\ldots + r_1m_2 + m_1) = \sum_{q_{v-1}=0}^{r_{v-1}} W_{rv}^{Qv-1}\, x_{v-1}(q_{v-1,}\, m_{v-1}) \quad (2)$$

Equation 5.3 defines the computation for the intermediate stages: [*Ref.[20]*].

$$x_t(q_t,m_t) = W_{Nt-1}^{q_t m_t} \sum_{p=0}^{r_t-1} W_{rt}^{pm_t}\, x_{t-1}(N_tp+q_t\, m_{t-1}) \quad (3)$$

Where for both the equation 5.2 and 5.3, , 2 □□*t* □□*v* □1, 0 □ m_t□ r_i-*1* , 0 □□ q_i □*N-1* and 2 □□*i* □□*v*

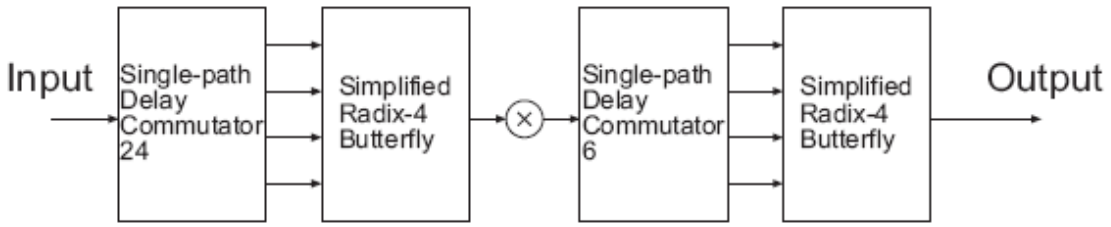

Figure 1: 16-*point pipelineR4SDC processor architecture.*

Butterfly:

The butterfly element performs the summation in Equation 1, 2 and 3. The summations can be replaced by six programmable adder/subtractors with the control circuits, as shown in Figure 2. Three complex adder/subtractors (each comprising of a real and an imaginary element) are used instead of eight complex adders. Control signal, stored in ROM unit selects the data fed into add/subs modules, according to the value of *mt.* This butterfly architecture generates *N* outputs consecutively in *N* word cycles, compared to the R4MDC butterfly which generates *N* outputs in *N/4* word cycles, with *N/3* word cycles idle. [1].

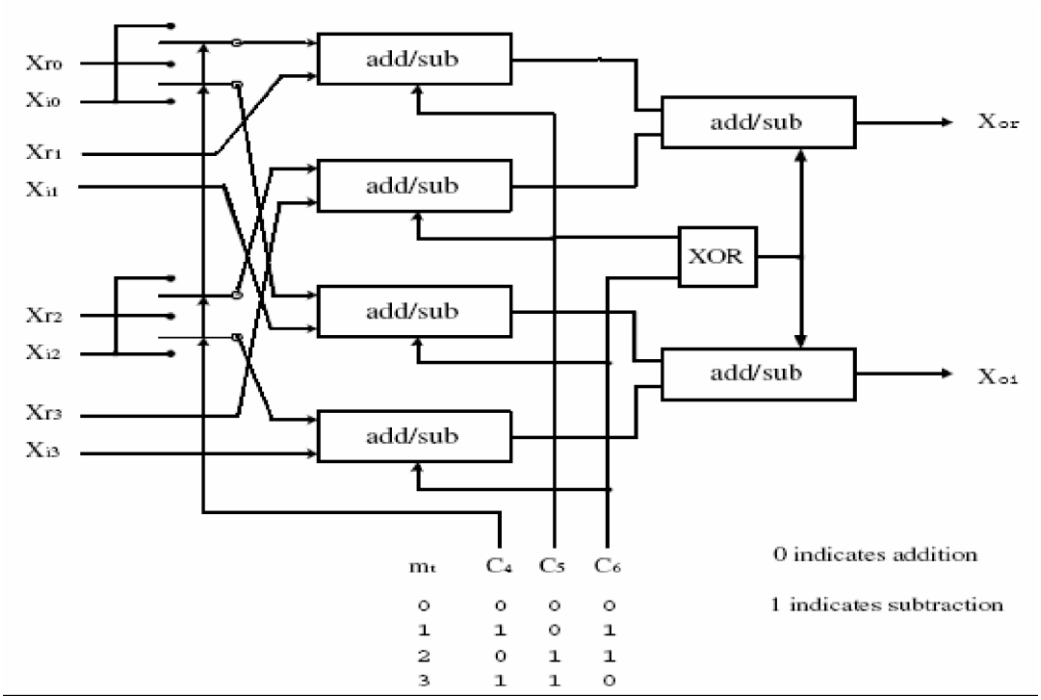

Figure 2: Conventional butterfly architecture for stage t in R4SDC pipelined FFT.
[1]

Conventional Complex Multiplier

In [Ref 8],a conventional complex multiplier accepts two complex inputs namely data (*Xr + jXi*) and coefficient (*Wr + jWi*) and produces a complex output (*XOr + jXOi*). It is constructed by using four real multipliers along an adder and a subtractor. The outputs and inputs are of the complex multiplier are related as:

$$XO_r=(X_rW_r - X_iW_i)$$
$$XO_i=(X_iW_r - X_rW_i)$$

The complex multiplier is shown in Figure 3. The product of the for real multipliers are truncated from 32 bits to 16 bits. The reduced precision achieves significant saving on hardware implementation, with acceptable error.

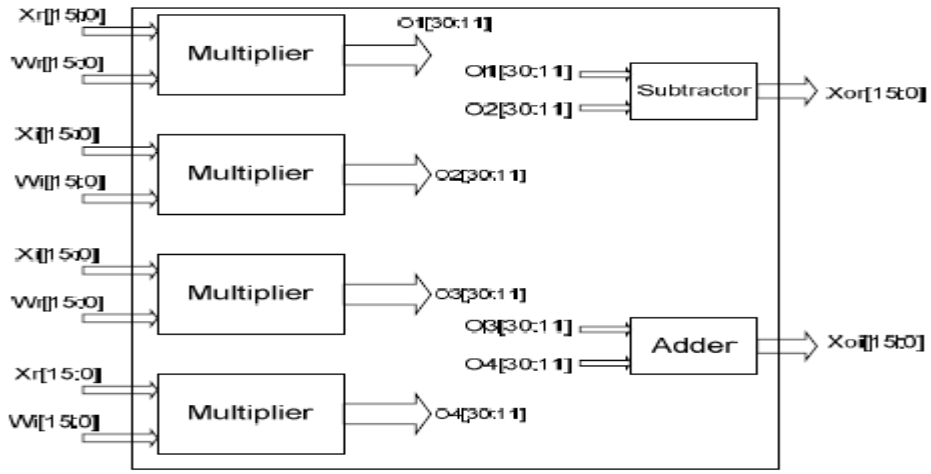

Figure 3: The block diagram of the Conventional Complex Multiplier.[2]

5.1.3 Commutator Architecture

In [9], the commutator architecture is conventional R4SDC FFTs is based on the Shift register architecture (SR) discussed in section 3.2, Chapter-3. Block diagram of the SR architecture is shown in Figure 4.

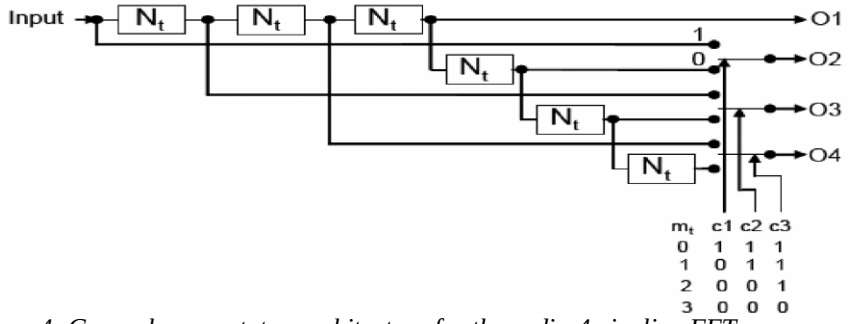

Figure 4: General commutator architecture for the radix-4 pipeline FFT processor.[9]

II. Methodology: Ordered R4SDC FFT Architecture

In this approach coefficient are reordered to save the power consumption by reducing the switching activity between the successive coefficients fed into the complex multiplier. Coefficients are ordered offline. Corresponding to the coefficient ordering, input is also ordered same as to make it Decimation in frequency algorithm and also to reduce the switching activity.

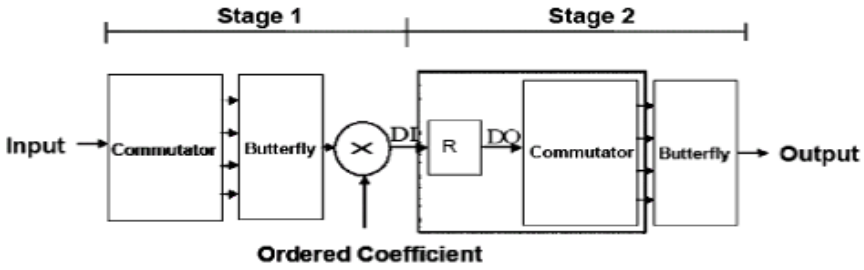

Figure5: 16-point ordered R4SDC pipelined FFT architecture [9]. R – RAM

The coefficients are reordered in order to minimize switching activity between successive coefficients by minimizing the hamming distance for each coefficient transition. The hamming distance is defined as the number of 1's of the XOR operation between two binary coefficients. Both original coefficient sequence and ordered coefficient sequence are encoded with the 16 bit fix point. The switching activity is accumulated by XOR the present coefficient by the previous coefficient sequence. To develop the minimum switching activity,we have developed the transition matrix of the hamming distance beween each coefficient as shown in table.

Our approach involves ordering the coefficient sequence so as to minimize swithing activity between successive coefficients fed to the multiplier for stage 1 of q 16-point FFT as listed in table 1.

Table 1
The transition matrix of switching activity
between each two coefficient with 16 word length

	W0	W1	W2	W3	W4	W6	W9
W0	0	15	17	19	3	21	13
W1	15	0	14	16	12	20	24
W2	17	14	0	14	14	16	14
W3	19	16	14	0	16	12	18
W4	3	12	14	16	0	20	16
W6	21	20	16	12	20	0	16
W9	13	24	14	18	16	16	0

From this transition matrix, we can arrange the twiddle factor in order to minimize the switching activity easily. The Coefficients are ordered so as to minimize switching activity between successive coefficients by minimizing the hamming distance between them.The ordered coefficient set is obtained by first arranging only imaginary part of the coefficient set on the basis of Hamming distance. It is followed by picking

up the corresponding real part of the coefficient or its two's complement depending upon the hamming distance with respect to the previously arranged real part.

The design complexity of ordered FFT and the size of the additional RAM increases as the size of the additional RAM increase as the size of the FFTs increases. Hence the reordering technique is suitable for stage-1 of a 16-point radix-4 FFT processor due to the need of restoring data ordering for the following stage.

Complex Multiplication

First, we discuss the implementations of complex multiplications with real multiplication.The product of complex numbers,X=A+jB and Y=C+jD is (A+jB)(C+jD)=(AC-BD)+j(AD+BC). The direct computations of complex multiplications requires four real multiplications and two two additions and thus requires large chip area and power consumption.

Another method to compute a complex multiplications is to modify the original computation is to modify the original computation as follows.

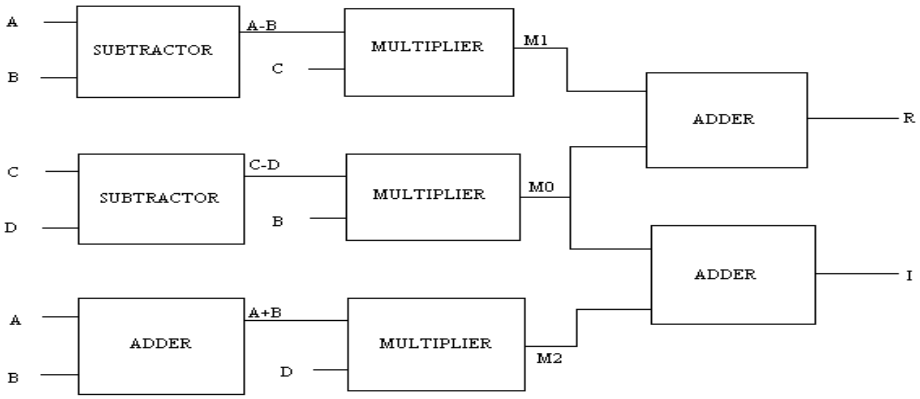

Figure 6 Multiplierless architecture for complex multiplier [9].

Butterfly Architecture: The most important element in FFT processor is a butterfly structure. It takes two signed fixed-point data from memory register and computes the FFT algorithm. The output results are written back in same memory location as the previous input stored. This method is called in-placement memory storage whereby it can reduce the hardware utilization. The butterfly architecture is shown in Fig. 6. The adder sums the input before being multiplied by the twiddle factor. The multiplier forms the partial product of the complex multiplication and produce two times bigger then input bit. Shift register would shift the bits to avoid overflow issue. Output of this butterfly would be kept in the register for the subsequent stage.

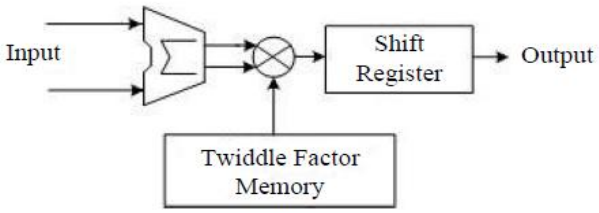

Figure 7 Butterfly architecture

III. Results:

The results are compared with the different FFT architecture implementations In this, as per the project requirements, Conventional 16-point and Scheme I 16-point FFT architectural implementation are discussed with the area and power calculations. All the other proposed architectural implementations and results are discussed briefly.

The 16-point R4SDC is synthesised at 16ns clock cycle, using the Cadence RTL Compiler targeted at 0.18 □ □ CMOS technology library. Power evaluations were carried out, usingCadence RTL compiler, at 16ns clock cycle for 16-point FFT. Table 5 and 6 provide information about the main modules for each implementation.

IV. Simulation Results

Analysis :
Commutator converts serial input to parallel output so that butterfly can receive these outputs at different clock with N_t delays.

Figure 8:Commutator

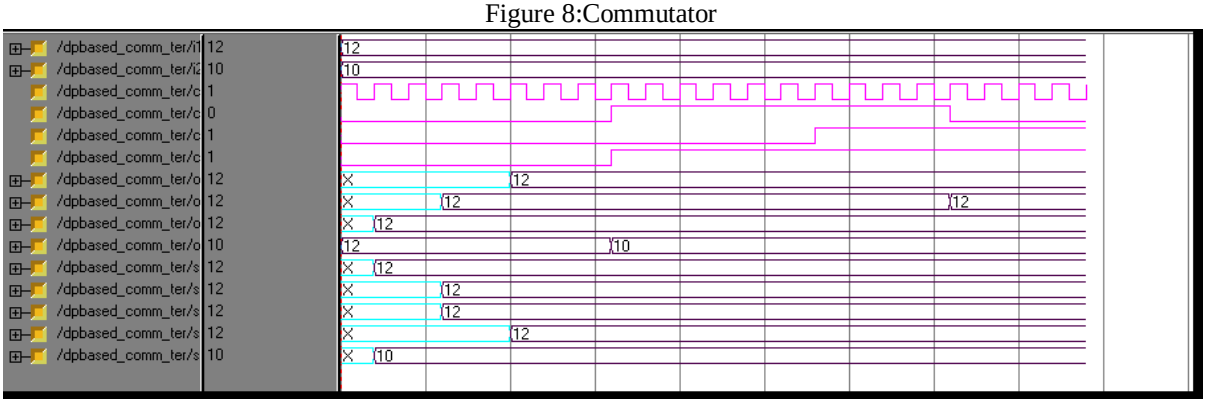

Analysis
The butterfly element is used to perform addition and subtraction. It accepts four input and produces four output.Here xre0,xre1,xre2,xre3,xim0,xim1,xim2,xim3 are the inputs and yre0,yre1,yre2,yre3,yim0,yim1,yim2,yim3 are the outputs.

Figure 9: Radix-4 FFT

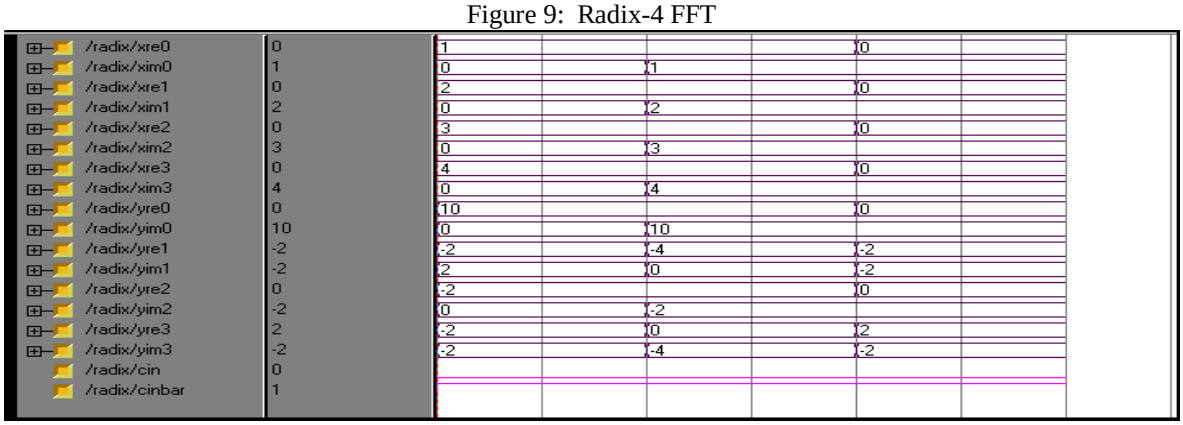

Analysis
Complex multiplier multiplier accepts two complex inputs namely data (*Xr* + *jXi*) and coefficient (*Wr* + *jWi*) and produces a complex output (*XOr* + *jXOi*). It is constructed by using four real multipliers along an adder and a subtractor.

Figure 10: Complex Multiplier

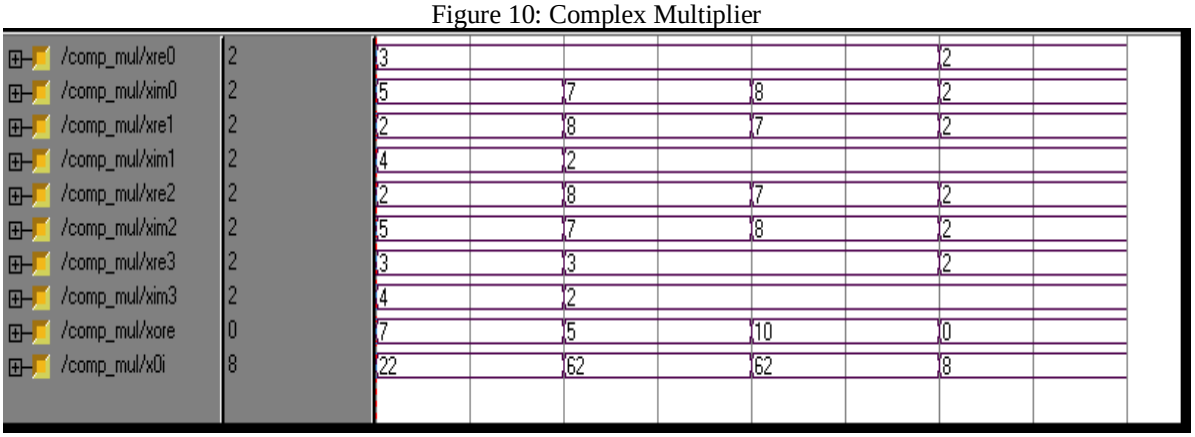

Analysis

The pipelined FFT Processor accepts serial input and produces the output depending upon the applied clock. The input is 32 bit complex data and output is 32 bit complex data. For easy understanding all the inputs and the outputs are shown.

Figure 11: Inputs for pipelined FFT

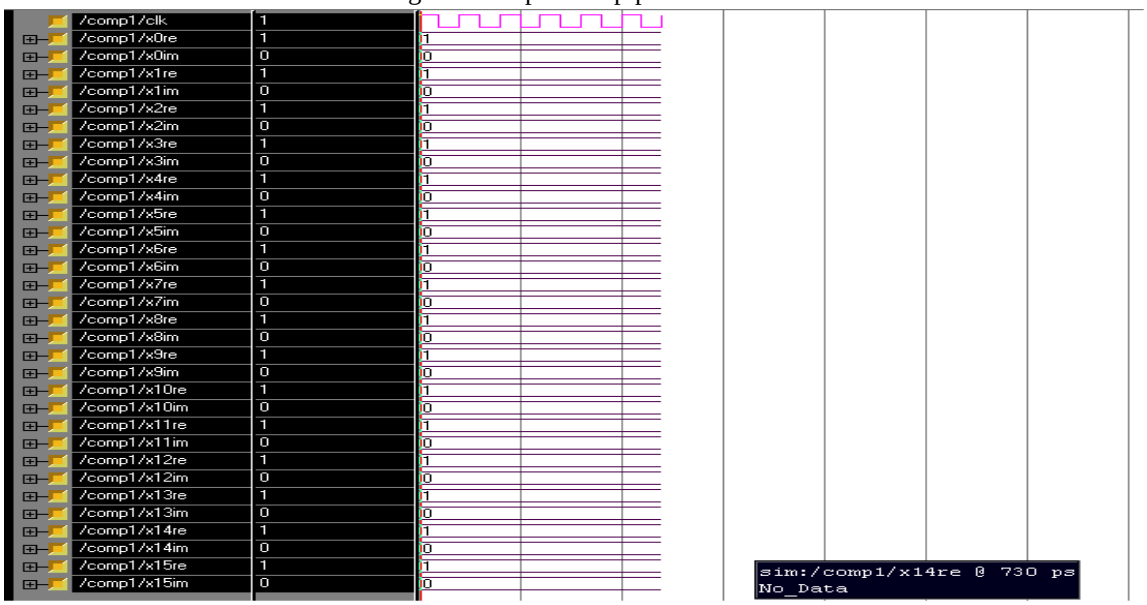

Analysis

The output is 32 bit complex data. Commutator accepts serial input and produces the parallel output with Nt delays. The size of commutator is 3N/2.so the output is delayed by 3N/2 bits.

Figure 12 outputs for pipelined FFT

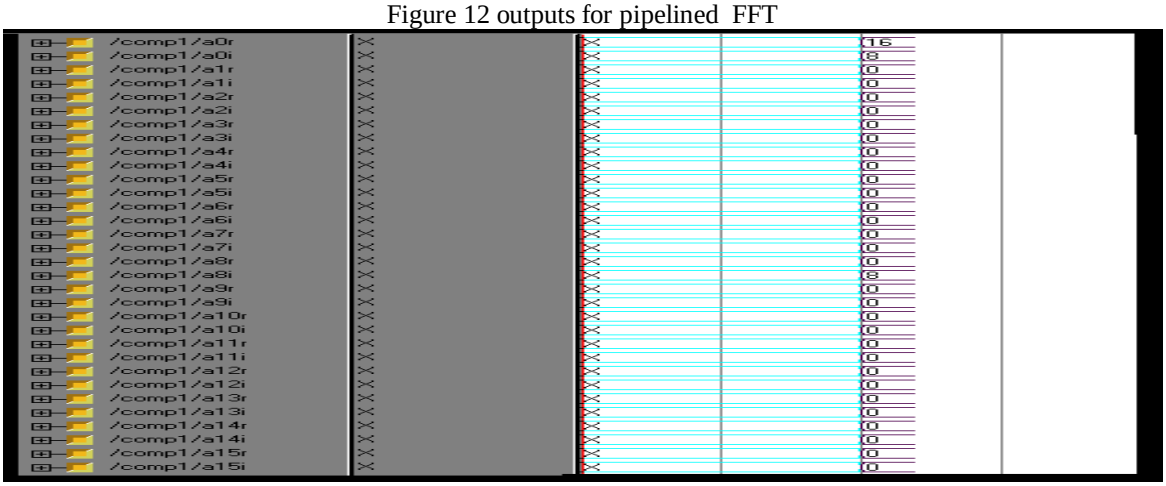

The graphical power and area comparison between the all the 5 architectures is shown in Figure 10 and 11.

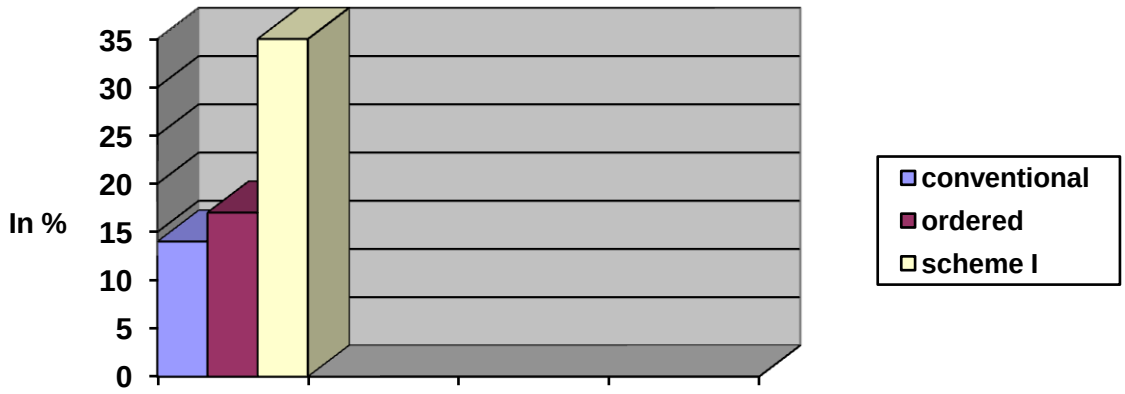

Figure 13: *Power reduction of Ordered and Scheme I-III relative to ordinary FFT*

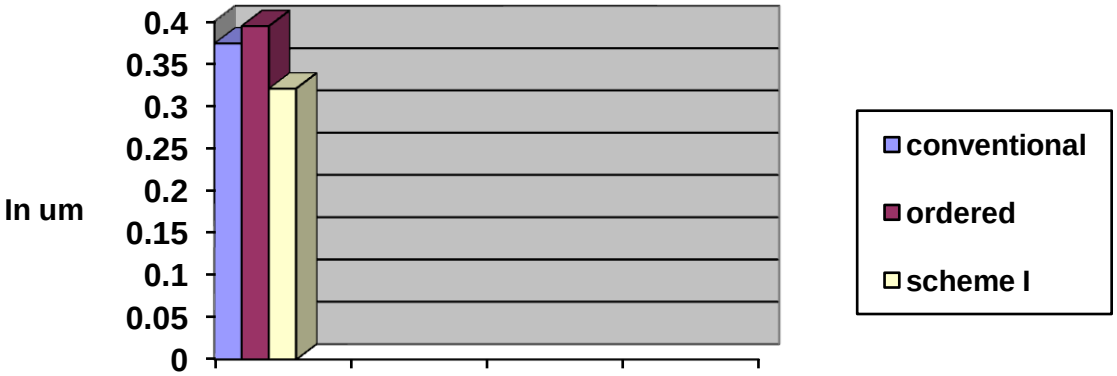

Figure 14: Area of Conventional FFT, Ordered FFT and Scheme I-III

This comparison result gives us very brief and concise information that which architectural combination is best for the design? As can bee seen by the figures above the scheme III outperforms all the other architectures both in power and area. So in respect with the above comparisons results we will compare the area and power for our designed architectures.

The comparative power and area results are shown in Figure 5.13 and 5.14 respectively. Clearly, for the scheme II-III for the 16-point FFT, the best possible power savings results are achieved.

Table 2

16 point FFT	Slack Time (ns)
Conventional	7.89
Scheme II	7.6
Scheme III	0.049

Timing Analysis for 16-point R4SDC FFT.

V. Summary.

In this work, we have discussed low power design techniques for multiplier and butterfly units. Based on the combination of the above two low power techniques with the ordered commutator architecture proposed in Chapter-4, low power 16-point R4SDC FFT architecture is implemented. Power and area parameters are calculated and discussed in the end of the chapter.

The multiplier-less architecture can also be utilised in the long FFTs, but where the area reduction is a major constraint, with a slight expense of power Scheme I or NBW type conventional multiplier can be used.

References:

[1]. Wei Han; Arslan, T.; Erdogan, A.T.; Hasan, M., "Low Power Commutator for Pipelined FFT Processors", *Circuits and Systems, 2005. ISCAS 2005. IEEE International Symposium on 23-26 May 2005 Page(s):5274 - 5277.*

[2]. Weidong Li,Lars Wanhammar," A Pipelined FFT processor",IEEE Transactions on consumer electronics,1999.

[3]. John G. Proakis, Dimitris G. Manolakis, "Digital Signal Processing", *Third Edition. Principles, Algorithm and Applications.*

[4]. Johansson, S.; Shousheng He; Nilsson, P., "*Wordlength optimization of a pipelined FFT processor*, Circuits and Systems, 1999, Volume 1, Aug. 1999 Page: 501 –503.

[5]. Baas, B.M., Student member, IEEE, "A Low-Power, High-Performance, 1024-point FFT processor, *Solid-State Circuits, IEEE Journal*, Volume 34, Issue 3, March 1999 Page: 380 – 387.

[6]. Schoushheng He; Mats Torkelson,IEEE, "A New approach to pipeline FFT processor", Applied electronics,IEEE journal,proceedings ofIPPS,1996

[7]. Jen Ming Wu and Yang Chun Fan "coefficient ordering based pipelined FFT/IFFT with minimum switching activity for a low power OFDM communications", Institute of communications Engineering.

[8]. B.Guoan and E. Jones,"A pipelined FFT processor for word sequential data",IEEE Transactions on Acoustics, Speech and Signal Processing,vol.37,pp.1982-1985,December 1989.

[9]. Wei Han; Arslan, T.; Erdogan, A.T.; Hasan, M., "Low Power Commutator for Pipelined FFT Processors", Circuits and Systems, 2005. ISCAS 2005. IEEE International Symposium on 23-26 May 2005 Page(s):5274 - 5277

IOSR Journal of VLSI and Signal Processing (IOSR-JVSP)
e-ISSN: 2319 – 4200, p-ISSN No. : 2319 – 4197 Volume 1, Issue 6 (Mar. – Apr. 2013), PP 76-83
www.iosrjournals.org

Multimodal Biometric Identification System Based On Iris & Fingerprint

Ms. Priyanka S. Patil[1], Prof.(Dr.) A. S. Abhyankar[2]
[1](*Department of E&TC(Signal Processing), VIIT College of Engineering Pune, India*)
[2](*Department of Computer Engineering, VIIT college of Engineering Pune, India)*

Abstract : *This paper is related to the development of an innovative multimodal biometric identification system. Unimodal biometric systems often face significant limitations due to sensitivity to noise intraclass variability and other factors. Multimodal biometric identification systems aim to fuse two or more physical or behavioral traits to provide optimal False Acceptance Rate (FAR) and False Rejection Rate (FRR), thus improving system accuracy and dependability. In greater detail, a Multimodal Biometric Identification System Based On Iris & Fingerprint. Both biometric traits (Iris & Fingerprint) are processed individually through all steps like segmentation ,feature extraction & matching. The multimodal system is fused using match level fusion at the verification stage on obtained matching score of iris and fingerprint. The performance of the biometric system shows improvement in the False Acceptance Rate (FAR) and False Reject Rate (FRR) .The proposed multimodal system achieves interesting results with several commonly used databases.*

Keywords *- Unimodal biometrics, multimodal biometric systems, iris and fingerprint biometry.*

I. INTRODUCTION

Biometrics, which refers to identify an individual based on his or her physiological or behavioral characteristics, has the capability to reliably distinguish between an authorized person and an imposter. Since biometric characteristics are distinctive, cannot be forgotten or lost, and the person to be authenticated needs to be physically present at the point of identification. Most biometric systems deployed in real-world applications are unimodal, i.e., they rely on the evidence of a single source of information for authentication (e.g., single fingerprint or Iris). unimodal biometric systems often face significant limitations due to sensitivity to noise, intraclass variability, data quality, non universality, and other factors. Limitations of unimodal biometric systems can be overcome by using multimodal biometric systems. Multimodal biometrics refers to the use of a combination of two or more biometric modalities in a verification / identification system. The goal of multi-biometrics is to reduce False accept rate (FAR), False reject rate (FRR).

A multi-biometric system can be classified into one of the 4 categories:

1.Multi-algorithm 2.Multi-instance
3.Multi-sample 4.Multimodal.

Multibiometrics data can be combined at different levels fusion:

1.Data-sensor level 2. Feature extraction level
3.Matching level 4. Decision level.

II. RELATED WORK

A variety of articles can be found, which propose different approaches for unimodal and multimodal biometric systems. Traditionally, unimodal biometric systems have many limitations. Multimodal biometric systems are based on different biometric features and/or introduce different fusion algorithms for these features. Many researchers have demonstrated that the fusion process is effective, because fused scores provide much better discrimination than individual scores. Such results have been achieved using a variety of fusion techniques . An unimodal fingerprint verification and classification system is presented in [16]. The system is based on a feedback path for the feature-extraction stage, followed by a feature-refinement stage to improve the matching performance. This improvement is illustrated in the contest of a minutiae-based fingerprint verification system. The Gabor filter is applied to the input image to improve its quality.

Ratha *et al.* [17] proposed a unimodal distortion-tolerant fingerprint authentication technique based on graph representation. Using the fingerprint minutiae features, a weighted graph of minutiae is constructed for both the query fingerprint and the reference fingerprint. The proposed algorithm has been tested with excellent results on a large private database with the use of an optical biometric sensor. Concerning iris recognition systems in [14], the Gabor filter and 2-D wavelet filter are used for feature extraction. This method is invariant to translation and rotation and is tolerant to illumination. The classification rate on using the Gabor is 98.3% and the accuracy with wavelet is 82.51% on the Institute of Automation of the Chinese Academy of Sciences (CASIA) database. In the approach proposed in [13], multichannel and Gabor filters have been used to capture

local texture information of the iris, which are used to construct a fixed-length feature vector. The results obtained were FAR = 0.01% and FRR = 2.17% on CASIA database. Generally, unimodal biometric recognition systems present different drawbacks due its dependency on the unique biometric feature. For example, feature distinctiveness, feature acquisition, processing errors, and features that are temporally unavailable can all affect system accuracy. A multimodal biometric system should overcome the aforementioned limits by integrating two or more biometric features.

Conti *et al*. [20] proposed a multimodal biometric system using two different fingerprint acquisitions. The matching module integrates fuzzy-logic methods for matching-score fusion. Experimental trials using both decision-level fusion and matching-score-level fusion were performed. Experimental results have shown an improvement of 6.7% using the matching score- level fusion rather than a monomodal authentication system.
Besbes *et al*. [12] proposed a multimodal biometric system using fingerprint and iris features. They use a hybrid approach based on: 1) fingerprint minutiae extraction and 2) iris template encoding through a mathematical representation of the extracted iris region. This approach is based on two recognition modalities and every part provides its own decision. The final decision is taken by considering the unimodal decision through an "AND" operator. No experimental results have been reported for recognition performance.

Aguilar *et al*. [21] proposed a multibiometric method using a combination of fast Fourier transform (FFT) and Gabor filters to enhance fingerprint imaging. Successively, a novel stage for recognition using local features and statistical parameters is used. The proposed system uses the fingerprints of both thumbs. Each fingerprint is separately processed; successively, the unimodal results are compared in order to give the final fused result. The tests have been performed on a fingerprint database composed of 50 subjects obtaining FAR = 0.2% and FRR = 1.4%.

Subbarayudu and Prasad [22] presented experimental results of the unimodal iris system, unimodal palmprint system, and multibiometric system (iris and palmprint). The system fusion utilizes a matching scores feature in which each system provides a matching score indicating the similarity of the feature vector with the template vector. The experiment was conducted on the Hong Kong Polytechnic University Palmprint database. A total of 600 images are collected from 100 different subjects. In contrast to the approaches found in literature and detailed earlier, the proposed approach introduces an innovative idea to unify and homogenize the final biometric descriptor using two different strong features—the fingerprint and the iris. In opposition to [23], this paper shows the improvements introduced by adopting the fusion process at the template level as well as the related comparisons against the unimodal elements and the classical matching-score fusion-based multimodal system. In addition, the system proposed in this paper has been tested on the official fingerprint FVC2002 DB2 and iris BATH databases [18], [24].

III. MULTIMODAL BIOMETRIC IDENTIFICATION SYSTEM

In this paper, we introduce a frequency approach [17], to generate a unified homogeneous template for fingerprint and iris features. In greater detail, the proposed approach performs fingerprint matching using the segmented regions (Regions Of Interests, ROIs) surrounding fingerprint minutia points[11]. On the other hand, iris preprocessing aims to detect the circular region surrounding the iris[5]. As a result, we adopted a algorithm-based codifier to encode both fingerprint and iris features, obtaining a unified template. Then we obtain matching score of individual biometric. Successively, the HD on the fused template has been used for the similarity index computation[12].

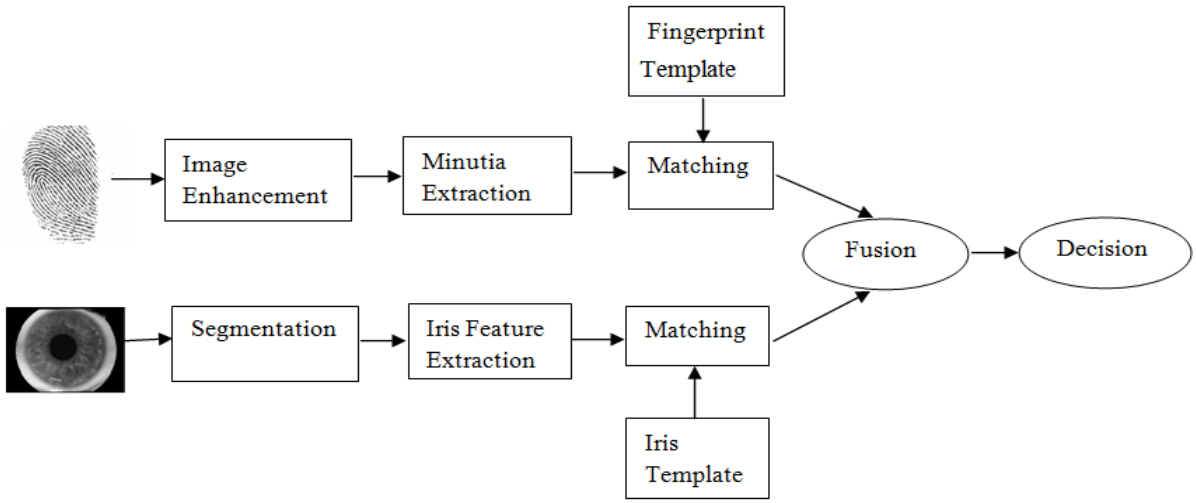

Fig 1. block diagram of multimodal biometric system .

In this structure of multimodal biometric identification system, two biometric models have been fused.

1. Fingerprint Recognition
2. Iris Recognition

Each individual biometric model has to go under different level of processing like Preprocessing, Normalization, Feature Extraction and Matching to get proper Matching score of both biometric individually and we apply fusion technique at matching score level with obtained matching score. The system can work either sequentially or parallel.

1. Fingerprint Recognition

Fingerprint recognition is the most consistent biometric modality in use, The main reason behind the use of fingerprint biometric is that it is the most proven technique to identify the individual. Digital fingerprints are more convenient and less disturbing than most of the other biometric methods and they are already accepted as an immutably single identifier. The fingerprint is basically the combination of ridges and valleys on the surface of the finger. However, revealed by rigorous research on fingerprint recognition, fingerprints are not distinguished by their ridges and furrows, but by Minutia, which are typical points on the ridges[11] . There are several minutia types: Termination (the immediate ending of a ridge), Bifurcation (the point on the ridge from which two branches derive),Island (a ridge that commences, travels a short distance and then ends), Ridge enclosures (a single ridge that bifurcates and reunites shortly afterward to continue as a single ridge), Spur (a bifurcation with a short ridge branching off a longer ridge), Crossover or bridge (a short ridge that runs between two parallel ridges)[11][7]. In this paper only two types of minutia points are take into consideration, which are termination and bifurcation. The major steps involved in fingerprint recognition using minutiae matching approach after image acquisition are:

1. Image Enhancement
2. Minutiae Extraction
3. Matching

1.1 Image Enhancement

A fingerprint image is corrupted due to various kinds of noises such as creases, smudges and holes. It is almost impossible to recover the true minutia points from the unrecoverable regions The fingerprint image is enhanced to make it clearer for easy further operations by increasing the contrast between ridges and furrows[15]. Image enhancement algorithm is used to improve the clarity of ridges/valley structures of fingerprint images in recoverable regions and to mask out the unrecoverable regions[11]. For this, we adopted an image normalization step using the arithmetic average M of the image gray levels and its variance V [12].

$$M(I) = \frac{1}{H*L}\sum_{i=1}^{H}\sum_{j=1}^{L} I(i,j) \qquad (1)$$

$$V(I) = \frac{1}{H*L}\sum_{i=1}^{H}\sum_{j=1}^{L} (I(i,j) - M)^2 \qquad (2)$$

1.2 Minutia Extraction

The endings and bifurcations of the fingerprint images are known as the minutia. The most commonly employed method of minutiae extraction is the Crossing Number (CN) concept.

(a) Ridge ending (b) Bifurcation

Fig 2. example of a ridge ending and a bifurcation.

The minutiae are extracted by processing the whole image pixel by pixel using a 3x3 matrix with the centre element being the focus of each process[14]. The CN value is then computed, which is defined as half the sum of the differences between pairs of adjacent pixels in the eight-neighborhood[11]. Using the properties of the CN as shown in table, the ridge pixel can then be classified as a ridge ending, bifurcation or non-minutiae point[7]. For example, a ridge pixel with a CN of one corresponds to a ridge ending, and a CN of three corresponds to a bifurcation. The Crossing Number (CN) method is used to perform minutiae extraction[11]. This method extracts the ridge endings and bifurcations from the skeleton image by examining the local neighborhood of each ridge pixel using a 3*3 window[11]. The CN for a ridge pixel *P* is given By,

$$CN = 0.5 \sum_{i=1}^{8} |P_i - P_{i+1}|, \quad P_{9=P_1} \qquad (3)$$

where *Pi* is the pixel value in the neighborhood of *P*. For a pixel *P*, its eight neighboring pixels are scanned in an anti-clockwise direction as follows:

P_4	P_3	P_2
P_5	P	P_1
P_6	P_7	P_8

After the CN for a ridge pixel has been computed, the pixel can then be classified according to the property of its CN value. A ridge pixel with a CN of one corresponds to a ridge ending, and a CN of three corresponds to a bifurcation[11]. For each extracted minutiae point, the following information is recorded:

- *x* and *y* coordinates,
- Orientation of the associated ridge segment, and
- Type of minutiae (ridge ending or bifurcation).

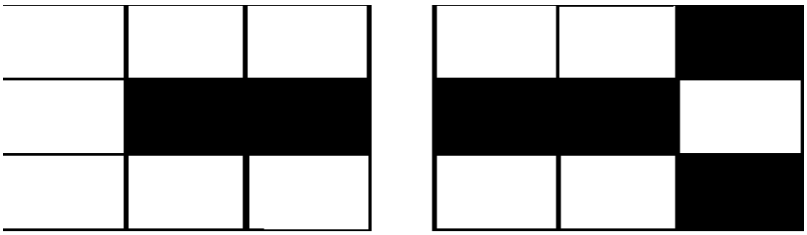

Fig 3. a) 1 Corresponds Ridge ending b) 3 Corresponds Bifurcation

However, there are a few cases where the extracted minutiae do not correspond to true minutiae points in the original image. In addition, it should be noted that in some cases the bifurcation and ridge ending points can be difficult to distinguish between each other[1]. This method not only increases the processing speed, but also reduces the possible error due to scars or noises in the fingerprint image[3]. Minutia extraction is processed in 4 steps:

- Fingerprint ridge thinning
- Minutia marking
- False minutia removal
- Unification of terminations and bifurcations.

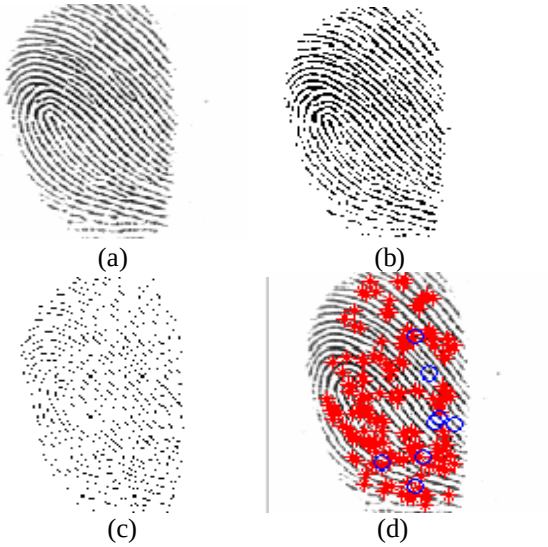

Fig 4. a)Input image, b) Binariesd image c)Thinned image, d) Minutia points of input image.

1.3 Matching

The minutia match algorithm settles on whether two set of minutia of two fingerprint images belong to the same finger or not .The first step consists in aligning the couple of fingerprint Images to be matched[3]. Thus we choose a minutia from each image and calculate the similarity of the associated ridges[10]. In the matching step, we count the matched minutia pairs of two set of transformed minutia points and we assume identical, two minutia having nearly the same position and direction[3].

2. IRIS RECOGNITION

Iris is plainly visible, colored ring that surrounds the pupil which is unique to each individual and remains constant over the life of a person. The iris is the annular ring between the sclera and pupil boundary and contains the flowery pattern unique to each individual. The eyeball has a circular black disk in the center known as pupil. The pupil dilates when exposed to light and contracts in dark. Thus the size of pupil varies with respect to light. There is no detailed correlation between the iris patterns of even identical twins, or the right and left eye of an individual[14]. For our developed approach of iris recognition, the input is an eye image, and the output is the matching score of the iris template. This texture information unique to each individual is extracted from rest of the eye image and is transformed into strip to apply pattern matching algorithm between the database and query images of iris[8]. It compares the difference between a pair of iris representations by computing their Hamming distance using XOR operator[12]. The algorithm consists in 4 steps :

1. Segmentation
2. Normalization
3. Feature Extraction
4. Matching

2.1 Segmentation

Iris image must be preprocessed before using it for the recognition purpose since the unwanted data including eyelid, pupil, sclera and eyelashes in the image should be excluded. The preprocessing module for iris was required to perform iris localization, iris normalization and image enhancement[6]. The Iris region is located within the two circles: the iris/sclera boundary and the iris/pupil one. We have used images provided by CASIA (Institute of Automation, Chinese Academy of Sciences)[6]. The images were taken exclusively for the purpose of iris recognition software research and implementation. Infra-red light was used for illuminating the eye, and hence they do not involve any specula reflections. For this reason, we do not proceed for a reflection error's removal. The segmentation step consists in applying Canny edge detection to generate an edge map, to isolate the actual iris region from a captured iris image[5]. In this process, roughly determine the inner and outer boundaries of iris region from iris image ,and then accurately locate the fine boundaries in the iris image with raw resolutions[6][10]. Image binarization were next used to extract the eyelid edge information. After this process, histogram equalization was used to implement image enhancement. then using circular Hough transform to detect the iris and pupil boundaries and deduce their radius and centre coordinates[13]. As a result parameters are stored: the radius, and (x, y) centre coordinates for both circles[12].

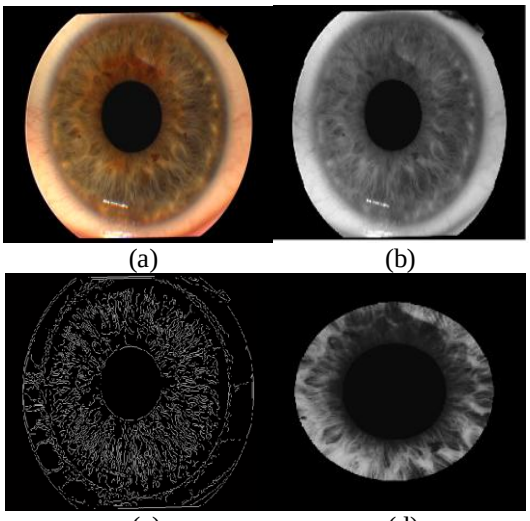

(a) (b)

(c) (d)

Fig 5. a) Original image, b) Gray image, (c) Binerised image, d) Segmented iris imge

2.2 Normalization

Once the iris region is successfully segmented from an eye image, the next stage is to transform the iris region so that it has fixed dimensions in order to allow comparison[6]s. The normalization process will produce iris regions, which have the same constant dimensions. The pupil region is not always concentric within the iris region, For normalization of iris regions a technique based on Daugman's rubber sheet model was employed[10][12]. The centre of the pupil was considered as the reference point, and radial vectors pass through the iris region**.**

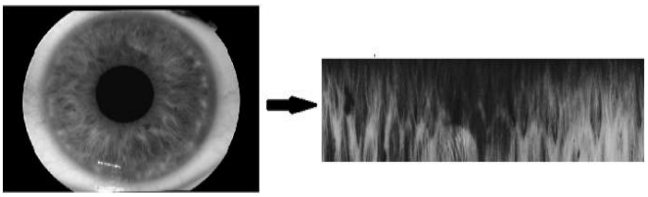

Fig 6. Normalized Iris Image

2.3 Feature extraction

The output of the normalization is noise free and is further proceed for feature extraction. In feature extraction, the template which is produced by normalization is converted into binary format for the matching process[1][6]. Feature Extraction is done by using bit plane slicing method. In order to provide accurate recognition of individuals, the most discriminating information present in an iris pattern must be extracted[13]. Only the significant features of the iris must be encoded so that comparisons between templates can be made. Most iris recognition systems make use of a band pass decomposition of the iris image to create a biometric template.

2.4 Matching

The comparison is done between iris codes (IC) generated for database and query images using hamming distance approach. In this approach the difference between the bits of two codes are counted and the number is divided by the total number of comparisons[12].

$$MS_{Iris} = \frac{1}{N}\sum_{i=1}^{N} A_i \oplus B_i \qquad (4)$$

where A is the binary vector (iris code) for database image and B is the binary vector for query image while N is the number of elements. This matching score (MS_{Iris}) is used as input for the fusion module where the final matching score is generated.

IV. FUSION OF IRIS & FINGERPRINT

No individual trait can provide 100% accuracy. Further, the results generated from the individual traits are good but the problem arises when the user is not able to give his iris image due to problem in exposure to light. As eye is the most sensitive organ of human body, the problem becomes severe when there exist some eye diseases. Thus in such a situation an individual cannot be recognized using the iris patterns and the biometric system comes to a standstill. Similarly, the problem faced by fingerprint recognition system is the presence of scars and cuts. The scars add noises to the fingerprint image which cannot be enhanced fully using enhancement module. Thus, the system takes noisy fingerprint as input which is not able to extract the minutiae points correctly and in turn, leads to false recognition of an individual. Thus to overcome the problems faced by individual traits of iris and fingerprint, a novel combination is proposed for the recognition system[5][10]. The integrated system also provide anti spoofing measures by making it difficult for an intruder to spoof multiple biometric traits simultaneously. Scores generated from individual traits are combined at matching score level using weighted sum of score technique[17]. Sum rule is used for the fusion of iris & fingerprint Matching score. A fusion system consist of two modules fusion and decision module. In the fusion module is well understood that need to normalize scores before combining them, that is seek to transform individual scores from each subsystem before combining[17]. In fact score from each subsystem can be of different nature. To solve this problem, the normalization transforms the score into common range include between 0 and 1 [17][13]. After that we use score combination method using a simple sum. Combining the average scores is to compute as,

$$s = \frac{1}{N}\sum_{i=1}^{N} s_i \qquad (5)$$

V. CONCLUSION

In this paper we introduced an innovative multimodal biometric identification system based on iris and fingerprint traits. Iris is the unique organ and remains stable throughout the lifetime. Fingerprint is more selective as compare to other biometric. That's why we take these traits. The features are extracted from iris & fingerprint image. Then template is formed & compare with stored one with the help of hamming distance. The Multimodal identification system is fused at Matching level fusion using sum rule at the verification stage. The results show improvements in the fingerprint verification phase and iris segmentation process. The proposed system works fine as it's FAR & FRR. The accuracy of the multimodal system is very high. So that multimodal biometric system has the potential to overcome the limitations of any individual biometric system. The multimodal biometric system provides more security to electronic data and resource access from unauthorized user. The performance of the multimodal biometric identification system shows significant improvement.

Acknowledgements

I am sincerely thankful to my guide Prof. Dr. A. S. Abhyankar for his relevant help, encouragement and providing the necessary guidance. I am also proud to thank our HOD (E&TC Department) Prof. P. D. Khandekar and our Principal Prof. Dr. B. S. Karkare for moral support. I am really thankful to all professors of VIIT for their guidance. Without their help it was tough job for me.

REFERENCES

Journal Papers:

[1] L. Hong, A. Jain, **"***Multimodal Biometrics***",** chapter 16 in A.Jain, R. Bolle , S. Pankanti, "Biometrics: Personal Identification in Networked Society", Kluwer Academic Publishers, Norwell, 1999.•

[2] S. Prabhakar, S. Pankanti, and A. K. Jain, "An Introduction to Biometric Recognition," IEEE Transactions on circuits and systems for video technology, VOL. 14, NO. 1, January 2004.

[3] Vincenzo Conti, Carmelo Militello, Filippo Sorbello, and Salvatore Vitabile, "A Frequency-based Approach for Features Fusion in Fingerprint and Iris Multimodal Biometric Identification Systems," IEEE transactions on systems, man, and cybernetics—part c: applications and reviews, VOL. 40, NO. 4, july 2010.

[4] Anil Jain Sharath Pankanti,Dept. of Computer Science & Engg. Exploratory Computer Vision Grp, *"Fingerprint Classification and Matching*,"

[5] R. Wildes, "*Iris Recognition: An emerging biometric technology*" Proceedings of the IEEE, vol.85, no.9, September 1997.

[6] Arun Ross, Anil Jain, Jain-Zhong Qian ―Information Fusion in Biometrics‖ Appeared in Proc. of 3rd Int'l Conference on Audio- and Video-Based Person Authentication (AVBPA), pp. 354-359, Sweden, June 6-8, 2001.

[7] A. K. Jain, A. Ross, and S. Pankanti, "An introduction to biometric recognition," *IEEE Trans. Circuits Syst. Video Technol.*, vol. 14, no. 1, pp. 4–20, Jan. 2004.

[8] Chan K.C, Y.S Moon and Cheng, "Fast fingerprint verification using subregions of fingerprint images", *IEEE Trans.on Circuits and Systems for video technology*, vol 14, Jan 2004.

[9] F. Besbes, H. Trichili, and B. Solaiman, "Multimodal biometric system based on fingerprint identification and Iris recognition," in *Proc. 3rd Int. IEEE Conf. Inf. Commun. Technol.: From Theory to Applications (ICTTA 2008)*, pp. 1–5. DOI: 10.1109/ICTTA.2008.4530129.

[10] L. Ma, Y. Wang and D. Zhang, ―Efficient iris recognition by characterizing key local variations‖ IEEE Trans. Image Process., vol. 13, no. 6, pp. 739–750, Jun. 2004.

[11] Y. Zhu, T. Tan, and Y. Wang, "Biometric personal identification on iris patterns," in *Proc. 15th Int. Conf. Pattern Recogn.*, 2000, vol. 2, pp. 805–808.

[12] L. Hong, Y.Wan, and A. Jain, "Fingerprint image enhancement, algorithm and performance evaluation," *IEEE Trans. Pattern Anal. Mach. Intell.*, vol. 20, no. 8, pp. 777–789, Aug. 1998.

[13] S. Prabhakar, A. K. Jain, and J.Wang, "Minutiae verification and classification,"presented at the Dept. Comput. Eng. Sci., Univ. Michigan State,East Lansing, MI, 1998.

[14] N. K. Ratha, R. M. Bolle, V. D. Pandit, and V. Vaish, "Robust fingerprint authentication using local structural similarity," in *Proc. 5th IEEE Workshop Appl. Comput. Vis.*, Dec. 4–6, 2000, pp. 29–34. DOI 10.1109/WACV.2000.895399.

[15] Fingerprint Verification Competition FVC2002. (2009, Nov.). [Online]. Available: http://bias.csr.unibo.it/fvc2002/

[16] J. Cui, J. P. Li, and X. J. Lu, "Study on multi-biometric feature fusion and recognition model," in *Proc. Int. IEEE Conf. Apperceiving Comput. Intell. Anal. (ICACIA)*, 2008, pp. 66–69. DOI: 10.1109/ICACIA.2008.4769972.

[17] V. Conti, G. Milici, P. Ribino, S. Vitabile, and F. Sorbello, "Fuzzy fusion in multimodal biometric systems," in *Proc. 11th LNAI Int. Conf. Knowl.Based Intell. Inf. Eng. Syst. (KES 2007/WIRN 2007),* Part I LNAI 4692. B. Apolloni *et al.*, Eds. Berlin, Germany: Springer-Verlag, 2010, pp. 108–115.

[18] G. Aguilar, G. Sanchez, K. Toscano, M. Nakano, and H. Perez, "Multimodal biometric system using fingerprint," in *Proc. Int. Conf. Intell. Adv.Syst. 2007*, pp. 145–150. DOI:10.1109/ICIAS.2007.4658364.

[19] V. C. Subbarayudu and M. V. N. K. Prasad, "Multimodal biometric system," in *Proc. 1st Int. IEEE Conf. Emerging Trends Eng. Technol.*, 2008, pp. 635–640. DOI 10.1109/ICETET.2008.93.

[20] F. Yang and B. Ma, "A new mixed-mode biometrics information fusion based-on fingerprint, hand-geometry and palm-print," in *Proc. 4th Int. IEEE Conf. Image Graph.*, 2007, pp. 689–693. DOI:10.1109/ICIG.2007.39.

[21] BATH Iris Database, University of Bath Iris Image Database. (2009, Nov.). [Online]. Available: http://www.bath.ac.uk/eleceng/ research/sipg/irisweb/

Books:

[22] A.Ross, K. Nandakumar, A. Jain, **"**Handbook of Multibiometrics**",** Springer, New York, 2006•

[23] "Multimodal Biometric Systems",chapter7 in D. Maltoni , D. Maio , A.K. Jain, S . Prabhakar, "*Handbook of Fingerprint Recognition*", *Springer-Verlag ,New York,2003.•"*

Theses:

[24] John Daugman. "How Iris Recognition Work" .IEEE Transaction on Circuits and Systems for VIDEO TECHNOLOGY, VOL. 14, No. 1, January 2004.

AUTHOR'S PROFILE

Ms. Priyanka S. Patil

Received the degree of B.E in Electronics and Telecommunication Engineering from BVCOEW Engineering College, Pune, Maharashtra in 2009 and pursuing M.E. in Electronics & Telecommunication Engineering from VIIT College of Engineering, Pune. With having 1 year teaching experience.

Prof.(Dr.) A. S. Abhyankar

Ph.D. in (Electrical and Computer Engineering) Clarkson University, NY, USA, · M.S. in (Electrical and Computer Engineering) Clarkson University, NY, USA, · B.E. in (E&TC) University Of Pune. He is Dean Research & Development Professor, Department of Computer Engineering at VIIT college of Engineering. With teaching & research experience of 10 years and industrial experience of 2 years. He has published papers in National-International conferences & International Journals. His Area of interest in Pattern Recognition, Digital Signal and Image Processing, Wavelet Analysis, Biomedical Signals, Biometrics, Bio-informatics.